THE UNIVERSITY *of* EDINBURGH

Utilizing Flow Characteristics to Increase Performance in Swimming

Thesis submitted for the degree of Doctor of Philosophy

Georgios Machtsiras

Supervisors: Prof. Ross H. Sanders & Dr. Prashant Valluri

Submitted to The University of Edinburgh: June, 2012

Abstract

Performance when gliding in the streamlined position depends on a swimmer's morphological characteristics, body orientation and water characteristics. The purpose of this thesis was twofold. First to identify and assess the effect of controllable factors that contribute to glide performance and second to form the foundations of an improved approach of simulating the fluid flow around the swimmers' body. To address the purposes of the thesis four investigations were conducted.

Study 1. The effect of the head position on glide performance was investigated. When the high, medium and low head positions were compared, it was found that swimmers experience significantly greater resistance and decelerate faster when they adopt a high head position. It was also found that there is no significant difference between the medium and low head position indicating for the first time that swimmers can choose any of the positions according to their natural tendency.

Study 2. The second study examined the effect of gliding depth on gliding performance. A range of depths was investigated ranging from 0.8 m to 0.2 m from the water surface. The results demonstrated significantly higher glide factor values for glides at a greater depth when compared to glides closer to the water surface highlighting the retarding effect of wave drag when gliding close to the surface. The optimum gliding performance was reported for glides at 0.8 m from the surface.

Study 3. The third study investigated the effect of full body swimsuits on glide performance. According to the findings, it is demonstrated for the first time that the improved gliding performance when wearing full body swimsuits is linked to changes in swimmers' morphology due to compression.

Study 4. In the fourth study the magnitude of resistive forces applied on a swimmer's body when gliding underwater was assessed with the use of computational fluid dynamics (CFD) and the LES approach. The results showed a close match between the glide factor values of the experimental and the computational findings demonstrating the effectiveness of the CFD method when the LES approach is employed.

Author Declaration

Edinburgh June 2012,

I hereby declare that:

a) I have composed this thesis

b) This thesis include my own work and

c) This work has not been submitted for any other degree or professional qualification except as specified.

Georgios Machtsiras

Georgios Machtsiras : _____ **Date:** _____

Prof. Ross H. Sanders: _____ **Date:** _____

Acknowledgements

I would like to thank my supervisors Prof. Ross Sanders, Dr Prashant Valluri and Prof. William Easson for their advice and guidance. I appreciate their person interest and encouragement.

Tim Niblett (Virtual Mirrors Ltd) and Dr Arthur Stewart (Robert Gordon University) for providing me access to their 3D scanning facilities.

My colleagues and friends, Roozbeh Naemi for his support with the use of MATLAB and the application of the Hydro-Kinematic method, Carla McCabe for her encouragement, Andre Salles for his recommendations on 3D CAD designing and Jonathan Master for the inspiring CFD conversations.

The swimmers (I am not supposed to reveal their names) that volunteered to participate to the study and their coach, Chris Jones.

The members of staff of the Centre for Sport and Exercise of the UoE (Ewan Heeles and Angela Lucas-Herald) as well as Robbie Kupris for helping me with the data collection.

Last but not least I would like to thank my parents Vangelis and Sofia and my sister Athena for always being there for me.

Table of Contents

Abstract ..... **I**

Author Declaration ..... **II**

Acknowledgements ..... **III**

Table of Contents ..... **IV**

List of Figures ..... **XII**

List of Tables ..... **XVI**

List of Abbreviations ..... **XVII**

Chapter 1

Introduction **1**

1.1. Purpose of the study 5

1.2. Thesis structure 7

Chapter 2

Literature Review **8**

2.1. The Glide Phase 8

2.2. Glide Hydrodynamics 9

2.2.1. The main characteristics of the resistive forces when gliding in the water 9

2.2.2. Contributions to resistance 9

2.2.2.1. Frictional resistance 9

2.2.2.1.1. Decreasing frictional resistance 11

2.2.2.1.2. Frictional resistance studies 12

2.2.2.2. Pressure resistance 13
2.2.2.2.1. Decreasing pressure resistance 14
2.2.2.2.2. Pressure resistance studies 14
2.2.2.3. Wave resistance 15
2.2.2.3.1. Decreasing wave resistance 17
2.2.2.3.2. Wave resistance studies 17
2.2.3. Added mass 17
2.3. Resistance measurement methods 19
2.3.1. Passive drag 19
2.3.1.1. Passive drag measurement methods 19
2.3.1.1.1. Towing methods 19
2.3.1.1.2. Flume analysis 21
2.3.1.1.3. Kinematic analysis 21
2.3.1.1.4. Other methods 22
2.3.2. Active drag 22
2.3.2.1. Active drag measurement methods 23
2.3.2.1.1. Direct methods 23
2.3.2.1.2. Indirect methods 23
2.3.2.1.3. Other methods 24
2.4. Body Scanning 24
2.4.1. Laser body scanners 25
2.4.2. LED body scanners 26
2.4.3. White-light body scanners 26
2.4.4. Other methods to generate 3D models of swimmers 27
2.5. CFD analysis 28
2.5.1. CFD, the method 29

2.5.1.1. Mathematical modelling 31
2.5.1.2. Discretization of the mathematical model..... 32
2.5.1.3. Discretization of the space domain..... 33
2.5.1.4. Temporal discretization schemes..... 35
2.5.1.5. Turbulence models..... 36
2.5.1.5.1. Reynolds-Averaged Navier-Stokes equations 36
2.5.1.5.2. Large Eddy Simulation..... 37
2.5.1.5.3. Direct Numerical Simulation..... 37
2.5.4. CFD Software..... 38
2.5.5. CFD in Sports..... 38
2.5.6. CFD in swimming 39
2.5.6.1. Passive drag assessment with the use of CFD..... 39
2.5.6.2. Active drag assessment with the use of CFD..... 40
2.6. Anthropometry.....42
2.6.1. Measurement approaches..... 42
2.6.2. Anthropometric measurement techniques 43
2.6.3. Frontal surface area calculation..... 43
2.6.4. Anthropometry and resistance..... 47

Chapter 3

Method 49

3.1. Participants 51
3.2. Participant preparation 52
3.3. Calculation of participant's anthropometric characteristics.....53
3.4. Swimming test 54
3.4.1. Experimental design 54

3.4.2. Swimming pool information 54
3.4.3. Camera set up 55
3.4.4. Calibrated area 56
3.4.5. Marking 57
3.4.6. Data collection 59
3.4.6.1. Warm up 59
3.4.6.2. Testing procedures 59
3.4.6.3. Collection of kinematic data 59
3.4.6.4. Feedback 60
3.4.7. Data analysis 60
3.4.7.1. Trimming 60
3.4.7.2. Digitizing 61
3.4.7.3. Analysis 61
3.4.7.4. Glide factor calculation 61
3.5. 3D body scans 63
3.5.1. Experimental design 63
3.5.2. 3D scanner information 63
3.5.3. 3D Scanner set up 64
3.5.4. Calibrated area 65
3.5.5. Marking 65
3.5.6. Data collection 65
3.5.6.1. Establishing similar glide and scanned joint angles 66
3.5.7. Data analysis 66
3.5.7.1. Fixing the models with the use of the Magics and the Rhinoceros software 67
3.5.7.2. Swimmer's height in the streamlined position 68

3.5.7.3. Volume and area measurements with the use of the 3D models..... 68

Chapter 4

Study 1: The effect of head position on glide performance 70

4.1. Introduction 70

4.2. Method 74

4.2.1. Statistical analysis 78

4.3. Results 79

4.3.1. Accuracy of the glide factor computation approach..... 80

4.3.2. Glide factor 80

4.3.3. Frontal Surface Area..... 82

4.4. Discussion.....84

4.5. Conclusion.....86

4.5.1. Limitations and recommendations 86

Chapter 5

Study 2: The effect of gliding depth on glide performance 87

5.1. Introduction 87

5.2 Method 91

5.2.1. Statistical analysis 92

5.3 Results 93

5.4 Discussion.....95

5.5 Conclusion.....97

5.5.1 Limitations and recommendations 97

Chapter 6

Study 3: The effect of full body swimsuits on glide performance 98

6.1. Introduction 98

6.2. Method 103

6.2.1. Statistical analysis 105

6.3. Results 106

6.3.1 Glide factor 106

6.3.2 Frontal Surface Area.....108

6.3.3 Cross Sectional Area Measurement.....109

6.4. Discussion.....110

6.5. Conclusion.....112

6.5.1 Limitations and recommendations 113

Chapter 7

Study 4: Glide performance assessment with the use of CFD.....114

7.1. Introduction 114

7.2. Numerical Method 120

7.2.1. Scaling, transformation and rotation 120

7.2.2. Domain.....120

7.2.3. Mesh generation 121

7.2.4. CFD analysis 121

7.2.4.1. Boundary conditions 121

7.2.4.2 Flow model and simulation parameters 123

7.2.4.3. CFD reports 125

7.2.5. Statistical analysis 125

7.3. Simulation quality.....126

7.3.1. Mesh independence tests 126
7.3.2. Temporal independence tests 127
7.3. Results and Discussion 128
7.3.1. Validation 128
7.3.2. Velocity, vorticity and drag fields 131
7.3.3. Comparison with previous studies 138
7.4. Conclusion 139
7.4.1. Limitations and recommendations 140

Chapter 8

Conclusionsand Future Directions 141
8.1. Conclusions 141
8.1.1. Experimental methods 142
8.1.1.1. Head position and glide performance 143
8.1.1.2. Gliding depth and glide performance 143
8.1.1.3. Full body swim suits and glide performance 143
8.1.2. Modeling methods 144
8.1.2.1. CFD to assess glide performance 145
8.1.3. General conclusions 145
8.2. Recommendations for future research 146
8.2.1. Glide performance assessment 146
8.2.2. CFD analysis 147
8.2.3. Anthropometry 147

References 148
Appendix A. Participant preparation documents 162

Informed consent form 163

Participant information sheet.....164

Pre activity questionnaire 166

Appendix B. The frontal surface area of the participants.....167

Appendix C. CAD model mesh size.....174

Appendix D. The high and the medium head gliding position 177

List of Figures

2.1	The fluid flow velocity profile at the boundary layer.	10
2.2	White-light scanner output.	26
2.3	The CFD analysis process.	30
2.4	Structured grid around a rectangular object.	34
2.5	Structured grid around a rectangular object (close view).	34
2.6	Unstructured grid around a rectangular object.	35
2.7	Unstructured grid around a rectangular object (close view).	35
2.8	The relationship between the models used to simulate fluid flow and the computational cost and solution fidelity (adopted by Mockett *et al*., 2011).	38
3.1	The general methodological approach followed in this thesis.	50
3.2	Representation of swimmer's anthropometrical characteristics.	51
3.3	Participants were weighed underwater with the use of a load cell.	53
3.4	Representation of the underwater and the above water camera position (not scaled) and their field of view.	55
3.5	The fontal cover of the camera housing made from perspex.	56
3.6	The calibrated area with the 9 landmarks across the gliding path.	57
3.7	The location of markers when the swimmer was wearing the normal swimsuit.	58
3.8	The location of markers when the swimmer was wearing the full body swimsuit.	58
3.9	Difference in the GG values computed from the displacement data of the hip markers in comparison to the averaged displacement data of the wrist, shoulder, goggle, hip, knee and ankle markers.	62
3.10	The swimmer's goggles were painted white and their suits were covered in talc powder when that was necessary.	64
3.11	The scan of the upper part of the body (a) was merged with the scan of the lower part of the body (b) to get the full body model (c).	65
3.12	The goniometer used to calculate joint angles.	66

3.13	The scanned models were refined by filling the holes and smoothing the surface of the scanned mesh.	67
3.14	The total height in the streamline position as well as the ankle to the bottom of the toes length was measured from the 3D models.	68
3.15	Ankle to bottom of the toes length measurement with the use of the participant's 3D models.	69
4.1	The factors affecting performance when gliding after starts and turns.	71
4.2	Medium, high and low head position tested.	75
4.3	Side view of the male and the female swimmer in the 'medium head' position.	77
4.4	Medium, high and low head position adopted by the male swimmer.	79
4.5	Medium, high and low head position adopted by the female swimmer.	80
4.6	Glide factor values reported for each condition tested for the male participant. Bars represent the standard error of the mean.	81
4.7	Glide factor values reported for each condition tested for the female participant. Bars represent the standard error of the mean.	81
4.8	a). The frontal surface area of the male and b). the female participant for angles of attack ranging from 3 to -3 degrees.	82
4.9	FSA values reported for each condition tested for the male participant.	83
4.10	FSA values reported for each condition tested for the female participant.	83
5.1	The factors affecting performance when gliding after starts and turns.	88
5.2	Participants performed controlled glides at a depth 0.8 m, 0.6 m, 0.4 m and 0.2 m from the water surface.	92
5.3	Glide Factor values reported for each depth tested for the male participant. Bars represent the Standard Error of the Mean.	94
5.4	Glide Factor values reported for each depth tested for the female participant. Bars represent the Standard Error of the Mean.	94
6.1	The number of world records broken per year in swimming. Source: Swimming Statistics (http://www.scmsom.se/).	98
6.2	The factors affecting gliding performance.	100
6.3	a) The normal and full body swimsuit condition tested b) The Speedo LZR and the Jacked01full body suit.	103

6.4	The male participant when wearing the full body and the normal swimsuit.	104
6.5	The female participant when wearing the full body and the normal swimsuit.	105
6.6	Glide Factor values reported for each condition tested for the male participant. Bars represent the Standard Error of the Mean.	106
6.7	Glide Factor values reported for each condition tested for the female participant. Bars represent the Standard Error of the mean.	107
6.8	Frontal surface area values reported for each condition tested for the male participant.	108
6.9	Frontal surface area values reported for each condition tested for the female participant.	109
6.10	Cross sectional area values reported for each condition tested for the male participant.	110
6.11	Cross sectional area values reported for each condition tested for the female participant.	110
7.1	(a) The surface mesh of the swimmer consisted of 10,676 triangular surface elements. (b) The bounding box with dimensions equal to 5.6 m x 2.6 m x 2 m.	121
7.2	The boundaries of the computational domain.	122
7.3	Correspondence between gliding velocity, gliding time and iteration number. This information was input to the simulation software as inlet velocity.	123
7.4	(a) 20 prism cells layers were modeled to model with higher accuracy the transition boundary layer of the swimmer. The demonstrated region is at the lower back. (b) The volume mesh generated with the use of the ICEM software.	127
7.5	Irregularities in the drag force reported at velocity transition (the extreme values were not considered for the analysis).	129
7.6	Drag force reported with the use of the LES and the k-ε model.	130
7.7	Streamlines demonstrating the flow direction and the velocity magnitude.	132
7.8	Vectors showing the velocity of the water around the swimmer's body.	133
7.9	Wall shear stress magnitude scalar plots demonstrating the areas of the body with the highest wall shear.	134
7.10	Scalar plots demonstrating the vertical component of velocity (Y axis). The positive and negative values demonstrate the direction (positive Y+ and negative Y-).	135

7.11	Scalar plots demonstrating the lateral direction of velocity (Z axis). The positive and negative values demonstrate the direction (positive Z+ and negative Z-).	136
7.12	Scalar plots demonstrating the z component of vorticity. Positive values indicate regions of anticlockwise recirculation whereas negative values indicate regions of clockwise recirculation.	136
7.13	Isosurfaces of the z component of vorticity.	137
AP1	The frontal surface area profile for the female swimmer for angles of attack ranging from -3 to 3 degrees.	168
AP2	The frontal surface of the female swimmer in the medium head position.	168
AP3	The frontal surface area of the female swimmer in the high head position.	169
AP4	The frontal surface of the female swimmer in the low head position.	169
AP5	The frontal surface area profile for the female swimmer when wearing the full body and the normal swimsuit for angles of attack ranging from -3 to 3 degrees.	170
AP6	The frontal surface of the female swimmer when wearing the full body swimsuit.	170
AP7	The frontal surface area profile for the male swimmer for angles of attack ranging from -3 to 3 degrees.	171
AP8	The frontal surface of the male swimmer in the medium head position.	171
AP9	The frontal surface area of the male swimmer in the high head position.	172
AP10	The frontal surface of the male swimmer in the low head position.	172
AP11	The frontal surface area profile for the male swimmer when wearing the full body and the normal swimsuit for angles of attack ranging from -3 to 3 degrees.	173
AP12	The frontal surface of the male swimmer when wearing the full body swimsuit.	173
AP13	Maximum mesh size 5 mm.	175
AP14	Maximum mesh size 8 mm.	175
AP15	Maximum mesh size 9 mm.	175
AP16	Maximum mesh size 10 mm.	176
AP17	Maximum mesh size 20 mm.	176
AP18	Maximum mesh size 40 mm.	176
AP 19	Michael Phelps gliding underwater with a low head position.	178
AP 20	Ian Thorpe gliding underwater with a medium head position.	178

List of Tables

2.1	Passive drag assessment studies with the use of computational fluid dynamics.	40
2.2	Active drag assessment studies with the use of computational fluid dynamics.	41
3.1	Participants' age, body mass, height and maximum cross sectional area.	51
4.1	Average head angle values for each head position adopted by the participants.	76
4.2	SD_{pooled} data, significance levels and effect sizes for each swimmer and for all head angles tested.	82
5.1	SD_{pooled} data, significance levels and Effect Sizes for each swimmer and for all four glide depths tested.	95
6.1	SD_{pooled} data, significance levels and Effect Sizes for both swimmers.	107
6.2	Mass and standard deviation values of both swimmers when wearing the normal competitive and the full body polyurethane swimsuit.	108
7.1	Previous CFD studies in swimming biomechanics involving 3D full body models (the prism cell layers are employed to increase accuracy).	117
7.2	Mesh independence checks were performed to define the optimum mesh size (Initial velocity, υ_0=2 ms^{-1}).	126
7.3	Temporal dependence checks were performed to define the optimum time step size (υ = 2 ms^{-1}).	128
7.4	Glide factor values reported for the experimental and the numerical analysis.	131

List of Abbreviations

BH	Body height
BM	Body mass
BSA	Body surface area
BV	Body volume
CAD	Computer aided design
CARE	Centre for Aquatics Research and Education
CFD	Computational fluid dynamics
CG	Glide factor
CT	Computerised tomography
DLT	Direct linear transformation
DNS	Direct numerical simulation
FDM	Finite difference method
FEM	Finite element method
FINA	Federation Internationale de Natation
FSA	Frontal surface area
FVM	Finite volume method
HKM	Hydro-Kinematic method
LED	Light emitting diodes
LES	Large eddy simulation
MCSD	Maximum cross sectional diameter
MRI	Magnetic resonance imaging
NS	Navier-Stokes
RANS	Reynolds-averaged Navier-Stokes
RNG	Re-normalisation group
RSM	Reynolds stress model
SD	Standard deviation
STL	Stereolithography

Chapter 1

Introduction

Both in competitive and recreational swimming, athletes adopt a streamlined posture in the glide phase of starts and turns as well as in the glide phase of the breaststroke cycle. Swimmers produce no propulsive forces and the body decelerates due to the resistive drag force of the water. Because the swimmer is not active in attempting to produce propulsive movements during the glide phase, the resistive drag is termed 'passive' drag (Wilson and Thorp, 2003). To minimise passive drag and increase gliding performance, swimmers adjust their posture to minimize their frontal surface area exposed to the flow. Typically the posture of competitive swimmers is characterised by fully extended elbows, one hand over the top of the other, the head between the arms, the knees fully extended and the ankles together and plantar flexed.

Unlike marine mammals, humans did not show a continuum for aquatic locomotor optimization during evolution (Williams, 1997).The human shape is neither smooth nor well tapered. The shoulders project from the trunk at sharp angles, the hips are wider than the waist and the lower and the upper limbs are irregular in shape. Efficiency values reported for human underwater aquatic locomotion (11-29%, von Loebbecke *et al.,* 2009) indicate that the ability to minimise resistive drag is far inferior to that of aquatic species like the harbour porpoise (56%, von Loebbecke *et al.,* 2009).

Several studies of the effect of morphological characteristics on swimming performance (Cureton, 1975; Huijing *et al.,* 1988 and Toussaint *et al.,* 1990) as well as others on gliding performance (Clarys *et al.,* 1974; Chatard, 1990; Lyttle, 1998 and Benjanuvatra *et al.,* 2001) concluded that body form is a significant contributor.

However, gliding performance does not depend only on swimmers' genetically defined morphological characteristics but also on other factors that are controllable and can be adjusted by swimmers. During the passive glide phase swimmers can optimize their body posture and body orientation to the flow to minimise passive drag.

Hydrodynamic resistance of a body during a passive glide is equal to the sum of frictional, pressure and wave contributions contributing respectively by 0.05%, 94.9% and 5% to the total resistance (Vorontsov and Rumyantsev, 2000). For glides deeper than 0.6 m 'pressure drag' that is the result of pressure differences between the front and the rear part of the swimmer's body, predominates (Lyttle, 1999). Pressure drag is determined by the posture and shape characteristics of the body as well as its orientation to the flow. Thus, total resistance is strongly dependent on swimmers' postures. At depths less than 0.6 m 'wave drag' needs to be considered as well as pressure drag. Wave drag is greatest when a swimmer is near the surface and decreases with depth. Therefore, swimmers must consider their glide depth and trajectory in combination with their posture and orientation (Lyttle *et al.*, 1998). Frictional drag, due to the frictional force of fluid particles acting on the swimmer's body, is small relative to the other contributions to drag (Vorontsov and Rumyantsev, 2000).

Measures of the passive drag provide useful information regarding the amount of the resistive forces swimmers experience and have been used to quantify gliding performance. Several methods have been used to measure passive drag with varying success. Dubois-Reymond tried to measure resistance by towing his subjects behind a rowboat in 1905. Since then towing devices have been advanced, testing environments improved and more accurate data collected from numerous research groups by means of towing devices/apparatus (Karpovich, 1933; Alley, 1952; Counsilman,1955; Hairabedian, 1964; Clarys *et al.*, 1974;Van Manen and Rijken, 1975; Jiskoot and Clarys, 1975; Clarys and Jiskoot, 1975; Clarys, 1979; Williams and Kooyman, 1985; Chatard, *et al.*, 1990; Sheehan and Laughrin, 1992;

Kolmogorov and Duplisheva, 1992; Klauck, 1998; Lyttle *et al.*, 1998; Benjanuvatra *et.al.*, 2001 and Mollendorf *et al.*, 2004). Testing in moving water channels (flumes) has been conducted by Miyashita and Tsunoda, (1978), Maiello *et al.* (1998), Roberts *et al.* (2003), Chatard and Wilson (2003) and Vennell *et al.*(2006). Analysis of kinematic data obtained from actual glides of unrestrained swimmers has been conducted by several researchers including Klauck and Daniel (1976), Oppenheim, (1997), Naemi and Sanders (2008) and Elipot *et al.* (2009). Recently, computational fluid dynamics (CFD) analysis has been conducted (Bixler *et al.*, 2007; Marinho *et al.*, 2009 and Zaidi *et al.*, 2010).

In this thesis the effect of controllable factors that can be adjusted by the swimmers when gliding (and affect gliding performance) will be assessed. The quantitative results will be computed with the 'Hydro-Kinematic' method (Naemi and Sanders, 2008), a method used to quantify glide efficiency from kinematic data. Additionally, gliding efficiency will be assessed also with the use of CFD, a method used to simulate fluid dynamics phenomena. A comparison between the experimental and the numerical findings will allow a validation of the latter.

Controllable factors affecting glide performance

Head position

Bulgakova and Makarenko (1996) identified that drag forces were significantly lower when the head was positioned between the arms when gliding underwater. However, experimental limitations prevented the researchers from examining the effect of head position on glide performance. Kinematic analysis of swimmers in the streamlined position has been performed after a start to identify the loss of speed during the underwater gliding motion (Elipot *et al.*, 2009). However, the head angle was not calculated and its effect on swimmers' deceleration was not assessed. Kinematic analysis of swimmers gliding in the streamlined position with altered head orientations would provide the necessary information to accurately assess the effect of body posture on drag forces. This information would enable identification of the optimum head position.

Gliding depth

Lyttle *et. al.* (1998) confirmed that resistive forces for human swimmers experienced when gliding close to the surface, like those of other objects (Hertel, 1966), are higher than those experienced at greater depths due to wave drag. This has important implications for the depth of the glide during the glide phase of starts and turns and for the trajectory used when surfacing (Pease, 2009). By analysing the kinematic data of swimmers gliding at different depths when not attached to towing devices, the effect of wave drag on glide efficiency could be assessed.

Swimming suits

Full body swimming suits were common in national and international swimming competitions until the beginning of 2010 when the Federation Internationale de Natation (FINA) set new regulations for swimsuits. Significant improvement in swimming times when wearing them (Chatard and Wilson, 2008) highlight the effect of technology on swimming performance. Suit technology involves innovative materials with special properties. Advanced fabrics are advertised to compress body and create the most hydrodynamic shape across the whole body. Towing studies assessing the effect of swimming suits on performance showed that passive drag reduces significantly (Benjanuvatra *et al.,* 2002; Mollendorf *et al.,* 2004 and Pendergast *et al.,* 2006) when wearing the suits. However, the measurements were conducted when the swimmers were towed and not under realistic gliding conditions. Kinematic analysis of glides of swimmers wearing full body swim suits will allow us to assess their effect under real conditions.

Computational Fluid Dynamics

The possibility of using CFD to analyze swimming was recognized by Bixler and Schloder (1996) and applied years later to analyze the hydrodynamic resistance of a gliding swimmer (Bixler *et al.,* 2007; Marinho *et al.,* 2009 and Zaidi *et al.,* 2010; Popa *et al.,* 2011). However, to date, the numerical CFD approach has not been validated against experimental gliding performance data when the swimmer is freely gliding. A comparison between experimental and numerical findings of the same

swimmer analysed under transient conditions (when the swimmer is decelerating) would allow the validation of the numerical approach. Furthermore, such a comparison would enable validation of the different models that can be used when running the CFD fluid flow simulations.

1.1. Purpose of the study

The purpose of this study was twofold. First was to identify and assess the effect of controllable factors that contribute to glide performance. The second was to set the foundation of an improved approach of simulating fluid flows around a swimmer's body.

To address these purposes four investigations were conducted:

1. The effect of head position on glide performance.
2. The effect of gliding depth on glide performance.
3. The effect of full body swimming suits on glide performance
4. Glide performance assessment with the use of Computational Fluid Dynamics.

This information can be used by sport scientists and sport engineers to understand the hydrodynamics of a swimmer's glide, optimize swimmer's glide posture, further advance swimming suit design and apply Computational Fluid Dynamics with greater accuracy.

Study 1: The effect of head position on glide performance

Not all elite swimmers streamline their body in the same way. Investigation of the magnitude of glide efficiency when swimmers are gliding with their head in low, medium and high position will enable to identify the optimum posture for the head. This study addresses the question:

- What is the effect of head position on glide performance?

Study 2: The effect of gliding depth on glide performance

A comprehensive evaluation of the gliding depth effect while allowing free movement of the participant as in competition will allow swimmers to identify the optimum gliding depth after starts and turns. This study addresses the question:

- What is the effect of gliding depth on glide performance?

The effect of wave drag assessed by the Hydro-Kinematic method will also enable the comparison against previous results from towing testing (Lyttle, 1998).

Study 3: The effect of full body swimming suits on glide performance

Assessment of glide efficiency when swimmers wear normal and full body swimming suits will allow scientists to identify gliding performance improvement due to the swimming suit used. This study addresses the question:

- What is the effect of full body swimming suits on glide performance?

Study 4: Glide performance assessment with the use of Computational Fluid Dynamics

A comparison between the numerical and the experimental findings would enable the optimum settings of variables in the Computational Fluid Dynamics simulation software to obtain accurate results. This study addresses the question:

- What is the effect of turbulence model selection on the accuracy of the analysis?

1.2. Thesis structure

This thesis is organised into eight chapters.

Chapter one introduces the areas of interest that will be investigated in this thesis.

Chapter two reviews the literature related to the purposes of the thesis.

Chapter three presents and describes the methods that were common within all experimental studies.

Chapters' four to seven describes each of the four studies.

Chapter eight summarises the outcome of this thesis and provides suggestions for future research.

Chapter 2

Literature Review

In this section of the thesis the factors that affect performance when gliding are outlined and the previous studies conducted to assess hydrodynamic resistance are discussed in detail. Particular emphasis is accorded the hydrodynamic resistance measurement techniques employed in the past and the limitations that each one of them possesses. Finally, the approaches employed in previous studies to assess the anthropometric characteristics of swimmers are reviewed as well as their relative accuracy.

Accurate and detailed measurement of the resistive forces when swimming is required not only to increase performance but also to give a deeper insight into the physical phenomena that define the characteristics of the flow. This is done in two stages; first by defining how different factors affect performance (causal relationships between variables) and second by analysing the effect of the independent variables from a theoretical perspective. Therefore, in this chapter a theoretical background relating to the hydrodynamic forces applied when gliding underwater is developed.

2.1. The Glide Phase

Lower race times are achieved when swimmers glide for longer underwater in the streamline position after a start or a turn (Hay, 1986). Thus, researchers seek an explanation of the mechanisms that define performance during this phase of the race. The following paragraphs describe the contributions to drag as well as the different methods applied to compute drag forces.

2.2. Glide Hydrodynamics

2.2.1. The main characteristics of the resistive forces when gliding in the water

As the swimmer glides in the water, forces retard the motion. The direction of these forces is opposite the direction of motion and are usually referred to as drag. Because of the high density and viscosity of the water, the resistive forces are an important factor in determining performance when gliding. Therefore, to improve race times, a swimmer needs to comprehend the physical principles that govern the motion of fluids and also the nature of the interaction between the fluid flow and the body. The different factors that affect hydrodynamic resistance need to be studied and considered when training in order to minimize drag and maximize gliding velocity.

2.2.2. Contributions to resistance

William Froude in 1955 with his experiments in naval engineering research established the foundations of the notion that different sources of resistance might be separated and treated independently (Molland, 2008). Nowadays resistance is considered to be equal to the sum of the frictional (F_f), pressure (F_p) and wave (F_w) contributions.

$$F_{total} = F_{frictional} + F_{pressure} + F_{wave} \quad \text{Equation 2.1}$$

2.2.2.1. Frictional resistance

Frictional resistance or skin drag is the result of the viscous shear between the skin surface and the fluid particles moving along the swimmer's body. The velocity of the fluid particles at the interface is equal to the velocity of the swimmer. As the distance from the body surface is increasing, the flow velocity increases as well until it reaches the free stream velocity. The area between the interface and the point where the flow velocity is equal to 99% of the free stream velocity is called the boundary layer (Schlichting and Gersten, 2000, Figure 2.2).

The frictional resistance can be computed according to Equation 2.2

$$F_{fr} = \frac{1}{2} \cdot C_{fr} \cdot \rho \cdot S \cdot v^2 \qquad \text{Equation 2.2}$$

where C_{fr} is the friction drag coefficient, ρ is the fluid density, S is the wetted body surface area and v is the velocity of the moving body.

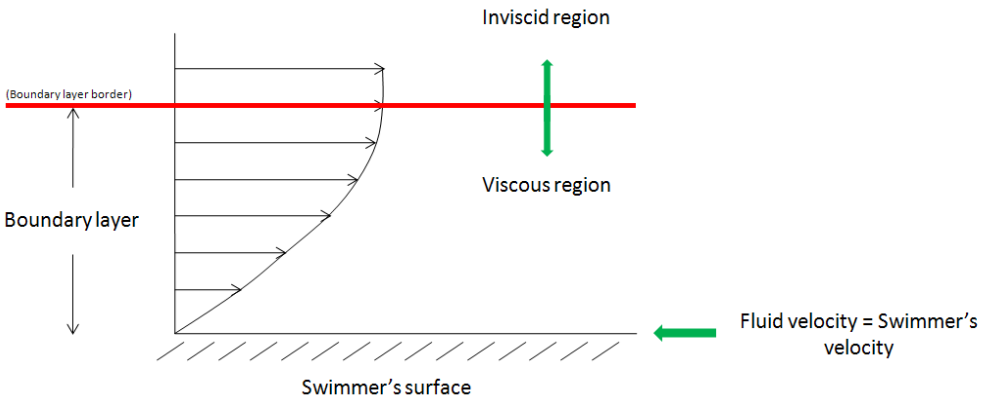

Figure 2.1Thefluid flow velocity profile at the boundary layer

The magnitude of frictional resistance depends on: (i) the total immerged surface area of the swimmer and (ii) the flow conditions within the boundary layer (Webb, 1975). The flow within the boundary layer can be (i) laminar (ii) turbulent or (iii) transitional depending on the size, shape, and velocity of the swimmer as well as the density and viscosity of the water. The Reynolds number (Re), a dimensionless parameter, is the ratio of inertial to viscous forces that describe the type of flow according to the Equation 2.3.

$$Re = \frac{\rho \cdot v \cdot L}{\mu} \qquad \text{Equation 2.3}$$

where ρ is the water density, v is the flow velocity, L is the body length and μ is the coefficient of dynamic viscosity.

In laminar flows, the fluid flows in parallel layers without any disturbances and disruption between the layers. Laminar flow around a swimmer's body is achieved by adopting a streamlined position and keeping the velocity low. As the velocity increases and the body contours are not smooth, the flow 'separates' and becomes turbulent.

Separation and turbulent flow occurs when friction within the boundary layer increases. The formation of eddies after the point at which the flow separates results in variation of pressure and velocity as well as the formation of unsteady vortices.

For competitive swimming Re is of the order of $2x10^5$ to $2.5x10^6$ (Clarys, 1979). The size and shape of swimmers is such that, at these Reynold's numbers, the flow is predominately turbulent.

2.2.2.1.1. Decreasing frictional resistance

Swimmers can minimize the effect of frictional resistance by decreasing the amount of water dragged along with their body when gliding underwater. This can be achieved by improving the smoothness of the body surface, removing skin hair, or adjusting the tightness of the swimsuit.

At the beginning of the 21st century, scientists were convinced that smooth swimsuits covering most of the body surface could decrease friction drag and allow faster swimming times. Scientific evidence supporting the effectiveness of full body suits was published at that time (Mollendorf *et al.,* 2004) but the source of improvement was still not established. Manufacturers claimed that the suit surface mimics that of sharks skin hence the frictional resistance is decreased but no evidence was provided to support the statement. It was a decade later when Oeffner and Lauder (2012) used a flapping foil robotic device to compare the self propelled swimming speed achieved when the surface of the device was covered by shark skin and by Speedo 'shark like skin' fabric. According to the results, the Speedo 'shark-like skin' fabric

did not improve the speed. The findings of the study suggest that other factors help swimmers improve performance and not the frictional drag reduction.

Even before the introduction of full body swimsuits, athletes used to shave their body in an attempt to decrease frictional drag. In two previous studies, Sharp and Costill (1989) and Sharp *et al.* (1988) found that shaved swimmers demonstrate less energy expenditure, greater velocity and greater distance per stroke. In both studies it was also found that shaved swimmers decelerate significantly less than when unshaved when they glide after a push from the wall indicating that passive drag has been decreased. However, the method of Sharp and Costill (1989) and Sharp *et al*. (1988) do not enable assessment of whether body hair removal actually reduces turbulence in the boundary layer and consequently it is unclear whether frictional drag or another type of resistance has been decreased.

2.2.2.1.2. Frictional resistance studies

Besides the aforementioned studies of Oeffner and Lauder (2012) that aimed to identify whether the Speedo suit surface mimics that of shark's skin and that of Sharp and Costill (1989) assessing the effect of skin shaving on swimming performance, friction drag was also investigated by Pendergast *et al*. (2006) from a theoretical perspective. He considered also the interaction between frictional and the other forms of drag. The investigators tried to reduce the effect of drag by introducing turbulators on the surface of the suit with the use of circular wires positioned around the circumference of the body. Total drag was decomposed theoretically to the frictional, pressure and wave component and even though total drag was significantly decreased, friction drag did not increase significantly. Moria *et al.* (2010), with the use of a wind tunnel, experimentally assessed the aerodynamics and the surface friction of two commercially available swimsuits (Speedo® LZR Racer and Speedo® Fast Skin-II) when covering a cylinder and found that there was no apparent variation in the drag coefficient computed. Furthermore there was no significant difference between the drag coefficient values computed with the Speedo® LZR Racer and the bare cylinder. The results of the study are

interesting for two reasons, first because polyurethane made suits (Speedo® LZR Racer) seem not to decrease further the frictional drag (when compared to the non-polyurethane suits) and second because the results indicate that the benefit when wearing full body swimsuits is potentially not linked to frictional drag. However, to come to a safe conclusion a similar study should be conducted in a flume and not in a wind tunnel in order to assess the effectiveness of the suits in the environment in which they are used.

2.2.2.2. Pressure resistance

Pressure resistance or form drag is caused by the boundary layer separation that results in differential pressure between the front and the rear of the swimmer's body or their limbs. As the swimmer moves through stationary water, the water is pushed to the sides of the body and follows its curvature. However, the flow does not remain attached to the skin for the whole length of the body and separates. The length between the front of the swimmer and the location where the separation point occurs is affected by the morphology of the swimmer, the gliding velocity, the frontal surface area and the density of the water. After the boundary layer has separated from the skin, it interacts with the outer flow and as a result the flow is forced to follow a circular motion along the body. The circular flow forms an area of low pressure at the rear of the swimmer called also the 'wake' causing differential pressure between the front and the rear of the swimmer. The wake becomes wider and its volume increases when the boundary layer separation occurs closer to the front of the body.

Pressure drag can be estimated according to Equation 2.4.

$$F_p = \frac{1}{2} \cdot C_p \cdot \rho \cdot A \cdot v^2 \qquad \text{Equation 2.4}$$

where C_P is the pressure drag coefficient, ρ is fluid density, A is the projected area to the flow and v is the velocity of the moving body.

According to the above equation pressure drag is highly related to velocity. As swimming velocity (v) increases, the boundary layer thickness is reduced and the point of separation occurs closer to the front of the body. Furthermore, pressure drag increases also when the frontal surface becomes greater, for example when the swimmer is not efficiently streamlined in relation to the gliding direction.

2.2.2.2.1. Decreasing pressure resistance

It has been shown that animals such as dolphins, that reach high velocities in the water, can maintain a fully attached turbulent boundary layer (Fish and Lauder, 2006). Experimentally it was found that a turbulent boundary layer delays the separation of the flow and consequently assists in maintaining the volume of the wake behind the gliding object, regardless of whether this is a dolphin or a human.

The size of the wake is directly related to drag and gliding performance. Hence, it is beneficial to a swimmer to maintain a turbulent and not separated boundary layer throughout the length of their body. The retarding effect of the turbulent flow within the boundary layer seems not to affect resistive forces as much as the early separation. To find solutions that would help swimmers decrease drag and improve performance sport scientists have induced turbulence in the boundary layer. Pendergast *et al*. (2006) added turbulators (wires wrapped around the circumference of the body) to the surface of a full body swimsuit and found that drag decreased by 13-16% when three turbulators were used. These research findings were used by TYR® to bring a revolutionary full body swimsuit to the market (in 2004) that could assist the swimmers to improve their performance. Similar attempts are popular for equipment used in other sports such as the dimples in the golf balls.

2.2.2.2.2. Pressure resistance studies

Besides the study conducted by Pendergast *et al*. (2006) aiming to decrease pressure drag by reducing the size of the wake, other studies focused on the effect of the frontal surface area and the anthropometric parameters of the body on pressure resistance. Vilas-Boas *et al*. (2010) assessed the difference in the cross sectional area

between the first and the second underwater gliding position of the breaststroke underwater phase and found that the area projected to the flow and the passive drag were significantly lower for the first gliding position. These findings agree with the findings of previous studies indicating that the passive drag is associated to the frontal surface area (Onoprienko, 1968). The effect of anthropometrical parameters to passive drag has been investigated by Lyttle *et al*. (2000) who found that the swimmer's height is associated negatively to passive drag. Furthermore, it was found that there was no difference in passive drag reported between the girls and the boys of the same age and similar heights. However, gender morphological characteristics are not evident at young ages and possibly the findings would differ if the participants were adult. Chatard *et al.* (1990), after towing 218 competitive swimmers, found that the surface area of the body is related to passive drag while the possible effect of the frontal surface area of the body was not considered. The effect of anthropometrical parameters on active drag has been also assessed but the difficulty to control a number of interfering variables (such as the swimming technique) when the participants are swimming affected the validity of the conducted studies and contradictory results were reported (Huijing *et al*., 1988 and Kolmogorov *et al.*, 1997). The effect of the size of the wake will be discussed in detail in section 2.2.3.

2.2.2.3. Wave resistance

Wave drag is caused by the formation of waves on the water surface. As the water is incompressible the fluid level rises when moving close to the surface and waves begin to form. Consecutively, the water level lowers in an attempt to get back to equilibrium as a result of the applied gravitational forces that in this case act as a restoring force. This way a series of waves are formed and via this mechanism energy is transferred from the swimmer to the water and consequently the gliding velocity of the swimmer decreases. Part of the swimmer's kinetic energy is lost in displacing water and consequently forming waves. The energy wasted to form these waves is proportional to the energy contained in the prime wave (Rumyantsev, 1982) while different approached have been applied to assess the magnitude of wave drag.

Wave resistance can be calculated according to the Equation 2.5.

$$F_w = \rho \cdot \left(\frac{A^2}{\lambda^2}\right) \cdot (V \cdot sina)^2 \cdot cosa \cdot \Delta t \qquad \text{Equation 2.5}$$

where ρ is water density, A is wave amplitude, λ is wave length, V is wave velocity and a is the angle between the direction of general centre of mass moment and the front of the prime wave (Rumyantsev, 1982).

When increasing speed, both the wave length and the wave amplitude increases. For competitive swimmers, maximum velocity corresponds to 'hull speed' (Kolmogorov and Duplishcheva, 1992) which occurs when the bow wave length becomes equal to water line length of the swimmer (swimmer's height). Any further increase in speed is inhibited since the swimmer is trapped in the interim space between crests of waves (Toussaint *et al.,* 2002). The relationship, between relative velocity and body height, that has been argued to be associated with wave drag, is defined by a dimensionless number called 'Froude number' determining the magnitude of resistance and can be calculated according to Equation 2.6(Newman, 1977).

$$F_r = \frac{v}{\sqrt{g \cdot L}} \qquad \text{Equation 2.6}$$

where v is swimming velocity, L is a swimmer's length and g is gravity acceleration ($9.81 ms^{-1}$).

For a value of F_r=0.42 the wavelength is equal to the swimmer's line length (height) and 'hull speed' is reached. Lower values of F_r are related to lower swimming velocity or greater swimmers length for a given speed.

2.2.2.3.1. Decreasing wave resistance

Similar to what has been found by Hertel (1966) for spindle shaped objects, wave drag for humans is also related to the gliding depth (Vennell *et al.*, 2006). Drag measurements on a towed mannequin demonstrated an increment of wave drag up to 2.4 times when tested on the surface compared to fully immersed condition. Furthermore, Lyttle *et al.* (1998) showed that the wave drag reported on surface would be negligible in underwater swimming, at 0.6m depth.

2.2.2.3.2. Wave resistance studies

Studies assessing the effect of wave resistance considered also the impact of anthropometrical parameters and the body shape. Lyttle *et al*. (1998) found that both the chest girth and the ponderal index (or slenderness index, $\text{ponderal index} = \frac{\text{mass}}{\text{height}^3}$) affect wave drag whereas Jiskoot and Maiello *et al*. (1998) measured the wave drag of a female swimmer when towed at different depths and found similar results to those reported for male swimmers (Lyttle *et al.*, 1998). The effect of the human shape on wave drag was analysed in depth by Pease and Vennell (2011) with a male and a female mannequin towed in a flume. It was found that the effect of waves on resistance was higher for the male mannequin when towed at the surface by 46.73% when the velocity was equal to 1.94 ms^{-1}.

2.2.3. Added mass

Added mass in swimming biomechanics is the mass of the water moving along with an accelerating or decelerating swimmer. The added mass added to the mass of the swimmer is called virtual mass.

Sources of added mass for an underwater gliding swimmer can be considered the mass of the water within the boundary layer that moves along with the swimmer as well as the mass of the water of the wake formed at the rear of the swimmer. To accurately assess the inertial characteristics of a swimmer, the virtual mass and not

just the body mass should be considered. The added mass can be calculated according to Equation 2.7 (Kirchhoff, 1998).

$$M_a = C_a \cdot V \cdot \rho \qquad \text{Equation 2.7}$$

where M_α is the added mass, C_α is the added mass coefficient, V is the body volume and ρ is the water density.

Eik *et al*. (2008), in an attempt to compute passive drag from gliding velocity decay data, considered also the effect of added mass and compared the findings to towing drag force data of the same swimmers. Even though there was a significant difference between the two sets of data, it was one of the first studies to consider added mass when assessing the gliding performance from kinematic data.

In an attempt to accurately assess the magnitude of added mass, Caspersen *et al*. (2010) employed the vertical oscillation test (where swimmers were attached to a vertical oscillating bar under water) and the oscillating frequency as well as the force resisting the oscillating movement (that is the hydrodynamic resistive force of the swimmer added by the mass of the swimmer and the mass of the equipment used) was measured with the use of a load cell attached to four springs and the vertical bar. The added mass was calculated according to Equation 2.8 and was found to be approximately equal to a quarter of the body mass. When the added mass values of the male and the female participants were compared, it was found that the added mass was significantly higher for the males, indicating that the body form plays a significant role in added mass.

$$M_a = \left(\frac{T^2 \kappa}{4\pi^2}\right) - M_t \qquad \text{Equation 2.8}$$

where T is the oscillating period, κ is the spring constant and M_t is the mass of the swimmer and the equipment.

2.3. Resistance measurement methods

Resistive forces act parallel to the flow direction and retard the forward motion. As it has been previously referred, when the swimmer is not active in attempting to produce propulsive movements, the resistive force experienced is termed 'passive' drag whereas the term 'active' drag refers to the resistive force acting on the swimmer when is actively propelling in the water (Wilson and Thorp, 2003).

2.3.1. Passive drag

Numerous studies have assessed the magnitude of the drag force when gliding in the streamline position for two reasons. First, because it has been found that the glide phase after starts and turns contribute significantly to the total event time (Chow *et al.*, 1984 and Vilas-Boas & Fernandes, 2003) and second because the passive glide allows a number of interfering variables, that are present when swimming, to be controlled. One example is the swimming technique that cannot be controlled.

2.3.1.1. Passive drag measurement methods

The passive drag assessment techniques involve towing swimmers in the streamline position, testing flume, kinematic analysis, inverse dynamics and CFD analysis.

2.3.1.1.1. Towing methods

Karpovich (1933) was the first to attempt a controlled assessment of passive drag. The experiments included passive towing in a pool with the use of an electric motor while recording the velocity of the swimmer. However, it was the velocity and not the drag that was measured during the testing and also the range of velocities analysed was limited (0.73 ms^{-1} to 1.18 ms^{-1}) and did not account for the velocity a swimmer glides after a start or turn that ranges between 2.5 ms^{-1} and 3.1 ms^{-1} for elite swimmers (Lyttle, 1999).

Alley (1952), assessed passive drag with the use of a platform suspended over the water for velocities between 0.34 $ms^{-1}$and 1.94 ms^{-1} the swimmers were towed

towards the platform and the drag force exerted by the swimmer's movement was measured. However, a swinging motion of the platform was reported.

Similarly, but with the use of equipment that did not swing, Counsilman (1955) assessed passive drag for different body orientations in relation to the flow (prone, side and two rolling orientations). All later studies employed equipment fixed on the pool side and the resistive forces were measured either with the use of a power meter, a dynamometer or a load cell (Hairabedian, 1964; Kent and Atla, 1971 and Chatard *et al*., 1990).

A different approach was employed by a number of other research groups (Sheehan and Laughrin, 1992 and Klauck, 1998) that used dropping weights to tow the swimmer while the resistance was computed from the velocity of the dropping weights.

Lyttle *et al*. (1999) and Benjanuvatra *et al*. (2001) employed a towing system that allowed the measurement of the resistive forces close to the swimmer with the use of a load cell. However, an object in front of the swimmer travelling at the same velocity is expected to affect the flow and decrease the accuracy of the measurement.

A number of research groups employed also a moving apparatus travelling with the swimmer either in a normal or an annular pool (Clarys *et al*. 1974; Van Manen and Rijken, 1975; Clarys, 1978; Clarys, 1979 and Mollendorf *et al*. 2004). Such systems allowed also the measurement of the drag forces when accelerating (Jiskoot and Clarys, 1975).

In all aforementioned towing studies it is expected to be difficult for the swimmer to maintain a streamlined position particularly when the velocity is low. Furthermore, changes in velocity with the moving apparatus are expected to affect the angle of attack of the swimmer.

2.3.1.1.2. Flume analysis

Testing in moving water channels (flumes) has been conducted to assess passive drag of both actual swimmer and mannequins (Miyashita and Tsunoda, 1978; Maiello *et al.*, 1998; Roberts *et al.*, 2003; Chatard and Wison, 2003; Vennell *et al.*, 2006 and Pease, 2009). The swimmer or the mannequin to be analysed is attached to a road and the drag is measured with the use of a load cell. Similarly to the towing studies, it is difficult for the swimmer to maintain a streamlined posture.

2.3.1.1.3. Kinematic analysis

Analysis of the kinematic data obtained from actual glides of unrestrained swimmers has been conducted by several researchers (Klauck and Daniel, 1976; Oppenheim, 1997; Eik *et al.*, 2008 and Naemi and Sanders, 2008).

The kinematic analysis to assess passive drag involves displacement calculation and drag assessment according to the Newton's second law of motion. Drag in this case is equal to the deceleration by the virtual mass of the swimmer (virtual mass = mass of the swimmer + added mass). However, not all studies have considered the added mass when assessing the gliding performance with the use of the kinematic analysis.

Neither Klauck and Daniel (1976) nor Oppenheim (1997) considered the added mass effect. All calculations were conducted assuming that the virtual mass is equal to the mass of the swimmer.

Eik *et al*. (2008), in an attempt to assess the accuracy of the kinematic analysis when taking into account the added mass effect, computed the drag coefficient when gliding underwater and compared the findings to towing results. A significant difference between the findings was reported, possibly due to the selection of non experienced swimmers to participate to the study and due to the low water temperatures during the testing session that prevented the participants from practising in advance.

Naemi and Sanders (2008) recently presented the Hydro-Kinematic method, a new approach with which the glide efficiency can be assessed from kinematic data. With the Hydro-Kinematic method, the displacement Equation 2.9 is fitted to the displacement-time kinematic data and from the curve with the best fit the glide factor (C_G), that is a measure of the glide efficiency, is calculated.

$$x = C_G \cdot ln\left[\frac{U_{x0}}{C_G} \cdot t + 1\right]$$ Equation 2.9

where C_G is the glide factor and U_{xo} is the initial velocity.

The method considers the effect of the added mass and additionally it is possible to compare the glide efficiency results between different velocities.

2.3.1.1.4. Other methods

Recently, computational fluid dynamics (CFD) has been conducted to assess passive drag (Bixler *et al.*, 2007; Marinho *et al.*, 2009 and Zaidi *et al.*, 2010). The methodologies employed are detailed in section 2.5.6.1.

2.3.2. Active drag

When the flow around a swimmer's body is disturbed by the limb movements, the reported resistive forces increase (Kolmogorov and Duplisheva, 1992). Kolmogorov and Duplisheva (1992) found that the active drag was 62% to 162% greater than the passive drag when male front crawl swimmers were examined.

Researchers estimated the active drag of swimmers during freestyle (di Prampero *et al.*, 1974; Holmer, 1974; Clarys, 1974; Rennie, 1975; Schleihauf *et al.*, 1983; Hollander *et al.*, 1986; Ungerechts and Niklas, 1994; Nomura *et al.*, 1994; Takagi *et al.*, 1999 and Wang Xin-Feng, 2006). However, even some of these studies may be applicable to other strokes, this has never been attempted and comparative results have not been reported.

2.3.2.1. Active drag measurement methods

There are two main approaches used to measure active drag. The direct methods based on force measurement techniques and the indirect methods based on oxygen consumption extrapolation techniques.

2.3.2.1.1. Direct methods

A direct active drag assessment method was applied for the first time by Hollander *et al.* (1986) who developed the 'Measurement of Active Drag' (MAD) system. With the MAD system the swimmer accelerates by pushing against fixed pads positioned below the water surface while both the force applied by the hands to the system as well as the energy consumed during the experiment is measured. The results are compared with the energy consumed during free swimming when the hand pushing force contributes both to thrust and to wake kinetic energy (in comparison with the MAD system where the total force contributes to propulsion). By the application of this method only propulsion coming from the upper part of the body is investigated, as the legs are supported and fixed together by a small buoy.

Another indirect method assessing active drag was employed by Kolmogorov and Duplischeva (1992). With this method, the participants swim with and without towing a hydrodynamic body creating known additional drag and the maximum swimming velocity is recorded. The active drag calculations rely on the assumption that the power output in the two conditions assessed is equal and that any difference is duo to the effect of the towed body. However, it is expected to be difficult to the swimmer to repeat the same swimming technique with and without the towed body.

2.3.2.1.2. Indirect methods

Di Prampero *et al.* (1974) measured oxygen consumption during submaximal swimming at constant speed while different known weights (forces), acting horizontally, were attached to the subjects by means of a rope and a safety belt. During the experiment, air samples were collected and oxygen consumption and energy expenditure were estimated. The comparison of the oxygen consumption

between the different conditions and free swimming was related with the extra drag in order to extrapolate resistance during free swimming and the subject's mechanical efficiency. According to the findings of the study, the drag when the participants are actively swimming is double that for passive towing (Di Prampero *et al.* 1974).

2.3.2.1.3. Other methods

Computational fluid dynamics is a third approach assessing active drag when swimming that will be discussed in detail in section 2.5.6.2.

2.4. Body Scanning

The assessment of size and shape of the human body until 1989 was conducted primarily with the use of standard anthropometric tools (such as the anthropometer, the spreading calliper, the sliding compass and the measuring tape). In 1989, as reported by D'Apuzzo (2009) the first full body scanner (the Loughborough Anthropometric Shadow Scanner) was developed at the Loughborough University in order to conduct anthropometric studies for the textile manufacturing industry (Jones *et al.*, 1989). Big scale projects such as the Civilian American and European Surface Anthropometry Resource project (with five thousand participants) were conducted with the use of full body scanners (Robinette, 1999).

The current application of 3D body scanning technology involves studies for the apparel industry, ergonomics, biomedical applications and reverse engineering. 3D body scans are used to design clothing using 3D human models as a guide (Wibowo *et al.*, 2012) while databases are created to recalibrate the size of the army uniforms. The ergonomy of new vehicles is evaluated with the use of human 3D models (Gunther, 2012) and 3D scans have been used to assess asymmetry and body composition (Ryder and Ball, 2012). 3D models are also combined with motion capture data for the movie industry in order to animate 'human like' models. Additionally, accurate modelling of the human form allows the use of 3D body scans for sports analysis. 3D models can be used to simulate the flow around an athlete in

sports in which the fluid resistance significantly affects performance. So far, body scans of swimmers, cyclists and bobsleigh athletes have been analysed (Dabnichki and Avital, 2006; Bixler *et al.*, 2007and Defraeye *et al*. (2010).

Currently there are three different types of scanners are available to generate the 3D model of a person. These are, laser, Light Emitting Diodes (LED), and the white-light scanners. Given that scanners differ in terms of resolution, the selection of the optimum type to be used depends on the level of accuracy required, the scanning range, the scanner portability and also the time required to perform a full scan.

For sports analysis in general and for swimming analysis in particular, it is important to capture the details of the body form with the 3D scan. Furthermore, it is desired to scan the full body of the athlete at one time, on site and as quickly as possible. However, none of the available products on the market combines all the desired characteristics.

2.4.1. Laser body scanners

Laser body scanners comprise a low energy laser and high speed digital cameras positioned on four vertical columns at the four corners of a square calibrated area that comprise the scanning field. The laser body scanners are heavy, require calibration and as such are not considered portable.

During the scanning process a laser stripe is deflected by a mirror or a prism and projected on the surface of the person positioned in the middle of the calibrated area. The person's surface is reflecting the beam back and this reflection is detected by the digital cameras. Discrete points are recorded on the surface of the scanned person and through this process three dimensional coordinates of the scanned points are acquired and a cloud of points is created. The majority of the laser body scanners perform the scanning process within 10-15 s.

2.4.2. LED body scanners

The LED body scanner operates similarly to the laser body scanner. However, instead of high speed digital cameras, position sensitive detector sensors are used to detect near infrared LED pulses. The accuracy of the laser and the LED scanners is comparable although the LED scanners are affected by the light and are operated in dark rooms (Hwang, 2001). Norton *et al.* (2002) compared the volume of the lower limbs of a number of participants obtained by 3D LED scanning (Hamamatsu, Photonics) and water displacement. A 0.6% difference between the two approaches was found.

2.4.3. White-light body scanners

The white-light scanners employ the shadow moiré fringe technique (a triangulation method) to generate 3D models of humans. A white light source is used to project multiple contour patterns on the surface of the participant from different angles while cameras record the deformed grating that describes the surface morphology. Recording from multiple cameras are combined as shown in Figure 2.2.

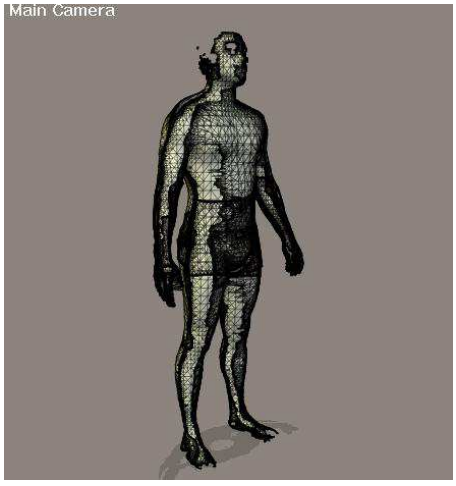

Figure 2.2 White-light scanner output

2.4.4. Other methods to generate 3D models of swimmers

Besides the laser and the white-light body scanning technology developed to be used exclusively for humans when standing, other 'indirect' approaches can also be employed to scan swimmers. However, in all other cases the level of accuracy is lower either because of technological (methodologies have not been advanced yet) or ergonomical (the participants need to remain for a long period of time stationary or in a recumbent posture) restrictions. These approached include CT (computerised tomography) and MRI (magnetic resonance imaging) scanners, hand held laser scanners, still photographs and motion sensors (such as the Microsoft Kinect).

CT and MRI scans have been used widely either separately or complementarily to produce 3D models of soft tissues and organs (Lee *et al*., 2008). The same devices have been used to generate models of the body surface. A CT scanner was employed by Marinho *et al.* (2010) to create a 3D model of a swimmer's hand. However, considering that during the scanning process the participant was in contact with the bed surface and that the outer layer of the body was deformed, the morph created would not be an accurate representation of the body shape. Another negative aspect of the CT scans is the high radiation exposure for both the participant and the investigator (Nickoloff and Alderson, 2001).

Hand held laser scanners have been designed to scan static objects and usually require longer times to complete the process. With the use of tracking devices (displacement censors, strain gauges or accelerometers) the position of the scanner in spaces (when used by the investigator) is defined and with similar triangulation mechanisms to the 3D laser body scanners, the final model is formed. Hand held laser scanners have been used to scan the body form of swimmer (Zaidi *et al*., 2010 and Popa *et al*., 2011). However, the accuracy of such devices is expected to be limited as it is not easy for the swimmers to stay in the streamlined position for long periods without any movement.

Still photographs have been used to assess the body volume of swimmer with the Ezone method (Deffeyes and Sanders, 2005) while the accuracy of the approach has been assessed (Machtsiras and Sanders, 2012) and a 3.1% difference was reported when the volume of the whole body was measured. However, besides the high accuracy values reported when the body volume was assessed, the body form is not captured. Advanced methodologies employing multiple photographs to generate 3D models (Autodesk, 123D) appear to capture also the body form but the accuracy of the method has not been assessed.

The Microsoft Kinect motion sensor (Microsoft Corporation, One Microsoft Way, Redmond WA, 2010) combines visual information from a 'red, green and blue'(RGB) camera, an infrared projector and an infrared sensor. The device implements the active triangulation principle in order to estimate the scene's depth with the use of the infrared apparatus (Dal Mutto *et al*., 2012). This function allows image-based 3D reconstruction and recently the device was used to scan humans and measure their size (Cook *et al.*, 2012). CAD software manufacturing companies (such as Geomagics) have recently presented Kinect data input capabilities for their packages with the ultimate aim being to use the Kinect device as a 3D capturing tool. However, the accuracy of the method has not been assessed yet.

2.5. CFD analysis

Computational fluid dynamics, a methodology used to simulate the fluid flow by solving the discretized form of the 3D Navier-Stokes equations was originally introduced to numerically calculate the flow around blunt bodies at supersonic speed (Moretti and Abett, 1966).

The ability of the method to predict accurately the fluid flow without the manipulation of huge and expensive constructions (such as wind tunnels and flumes) as well as the applicability of the method in a wide range of application areas (such as aerospace) accelerated its development.

CFD analysis, relying on the manipulation of thousands of calculations has not been widely applied before the early 1980's when the computing speed was still limited. Not surprisingly, the rapid increase in development and implementation of CFD analysis coincided with the advent of digital computers and correlated with the rapid increase in speed of supercomputers. Nowadays, CFD is widely used as a substantial research tool in physical sciences and sports either to enhance the understanding of physical phenomena (non industrial applications) or to support the optimization of equipment design (industrial applications).

2.5.1. CFD, the method

Besides the experimental approaches used to analyse the fluid phenomena, fluid flow problems can be also expressed in a way that can be resolved with the use of computers. This can be achieved by replacing the partial differential equations describing the physical phenomena with a system of algebraic equations, through the discretization process. Figure 2.3 illustrates the CFD analysis process.

Prerequisite for a CFD analysis is a 3D model of the object or person of interest to be analysed and also a software to run the CFD analysis (the types of which are detailed in section 2.5.4).

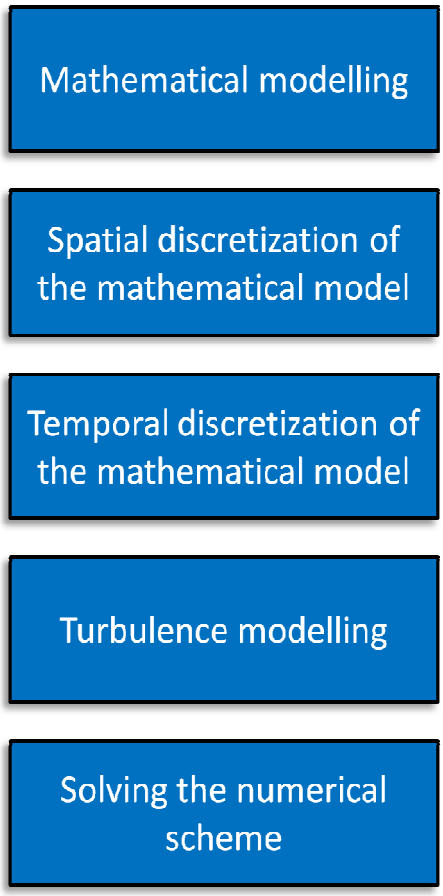

Figure 2.3 The CFD analysis process.

The accuracy of the analysis depends both on the resolution of the 3D model to be employed but also on the selection of the different parameters for each one of the first three stages of the analysis process presented in Figure 2.3. Consequently not all fluid flows can be resolved by the same mathematical model, contrarily a particular set of mathematical equations need to be selected and a particular discretization model needs to be applied according to the nature of the flow to be analysed. The most appropriate numerical grid type (spatial discretization) and turbulence model (turbulence modelling) need to be selected according to the requirements of the analysis to be conducted.

2.5.1.1. Mathematical modelling

Up to the early 1800's fluid dynamics theory was based on Euler's equations ignoring the effect of viscosity. Euler derived the continuity and momentum equation in 1753 while the same set of equation is used even today for inviscid flows. It was several years later when two researchers independently extended Euler's equations to include the effect of viscosity. In 1822 Claude Louis Marie Henri Navier in France and in 1845 George Gabriel Stoke in England, derived the governing equation of a viscous fluid. With the exception of the energy equation, the form of equations that Stoke described remained unchanged until today. The equations described are the so called Navier-Stokes equations named after the two researchers. The Navier-Stokes equations for the conservation of momentum for a viscous flow have been (terminologically) expanded and involve the entire system of flow equations for viscous flows, often reported as complete Navier-Stokes equations.

CFD is based on the fundamental physical principles of fluid dynamics. That is, the Navier-Stokes equations which comprise the conservation of mass, the conservation of momentum and the conservation of energy. Equations 2.9 and 2.10 illustrate the Cartesian form of the mass conservation and the momentum conservation equation respectively. The energy equation will not be presented as heat transfer was not considered in the analysis.

$$\frac{\partial \rho}{\partial t} + \frac{\partial (\rho u_i)}{\partial x_i} = 0 \qquad \text{Equation 2.9}$$

where ρ is the density, xi (i=1,2,3) or (x, y, z) are the Cartesian coordinates and u_i or (u_x, u_y, u_z) are the Cartesian components of the velocity vector **u**.

$$\frac{\partial(\rho u_i)}{\partial t} + \frac{\partial(\rho u_j u_i)}{\partial x_j} = \frac{\partial \tau_{ij}}{\partial x_j} - \frac{\partial p}{\partial x_i} + \rho g_i \qquad \text{Equation 2.10}$$

where g_i is the component of gravitational acceleration $\boldsymbol{g}$ in the direction of the Cartesian coordinate x_i, r is the position vector ($\boldsymbol{r} = x_i \boldsymbol{i}_i$) and τ is the strain rate tensor defined according to Equation 2.11.

$$\bar{\tau}_{ij} = \mu \left(\frac{\partial \bar{u}_i}{\partial x_j} + \frac{\partial \bar{u}_j}{\partial x_i} \right) \qquad \text{Equation 2.11}$$

2.5.1.2. Discretization of the mathematical model

A number of different types of numerical methods have been developed to replace the partial differential equations describing the physical phenomena by a system of algebraic equations. The most prevalent are the Finite Difference Method (FDM), the Finite Volume Method (FVM) and the Finite Element Method (FEM).

With the Finite difference method the partial differential equations are replaced by a system of algebraic difference quotients for two or more of the discrete grid points. The finite difference grid is, in most of the cases, structured (Figure 2.4 and 2.5) with each grid point regularly spaced as it is necessary for optimal convergence with FDM. Limitation to simulate flows around complex geometries led to the development of the finite volume method. The FDM can be categorized according to the grid structure (to structured or unstructured that is detailed in section 2.5.1.3) or according to the difference formulas used (forward, backward, centered) indicating the order of differencing (Equations 2.12, 2.13 and 2.14).

$$f'(x_i) = \frac{f(x_{i+1}) - f(x_i)}{h}$$ Equation 2.12

$$f'(x_i) = \frac{f(x_i) - f(x_{i-1})}{h}$$ Equation 2.13

$$f'(x_i) = \frac{f(x_{i+1}) - f(x_{i-1})}{2h}$$ Equation 2.14

where x is a function and h is the spacing between the grid points x, x_{i-1} and x_{i+1} respectively (as it is considered that $x-x_{i-1}= x_{i+1}-x$).

With the Finite volume method the discretization equations are derived by integrating the governing differential equations over a small region called the finite volume or the control volume. Each control volume is associated with a discrete point at which the dependent variable such as the velocity pressure and temperature are to be calculated. Such points are referred as grid points.

With the Finite element method the discretization equations divide the domain into unstructured finite elements in a manner similar to the finite volume method but with significantly greater numerical effort involved, thereby limiting its use (Blazek, 2001).

2.5.1.3. Discretization of the space domain

The computational domain, the boundaries and the geometries within the domain should be represented in a way that can be processed by the computer.

In CFD, the domain is split into smaller sub-domains using a grid. Each flow variable is defined at the grid points while the values at other locations are determined by interpolating the values at the grid points. The accuracy in this case depends on the number of cells in the grid. The points are placed either in a

structured or unstructured manner to split the domain spatially and form a structured or unstructured grid. The solution is also discretized temporarily by carrying out the calculations in discrete intervals to simulate the passage of time.

The structured grid is similar to a Cartesian grid and is formed of lines that do not cross each other as shown in Figures 2.4 and 2.5. The grid points are identified by three indices (*i, j, k*) one for each direction. Structured grids are used with the finite difference method.

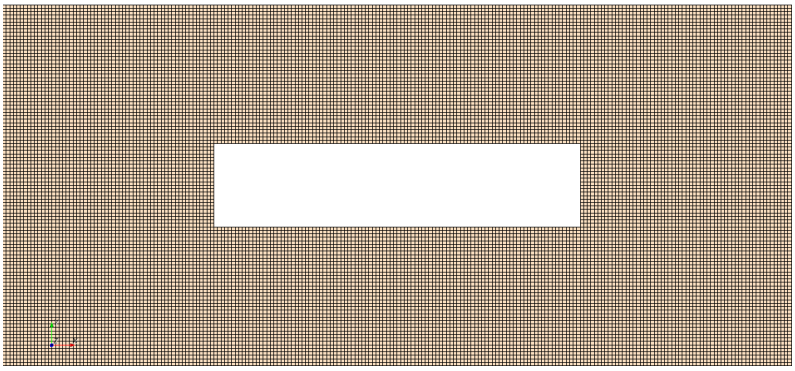

Figure 2.4 Structured grid around a rectangular object.

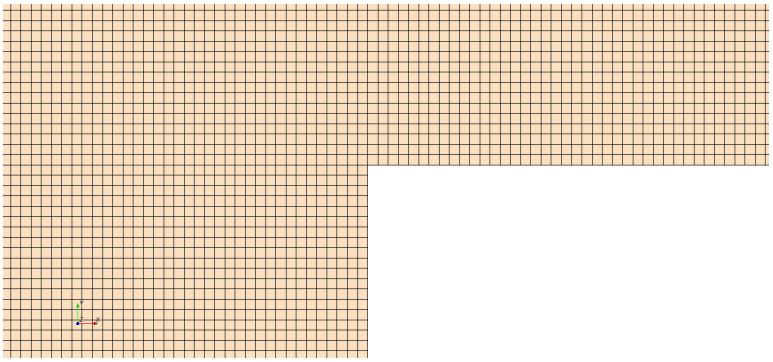

Figure 2.5 Structured grid around a rectangular object (close view).

In cases where complex geometries need to be analysed, a structured grid cannot be used. Then, an unstructured grid (similar to that seen in Figures 7.4 and 7.5) that can fit in complex domains can be employed. Unstructured grids are usually used with the finite volume and finite element method.

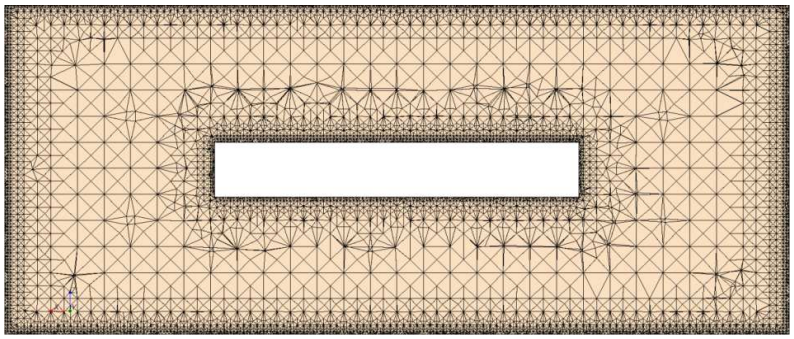

Figure 2.6 Unstructured grid around a rectangular object.

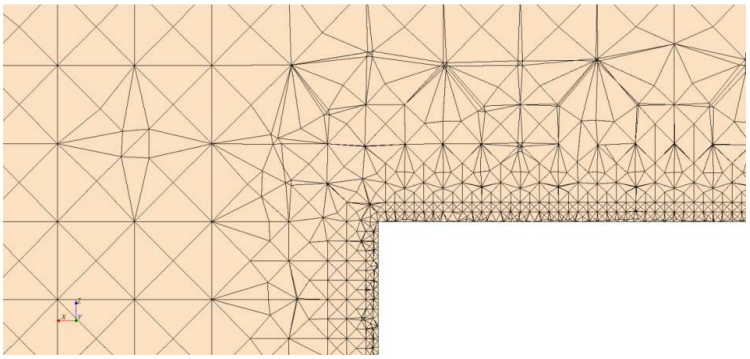

Figure 2.7 Unstructured grid around a rectangular object (close view).

2.5.1.4. Temporal discretization schemes

Besides space (spatial discretization), time (temporal discretization) should also be discretized when unsteady flows are considered for analysis. Temporal discretization involves splitting the simulation into discrete points in time with the use of a temporal discretization scheme.

The temporal discretization schemes can be either explicit or implicit and are chosen according to their stability, accuracy and computational cost. The accuracy of the temporal discretization can be determined from the truncation error that is aproduct of the time step restriction and the computational cost imposed by the scheme selected.

The two schemes (explicit and implicit) differ in terms of the information used to compute the scalar quantities at the time level n+1. The explicit treatment is using

information from the initial point (Equation 2.15) whereas the implicit treatment is using the final point (n+1, Equation 2.16).

$$\frac{\phi^{n+1} - \varphi^{n}}{\Delta t} = f(\varphi^{n}) \qquad \text{Equation 2.15}$$

where ϕ is a scalar quantity known at the time level n, f is the function incorporating the spatial discretization, n is the current time level, n+1 is the next time level and Δt is the time step size.

$$\frac{\phi^{n+1} - \varphi^{n}}{\Delta t} = f(\varphi^{n+1}) \qquad \text{Equation 2.16}$$

2.5.1.5. Turbulence models

The numerical solution of turbulent flows is extremely difficult due to the infinite number of scales that need to be resolved and the extremely dense grid required (with a number of cells proportional to Re^3). Therefore, a number of techniques have been suggested to simplify the process and either entirely model or partially model and partially resolve turbulence.

2.5.1.5.1. Reynolds-Averaged Navier-Stokes equations

The Reynolds-Averaged Navier-Stokes (RANS) equations are time averaged equations. The RANS equations model the detail of turbulent flows and provide only information about the averaged properties of the flow (mean velocity, mean pressure and mean stresses) and the effect of turbulence on the mean properties of the flow. To consider the effect of turbulence, it is necessary to employ one of the available turbulence models to predict the Reynolds stresses, the scalar transport terms and close the system of men flow equations. The turbulence models are classified to the one equation models and the two equations models according to the additional

equations required to be solved along with the RANS equations. The two equations models, such as the k-ε and k-ω are the most widely used.

2.5.1.5.2. Large Eddy Simulation

With the Large Eddy Simulation (LES) the behaviour of the large eddies is tracked while the small scales of the motion are modelled. Space filtering of the unsteady Navier-Stokes equations prior to the computations accepts the large eddies and rejects the small eddies. The effect of the small unresolved eddies are considered with the use of a sub grid scale model. Unsteady flow equations are resolved. With this technique CFD can be applied to complex geometries.

2.5.1.5.3. Direct Numerical Simulation

With the Direct Numerical Simulation that was employed for the first time in the beginning of the 70s (Orszag and Patterson, 1972) the mean flow and all turbulence fluctuations are computed rather than modelled as is the case with the RANS closure and also all scales of the motion are captured without the need of a sub grid scale model as is the case with the LES approach (Figure 2.8). Unsteady Navier-Stokes equations are solved on spatial grids that are sufficiently fine that they can resolve the Kolmogorov length scale at which energy dissipation takes place and with time step sufficiently small to resolve the fluctuations of the fastest fluctuations. The DNS method is highly computationally expensive and the maximum Reynolds number with which it can be used is limited (Coleman and Sandberg, 2010).

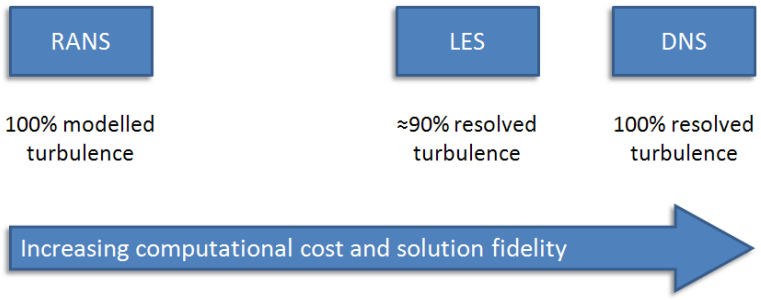

Figure 2.8 The relationship between the models used to simulate fluid flow and the computational cost and solution fidelity (adopted by Mockett *et al.*, 2011).

2.5.4. CFD Software

Technological institutes and universities often develop their own CFD code to meet their particular needs, such as Mittal *et al*. (2008) that developed a sharp interface immersed boundary method for incompressible flows with complex boundaries to simulate, amongst others, the butterfly kick (von Loebbecke *et al*., 2009). However, this is not common due to 1) the high cost and time involved to design such a code 2) the expertise required and 3) the regular upgrades needed. As a result the majority of simulations in a variety of disciplines rely on commercial packages. A number of CFD software packages (e.g. Fluent, CFX, STAR- CCM+) are available on the market differing either in price, reliability, applicability (not all packages are used in all industries), user friendliness (some packages often lack essential Graphic User Interface capabilities) and compatibility (ability to be used in combination with other CAD packages). The Fluent, the CFX and the STAR-CCM+ are amongst the most popular commercial packages used by educational institutions and the industry. Open source CFD code is also available (e.g. Open FOAM).

2.5.5. CFD in Sports

Formula 1 was the first industry to apply CFD analysis due to the high importance of aerodynamics in performance. CFD analysis in sport also involves soccer ball aerodynamics analysis, drafting in cycling investigation, sailing boat optimization,

oar blade design, aerodynamic behaviour assessment of ski jumpers and estimation of drag of golf balls.

Defraeye *et al*. (2010) used CFD to evaluate three different cycling positions (the upright, dropped and time-trial position). The athlete was positioned with his bicycle in a wind tunnel and drag forces were computed. A 7% difference between the experimental and CFD forces was reported indicating the level of accuracy that can be accomplished when simulating the flow around cyclists.

2.5.6. CFD in swimming

In swimming, CFD analysis was originally applied by Bixler and Schloder (1996) to evaluate the effects of accelerating a 2D flat circular plate through the water and his results suggested that 3D analysis could provide useful information. However, from 1996 up to now, only a small number of studies in swimming biomechanics employed these methods due to the difficulties in obtaining accurate 3D geometries and the high demand in processing power required to analyse the data. In 2002 Bixler and Riewald analysed a 3D swimmer's hand in steady flow conditions and three years later Rouboa *et al*. (2005) tested the effect of swimmer's hand acceleration on propulsive forces generation. It was not until 2007 that Bixler *et al*. (2007) tested a full body swimmer with CFD. From this short review we can conclude that CFD is a rather complicated methodology nevertheless with high potential.

2.5.6.1. Passive drag assessment with the use of CFD

Most of the studies that have been conducted so far to assess the swimming performance involved a steady state analysis of the whole body or sections of it. The inlet velocity was steady in these cases. There have been only a couple of studies in which transient analysis was employed (Table 2.1).

2D analyses have also been conducted with questionable accuracy as a complex three dimensional flow was approximated with a two dimensional simulation.

Table 2.1 Passive drag assessment studies with the use of computational fluid dynamics.

Author	2D/3D	Turbulence model	Type
Bixler and Schloder (1996)	2D	standard k-ε& RNG & RMS	steady state
Bixler and Riewald (2002)	3D	standard k-ε	transient
Gardano and Dabnichki (2006)	3D	N/A	steady state
Rouboa *et al*. (2006)	2D	standard k-ε	transient
Bixler *et al*. (2007)	3D	standard k-ε	steady state
Zaidi *et al*. (2008)	2D	standard k-ε	steady state
Zaidi *et al*. (2010)	3D	standard k-ε& standard k-ω	steady state
Minetti *et al*. (2009)	3D	SST	steady state
Bixler *et al*. (2007)	3D	standard k-ε	steady state
Marinho *et al*. (2009)	3D	standard k-ε	steady state
Zaidi *et al*. (2010)	3D	standard k-ε standard k-ω	steady state

where RNG is the Renormalized Group turbulence model, RSM is the Reynolds Stress model and SST is the Shear Stress Turbulence model.

2.5.6.2. Active drag assessment with the use of CFD

CFD has been also applied to analyse active drag. Table 2.2 presents the studies aiming to compute drag force when the swimmer was actively moving either on the surface or underwater. However, none of these studies has been validated against experimental findings.

Table 2.2 Active drag assessment studies with the use of computational fluid dynamics.

Author	2D/3D	Turbulence model	Type
Lecrivain *et al*. (2008)	3D	N/A	transient
von Loebbeke *et al*. (2009)	3D	IBM	transient
Keys (2010)	3D	realisable k-ε	transient

where IBM is the Immersed Boundary method.

3D motion capture techniques have been combined with CFD analysis to compute active drag when swimming (Lecrivain *et al.*, 2008; von Loebbeke *et al.*, 2009 and Keys, 2010). The accuracy of the final drag findings depend both on the methods employed to calculate the 3D locations of the tracked markers and also on the computational approach followed.

The 3D data used by Lecrivian *et al*. (2008) were collected at the University of Edinburgh and the methodologies and the equipment used were previously assessed and shown to produce data with RMS error equal to 0.05% for the X axis, 0.2% for the Y axis and 0.3% for the Z axis (Machtsiras and Sanders, 2009). Besides the precise 3D data, the human body form considered for the analysis was not scanned with a 3D body scanner and the numerical approach modelled and did not resolve the effect of turbulence. As a result, the accuracy of the analysis can be considered limited.

Von Loebbeke *et al.* (2009) used 2D data to animate a swimmer performing the butterfly kick underwater. The data were collected from a single camera while the two dimensional space was calibrated with the use of the known height of the swimmer when posing in the streamline position. The calculation of the displacement and the joint angles according to a reference frame comprised of only two known locations did not consider the effect of distortion. Additionally, the error is expected

to be further increased because the vertical axis was not calibrated. Considering also the case that the swimmer is not gliding perpendicular to the recording axis of the camera, the approach followed is expected to affect the accuracy of the findings. In this case the swimmer was scanned with a 3D body scanner and the simulation was conducted with the use of an in-house finite difference based immersed boundary method that was previously found to accurately simulate the flow past suddenly accelerated bodies (Mittal *et al*., 2007).

Keys (2010) used a 3D kinematic data collection setup similar to that of the University of Edinburgh but the accuracy of the system has not been reported. The swimmer was scanned with a 3D body scanner and produced an accurate geometry of the body form. However, the use of the realisable k-ε turbulence model for the fluid flow simulation introduced a source of error when calculating the active drag results.

2.6. Anthropometry

2.6.1. Measurement approaches

When the relationship between the passive drag and anthropometric characteristics of the swimmer is investigated, the accuracy of both methods should be considered and assessed.

Anthropometrical characteristics can be assessed either directly with the use of the standard anthropometrical tools or indirectly with the use of 2D images or 3D body scans. In an attempt to assess the accuracy of direct and indirect anthropometric measurement techniques, Taiar and Lodini (2005) compared frontal surface area measurement results computed with a direct (physical measurement when the swimmers were standing on pool side), a static (numerical measurement of still images of swimmers standing on poolside) and a dynamic approach (numerical measurement of still images of swimmers gliding underwater). The results suggested that the dynamic and the static approach were more repeatable than the direct.

Moreover, the difference in the computed values, expressed as percent discrepancy, was less than 0.5% between the direct and the static approach and less than 1% between the direct and the dynamic approach.

The frontal surface area calculation in this study was based on approximations taking into account lengths and widths of sections of the body. However considering that the transverse plane was not framed with the dynamic approach, it is expected that the error would be less if a third camera positioned either below or above the gliding path would be employed.

2.6.2. Anthropometric measurement techniques

Different approaches have been suggested for the measurement of anthropometric parameters of swimmers. Physical measurement of the participants in field has been encouraged by some research groups whereas others groups chose to collect visual data with the use of respective software and perform the analysis at a different time. A third approach is the detailed analysis of swimmer's 3D scanned model that has not been widely used yet.

2.6.3. Frontal surface area calculation

The significant effect of the angle of attack on resistive forces was identified many years ago. Onoprienko (1968) suggested that an increase from zero to five degrees in the angle of attack (that is the angle between the swimmer's body and the travelling direction) when actively swimming would raise the hydrodynamic resistance by 15%.

A number of different approaches employing approximation equations based on anthropometrical characteristics (such as the height of the swimmer) have been suggested for the calculation of the frontal surface area when gliding underwater (Clarys, 1979, Mollendorf *et al.*, 2004 and Vilas-Boas *et al.*, 2010). Nevertheless, more advanced methods employing digitization of the swimmers' outline when in the water have been applied by other research groups investigating the changes in the

frontal surface area when the athletes were actively swimming (Kolmogorov & Duplishcheva, 1992; Cappaert *et al.*, 1997 and Cappaert and Gordon, 1998). A third case that the frontal surface area was also considered was for the investigating of the added mass effect of swimmers (Caspersen *et al.*, 2010).

For the majority of the studies that explored the relationship between the resistive forces and the maximum frontal area, the anthropometric parameters were measured through planimetry (a method used to measure areas from two dimensional figures) when the participants were standing on land in the streamlined position (Clarys, 1979; Chatard *et al.*, 1990; Lyttle *et al.*, 1998; Benjanuvatra *et al.*, 2001; Caspersen *et al.*, 2010 and Vilas Boas *et al.*, 2010). In that case the outline of swimmer's trunk was digitized from scaled photographs to measure the maximum frontal area.

However, there are several limitations undermining the followed approach. The posture adopted when taking the picture cannot be considered similar to that when gliding in the water unless the joint angles and the angle of attack of the body are the same. Even minor discrepancies in these values would result in errors relative to actual frontal surface area when gliding. Moreover, the maximum cross-sectional area of the thorax does not account for the maximum frontal surface area exposed to the flow when the angle of attack is other than zero (Onoprienko, 1968). For this reason any other part of the body exposed to the flow should be included in the calculation. These comments support the idea that improved approaches are required that can improve the estimates of the frontal surface area in actual glides.

Mollendorf *et al.* (2004) considered the effect of the angle of attack in the frontal surface area and suggested an equation that could predict the difference in the estimated and actual values. However, no details were provided as to how the frontal area and the body surface area were originally computed or how the equation (Equation 2.17) has been validated.

$$A_f(\theta) = (A_{f0}) \cdot cos\theta + \left(\frac{A_s}{2}\right) \cdot sin\theta \qquad \text{Equation 2.17}$$

where $A_f(\theta)$ is the frontal surface area, A_{f0} is the frontal surface area when the swimmer is horizontal, and A_s is the body surface area.

When Zamparo *et al.* (2009) applied the same methods to compute the frontal surface area under different angles of attack, the body surface area was calculated according to Equation 2.18 proposed by Shuter and Aslani (2000) and the frontal surface area was calculated according to Equation 2.19 proposed by Clarys (1979). The Zamparo *et al.* (2009) calculations taking into account the angle of attack could be considered an upgraded approach to any previous method used but still relying on the Mollendorf *et al*. (2004) non validated equation.

$$BSA = BM^{0.411} \cdot BH^{0.655} \cdot 0.00949 \qquad \text{Equation 2.18}$$

where BSA is the body surface area, BM is the body mass and BH the body height.

$$MCDS = (6.9256 \cdot BM) + (3.5043 \cdot BH) - 377.156 \qquad \text{Equation 2.19}$$

where BM is the body mass and BH the body height.

Clarys (1979) photographed the participants of his study and planimetered the images to calculate the maximum cross-sectional diameter (MCSD) of the body. However, the shape of swimmers body is not cylindrical and the calculation of the diameter cannot be considered as an accurate approach to compute the frontal surface area. From his findings he concluded that the best predictors of the maximum cross-sectional diameter are the body height and body mass.

Lyttle *et al.* (1998) and Benjanuvatra *et al.* (2001) computed swimmer's cross sectional area according to Bloomfield *et al.* (1994). The girth was measured with a tape around the participant's chest.

Vilas Boas *et al.* (2010) developed a MATLAB routine to digitise the perimeter of the swimmer's body at the level of the maximum body cross-sectional area. Photographs were taken from above (transverse plane) and triangles were formed by linking the first with every following two digitised points. The total area taken by all triangles was summed to compute the body cross-sectional area. Even though this method takes into account that the shape of the frontal surface area is not cylindrical, the data is collected on poolside meaning that the swimmer's posture (joint angles) is not the same with the gliding posture and also that the effect of the angle of attack is not considered.

The same method of calculating the frontal surface area has been applied also by Caspersen *et al.* (2010) to evaluate the added mass effect in human swimmers. However, in his case the participants were vertically oscillating when attached to a bar, reassuring constant angle of attack during the movement. Therefore, the researchers correctly assumed that the frontal surface area is equal to the maximum cross-sectional area.

Consequently, even though planimetry is an easy way of computing the frontal surface area, there is some error when it is applied to studies that involve passive glide testing where the swimmers are not attached to any device and the angle of attack is changing. Furthermore, the joint angles when taking the pictures should be defined and be equal to the joint angles when gliding.

Kolmogorov and Duplishcheva (1992) approximated the frontal surface area according to Equation 2.20.

$$FSA = BV^{2/3}$$ Equation 2.20

where BV is the body volume.

Cappaert and Gordon (1998) who measured the frontal surface area when the participants were actively swimming placed an underwater camera at the 50m end of the pool to record the front view. The outline of swimmer's trunk, head, arms and legs was digitized and the frontal surface area was calculated. With this method the researchers considered the effect of the angle of attack and provided a methodology that could be also used to measure the frontal surface area when the swimmers are passively gliding. However, the author of this thesis is not aware of any study that actually applied this methodology to passively gliding swimmers. One reason could be the practical difficulties that are expected to be encountered with having the swimmer gliding in line with the axis of the camera.

2.6.4. Anthropometry and resistance

The morphological characteristics of male and female swimmers have not been assessed thoroughly. The curvature of the human body is expected to affect resistance but it has not been considered as a factor in most of the previous studies assessing the gliding performance.

Clarys (1979) measured the circumference of ten different locations of 63 male swimmers when standing on land and correlated the findings to passive drag results. According to the findings, for a certain increase in velocity when swimmers are towed underwater, resistance is affected by the body form. However, only male swimmers were analysed in this study and not in the streamlined position.

Pease and Vennell (2011) in an attempt to assess the effect of the human shape on wave drag, analysed a male and a female shaped mannequin and described their curvature as the rate of change of the cross sectional area in the axial plane.

According to the findings, a lower wave drag contribution was reported for the female shaped mannequin near the water surface. However, the same approach has never been applied so far to analyse actual swimmer.

Chapter 3

Method

The following chapter will outline the general methodological approach followed in this thesis and will present and describe the methods that were common to all four studies. The methods specific to each study are presented when describing those studies.

The approach to the general research questions comprises five stages (Figure 3.1). Stages one, two and the first two parts of stage three were common to all four studies whereas all five stages were employed for the fourth study.

Stage 1: Collection of swimmer kinematic data when gliding in the water. Video clips were digitized and displacement data and joint angles were calculated. From displacement data, the glide factor (C_G) was computed to assist with the identification of the most hydrodynamic condition of each study. Furthermore, C_G computation assisted with the validation of the fluid flow simulations around the swimmer's body (stage 5). Joint angles were calculated to monitor swimmers gliding posture throughout the glide and this information was later used to prescribe body alignment when performing the full body scans (stage 2).

Stage 2: Creation of the three-dimensional (3D) models of the swimmers with a full body LED scanner.

Stage 3: The models were then refined by filling the holes generated in areas that were out of the scanner scope when performing the scans, deleting any additional mesh captured (e.g. the ground) and smoothing the surface to reduce the level of noise of the models. The domain, that is the volume where the flow simulation occurs, was generated and split into smaller sub-domains (domain mesh generation) inside each one of which the discretized governing equations were solved. The

surface mesh of the model was generated with advanced automated meshing technology (boundary mesh generation).

Stage 4: A 3D model and displacement data were imported to the simulation software, to run the CFD analysis of a swimmer's geometry in order to identify the optimum simulating conditions (time step size and mesh density).

Stage 5: Simulation results were compared in the fourth study against glide factor (C_G) values calculated from swimmer displacement data to validate the mesh, domain and turbulence settings.

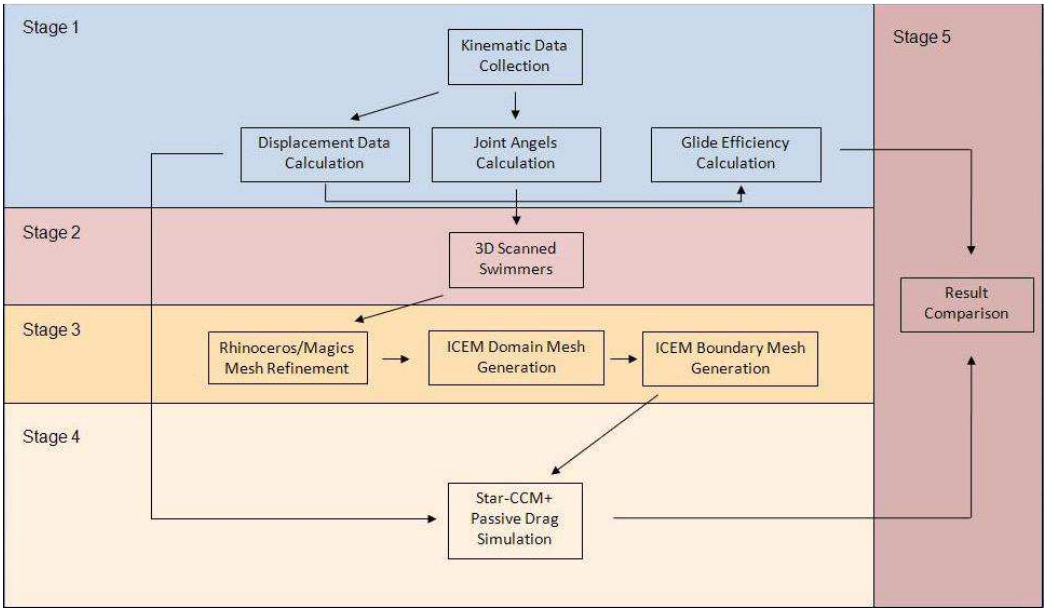

Figure 3.1 The general methodological approach followed in this thesis.

The outcome results of the first stage (C_G values calculated from the displacement data of each glide) were employed to assess the effect of the independent variable of each study (a. the head position, b. the gliding depth and c. the use of full body swim suits).

The methods that were common to all four studies and comprise stage 1, 2 and the first part of stage 3 of the diagram in figure 3.1 are detailed below. The second and

third part of stage 3 as well as stages 4 and 5 are detailed in Chapter 7 were the fourth study is described.

3.1. Participants

A male and a female adult swimmer of international level volunteered to participate in this study. Their descriptive and/or anthropometric characteristics are presented on Table 3.1 and Figure 3.3.

Table 3.1 Participants' age, body mass, height and maximum cross sectional area.

	Age (years)	Body mass (kg)	Height (cm)	Frontal surface area (m^2)*
Male	23	87.0	194	0.106291
Female	21	55.5	171	0.097627

*The frontal surface area reported, was computed when the angle of attack (that is the angle between the line connecting the wrist with the ankle joint and the horizontal) was equal to 0˚.

The total length of the male swimmer in the streamlined position when the angle of attack was 0˚ was equal to 264 cm and 231 cm for the female swimmer (Figure 3.2).

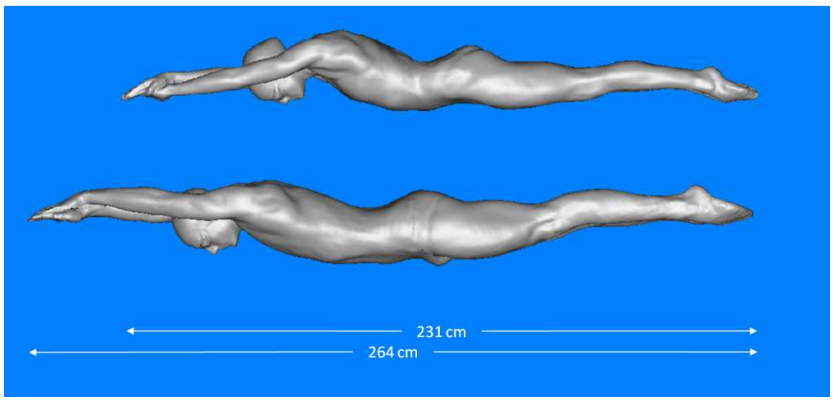

Figure 3.2 Representation of swimmer's anthropometrical characteristics.

Both swimmers were members of the British National Team at the time of the study and were selected according to their ability to perform consistently accurate controlled glides. The respective criteria considered for subjects participation were as follows: a) the longitudinal axis of the body does not deviate from horizontal b) joint angles do not change during the glide and c) body posture can be easily controlled (high glide factor) and d) there are no lateral deviations when gliding. These criteria were assessed using video data collected from the swimmers at the Centre for Aquatics Research and Education (CARE) of the University of Edinburgh.

In addition, the male swimmer could swim 200m butterfly in less than 1 min 56 s and the female swimmer could cover 100m butterfly in less than 59 s. These times demonstrate the participants' ability to produce high velocities equivalent to elite European swimmers(since the European swimming records when the study was conducted was 1 min 52 s for the 200 m men butterfly and 56 s for the 100 m women butterfly).

3.2. Participant preparation

To minimise the effect of confounding variables on performance, participants were required to avoid any stressful training before the testing sessions as well as caffeine (Graham, 2001) or alcohol ingestion (Brien and Lyons, 2000). Due to the long duration of the study and stay in a warm and humid environment, drinks were provided to the participants to avoid adverse effects of dehydration (Barr, 1999).

Prior to both testing sessions (swimming pool and scan), participants were provided with an information sheet (Appendix A) describing in detail the purpose of study, the procedures of the experiment and the benefits of their participation. After reading the information sheet and having any additional questions answered by the investigator, participants signed an informed consent (Appendix A). All testing procedures were approved in advance by The University of Edinburgh ethics committee.

3.3. Calculation of participant's anthropometric characteristics

Prior to data collection, participants were marked with a non-permanent black skin marker on six anatomical points (the wrist, the shoulder, the goggles, the hip, the knee and the ankle) their height was assessed using the stadiometer (SECA 712, SECA GmbH & Co. KG., Germany) and their body mass using weighing scales (SECA 225, SECA GmbH & Co. KG., Germany). Body weight in the water was also assessed in the swimming pool by weighing the participants with an axial compensated loadcell (Novatech F256, Novatech Measurements Ltd, UK) attached to a pool lift (Arjo pool lift, Arjo Ltd, UK) standing on pool side (Figure 3.3). Both participants were weighed three times after maximally exhaling and tucking both with a normal and a full body swimsuit, and the average value from all three trials was then used to describe body weight in the water. The underwater weight measurements were used to assess the effect of wearing the full body swimsuits on buoyancy.

Swimmers' experience and familiarization with the water environment ensured that they would remain steady for long enough period of time to get an accurate weight measurement.

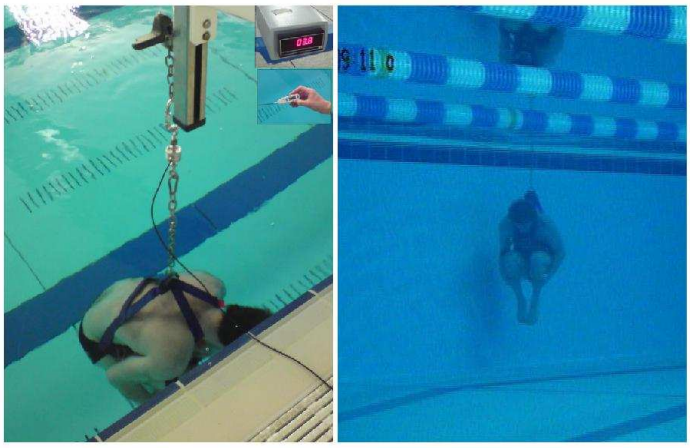

Figure 3.3 Participants were weighed underwater with the use of a load cell.

3.4. Swimming test

3.4.1. Experimental design

The testing protocol involved data collection for four different studies. Each study examined an independent research question but all of them involved controlled glides and 3D body scans of a male and a female participant.

Considering swimmers' unavailability to attend two different sessions in the pool and that both participants perform on average more than 250 pushes from the wall per training session or 450 pushes from the wall per training day, it was decided to collect all data for each participant in one testing session. For the requirements of this study the athletes had to perform in total 80 controlled glides that were significantly less than the average pushes from the wall the athletes perform in one session (considering also that some of the trials had to be repeated).

Moreover, in order to prevent any changes in participant's anthropometric and body composition characteristics participants were tested in the swimming pool and then were scanned with the 3D body scanner within 24 hours.

3.4.2. Swimming pool information

The swimming pool testing sessions were conducted in a 25 m x 13.5 m x 2 m, 6 lane indoor swimming pool (water temperature was 28 ˚C, ambient temperature was 29 ˚C and relative ambient humidity was 60 %) at The University of Edinburgh. Lane ropes were removed to minimise wave drag and to avoid obstruction of the underwater camera view. The covered windows at the swimming pool facilities prevented sunlight reflections that could affect the quality of the digitised data. Large lights and reflectors provided 1000 Lux of evenly distributed lighting to maintain high optical quality at the shutter speeds required to avoid blurring (1/120 s).

Wave turbulence was kept to a minimum by performing the glides far from the pool side and the bottom of the pool. Moreover, deck level swimming pool design assured

that any waves resulting from swimmers glides would not reflect back since the level of the water is the same with the level of the surrounding pool and any excess water is displaced through the overflow channels.

3.4.3. Camera set up

Two cameras (Elmo PTC-450C, Elmo CO., Ltd, Nagoya, Japan and JVC KY32 CCD, JVC Corporation, Yokohama, Japan) were employed for the filming requirements of the study; one positioned below the water surface and one above the water surface to record the swimmers' glides. The camera positions are shown in Figure 3.4. The below water camera was positioned perpendicular to the gliding path (13m from participants glide path) and 1 m below the surface. The above water camera was positioned above the gliding path of the swimmer with the axis aligned vertically to identify any lateral deviations from the prescribed gliding path.

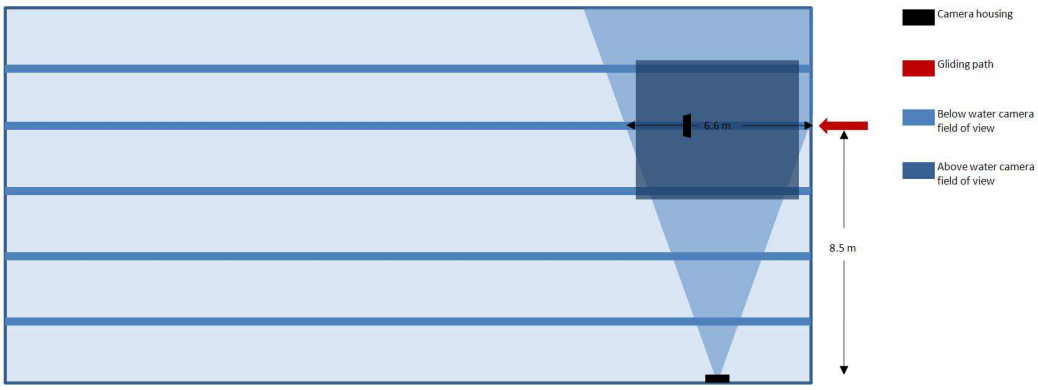

Figure 3.4 Representation of the underwater and the above water camera position (not scaled) and their field of view

The underwater camera was mounted into a rectilinear housing with a flat frontal cover made from perspex (Figure 3.5) the use of which has been reported not to affect underwater digitising accuracy (Psycharakis, 2006). Pan, tilt and zoom options were available. However, pan and tilt camera options were not utilized as it has been demonstrated that digitizing error increases when the camera is not perpendicular to the perspex cover (Kwon, 1999; Kwon and Casbolt, 2006). For this reason the camera was positioned physically without having to use the pan or tilt capabilities. Both cameras were recording at a sampling frequency of 25Hz.

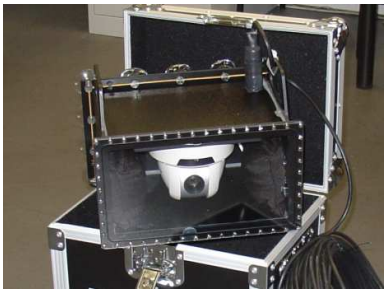

Figure 3.5 The fontal cover of the camera housing made from perspex.

3.4.4. Calibrated area

Nine markers with known coordinates in an 8.5 cm^2 area were digitized from video clips recorded with the underwater side view camera with 'GlideCoach' software (while the characteristics of the recording software are described in detail in section 3.4.6.3). Markers were positioned at the push off wall and at the bottom of the pool under swimmers' gliding path (Figure 3.6). The tracked coordinates on the swimmer's body were then converted to two dimensional coordinates using 2D Direct Linear Transformation (DLT) equations generated from the original set of markers.

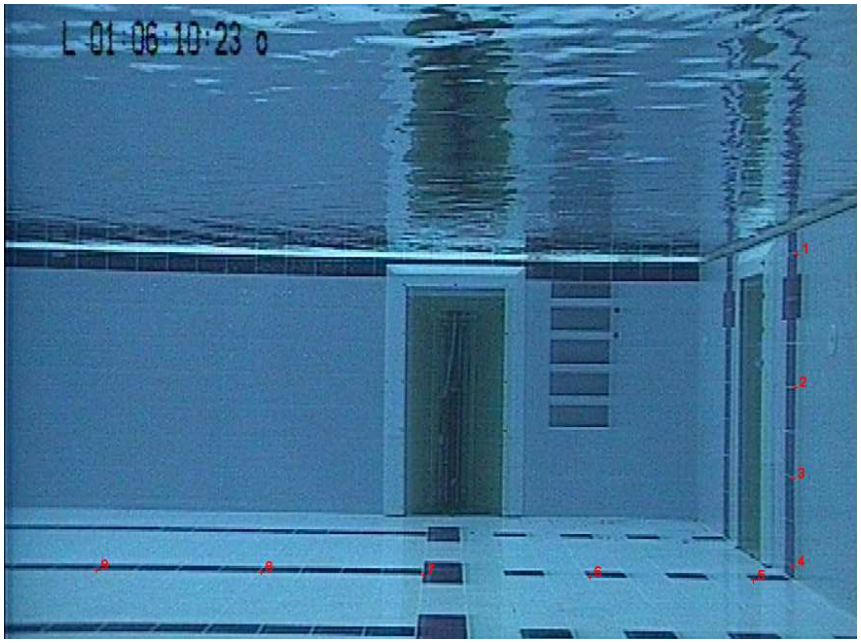

Figure 3.6 The calibrated area with the 9 landmarks across the gliding path.

3.4.5. Marking

Participants were marked for two reasons; first to track displacement as they glide and second to enable calculation of the joint angles. Only the left side of the swimmers was marked since the underwater camera was recording from the swimmer's left side during the glide. For the swimming trials, black non-permanent skin marker (Lumocolor, Staedler Mars GmbH & Co. KG, Germany) was used to form a circle of 40 mm diameter on six anatomical landmarks. Five of the landmarks corresponding to the joint centres of:the ankle, the knee, the hip, the shoulder and the wrist were marked at the lateral malleolus of the tibia, the lateral epicondyle of the femur, the greater trochanter of the femur, the head of the humerus and the styloid process of the ulna respectively. Swimmers goggles were also marked to enable head angle calculation. Goggles and not the centre of the limb were selected since swimmers glide with their arms elongated on either side of the head covering the majority of the limb including the centre of the head and preventing visual contact from the side view camera. When a full body swimsuit was worn, knee and hip joints were marked by placing adhesive stickers on the same anatomical points (lateral epicondyle of the femur and greater trochanter of the femur) over the swimsuit.

White stickers were used to enhance colour contrast with black suit. Their shape was square and their size 40 mm x 40 mm (Figures 3.7 and 3.8 show the markers on swimmers when wearing the normal and the full body swimsuit respectively).

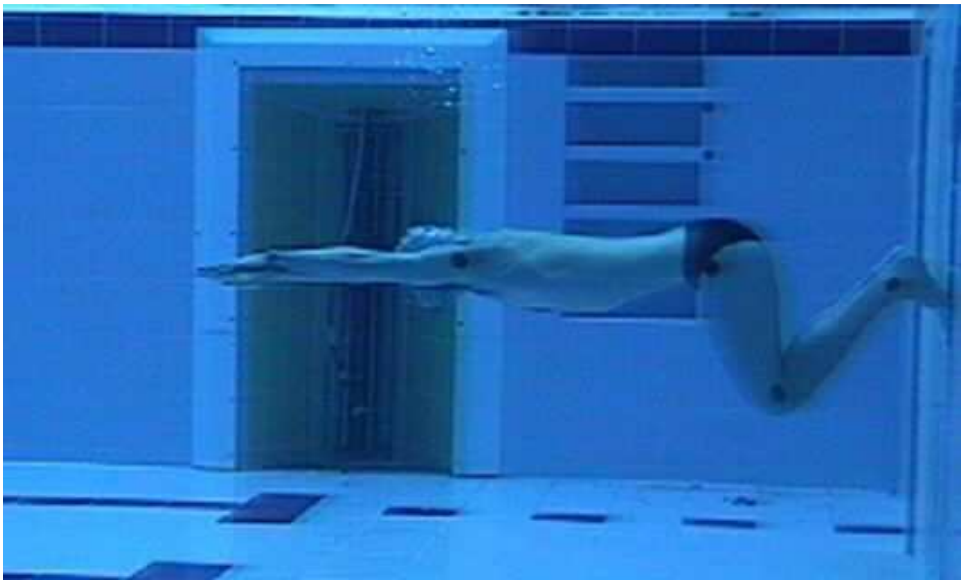

Figure 3.7 The location of markers when the swimmer was wearing the normal swimsuit.

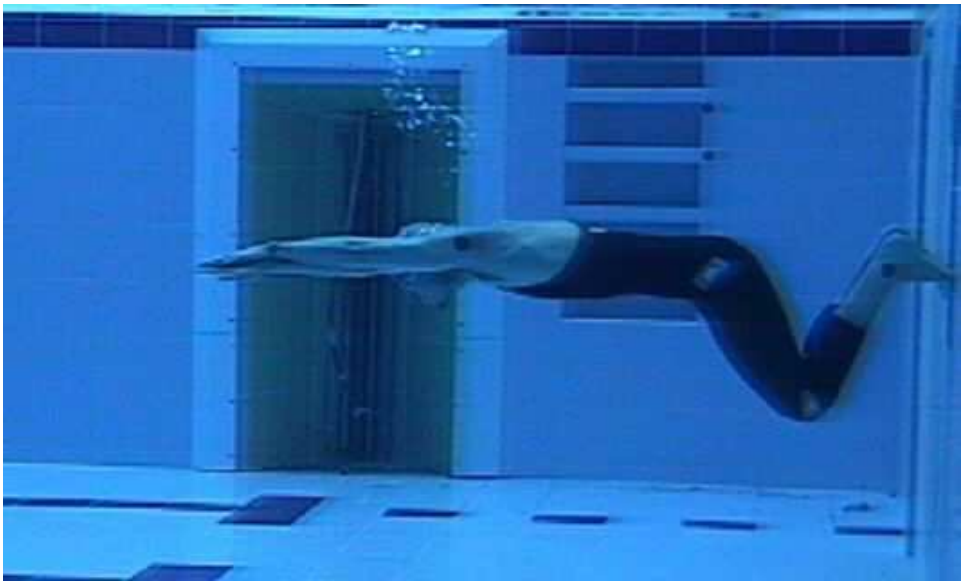

Figure 3.8 The location of markers when the swimmer was wearing the full body swimsuit.

3.4.6. Data collection

3.4.6.1. Warm up

The participants performed a warm up before the beginning of the test. The warm up consisted of 200 m moderate intensity swimming and a set of familiarization glides until the participants could glide consistently in a horizontal streamlined position.

3.4.6.2. Testing procedures

The data collection comprised three sections. Each section was designed to investigate the variable of interest in each study while controlling other variables that affect the glide performance. For each section, 10 controlled glides were considered for analysis.

The order of the variables assessed was randomly selected to prevent any order effects. Furthermore, the participant's involvement in previous studies and feedback sessions including controlled glides ensured that no learning effect would result from the glides repetition.

3.4.6.3. Collection of kinematic data

Kinematic data were collected with the 'GlideCoach' software; a tool designed to capture video clips when connected to a camera, digitize body landmarks and calculate the glide factor using the 'Hydro-Kinematic' method (Naemi and Sanders, 2008*)*. The GlideCoach software was specifically designed and developed at the University of Edinburgh to implement the Hydro-Kinematic method. The Hydro-Kinematic method is a technique quantifying the ability of the human body to maintain its velocity over time by calculating the glide factor (C_G) that allows the comparison between glide intervals both between and within individuals.

The kinematic data collection session comprised video recordings of the swimmers after pushing from the wall and gliding in the streamlined position for 1.5 s. The glide duration was limited to 1.5 s in order to prevent any effect of the glide duration to the gliding performance by retaining a consistent body posture.

Swimmers were instructed to push from the wall and adopt a streamlined position with their elbows fully extended, one hand over the top of the other, the head between the arms, the knees fully extended and the ankles together and plantar flexed. To maintain a horizontal position throughout the glide, swimmers submerged underwater and exhaled the air from their lungs to approximate neutral buoyancy. The volume of air each participant had to exhale relied on the personal perception of each swimmers while of both them practised during the warm up. The gliding conditions such as the gliding depth and the head position varied according to the aim of each particular study.

3.4.6.4. Feedback

Swimmers received feedback after each trial in order to optimize their gliding posture according to the requirements of the study. The investigator could monitor the participants gliding in real time from both below and above water views and provide feedback regarding the gliding depth, the joint angles and any lateral deflection of the body. Markers positioned underwater at certain heights (from the pool surface, 0 cm, 20 cm, 40 cm, 60 cm and 80 cm) on the pool side wall, were visible from the underwater camera view to the investigator when the swimmers were gliding and were used to provide feedback to the swimmers about their gliding depth.

3.4.7. Data analysis

After the end of the experimental session the data were transferred to a computer with the GlideCoach software installed and analysed.

3.4.7.1. Trimming

First the video clips were trimmed to include only the glide and not the underwater preparation phase, starting from the frame that the feet of the swimmers would leave the wall and finishing 1.5 s later. The trimmed file included 38 frames since the recording frequency of the cameras was 25Hz.

3.4.7.2. Digitizing

The trimmed files were digitized with the use of the GlideCoach software. The wrist, shoulder, goggles, hip, knee and ankle marker of the left side of the swimmer were selected and digitised with a semi-automatic method. The software tracked the selected markers but when that was necessary, the investigator manually corrected the miscalculated tracked locations.

3.4.7.3. Analysis

The 2D coordinates of the calibration markers were used to calculate the location of the digitised markers in space for each frame of the digitised video files.

3.4.7.4. Glide factor calculation

The GlideCoach software computed the glide factor values from the displacement data of the hip marker and both the digitised locations (of all markers) and the computed glide factors were exported from the software to get further analysed.

However, in order to identify whether there was an error involved with computing the glide factor from the displacement data of a single marker (hip) it was desired to compute also the glide factor according to the displacement data of all six markers (wrist, shoulder, goggles, hip, knee and ankle). The test was conducted under the assumption that any random digitising error would be cancelled by averaging the displacement data of all the digitised markers. For this reason, the displacement data of 10 trials of all six markers were exported from the GlideCoach software, averaged with the Microsoft Excel software package and then imported to MATLAB software (Naemi, 2006) to compute the glide factor with a custom function applied with the Curve Fitting Toolbox. The average difference between the C_G values computed from the displacement data of the single and the six markers was 3.75%. The C_G values computed from the displacement data of the six markers were closer to the average glide factor of all ten trials indicating that the C_G values are overestimated or underestimated when only a single marker is used (Figure 3.9). The difference seems to be associated with error during the digitising process. For this reason it was

decided not to use the direct output of the GlideCoach software but to compute the C_G considering the displacement data of all the six markers digitized.

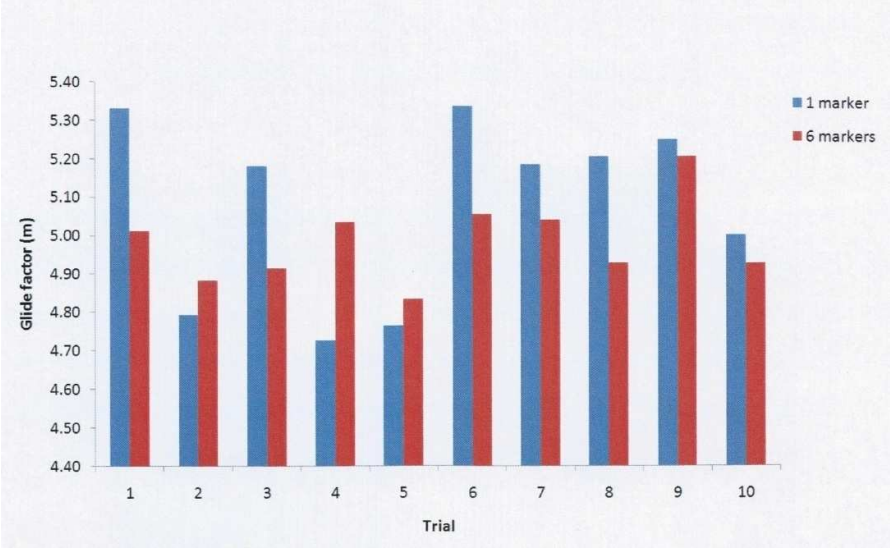

Figure 3.9. Difference in the G_G values computed from the displacement data of the hip markers in comparison to the averaged displacement data of the wrist, shoulder, goggle, hip, knee and ankle markers.

The glide factor was computed by fitting Equation 3.01 to the displacement/time data collected from the horizontal glides (Naemi and Sanders, 2008). The set of known initial velocity and glide factor values that allowed the best fit through the entire interval period provided the measure of the glide efficiency.

$$x = C_G \cdot \ln\left[\frac{V_{X0}}{C_G} \cdot t + 1\right] \qquad \text{Equation 3.01}$$

where C_G is the glide factor, V_{X0} is the initial velocity of the glide and t is the total duration of the glide.

3.5. 3D body scans

3.5.1. Experimental design

The data collection session involved four full body scans of both participants. The joint angles differed between the scanned models according to the requirements of each study.

To define the characteristics and the type of the scanner to be used in order to create accurate 3D representations of the participants, both a white-light and a LED body scanner were assessed in a pilot study. According to the findings a white-light body scanner cannot be used accurately to scan humans when not standing in the prescribed by the manufacturer standing position. For this reason it was decided to use an LED body scanner for the requirements of the study.

3.5.2. 3D scanner information

A 3D LED scanner (Hamamatsu Body Line Scanner, 9036 model, Hamamatsu Photonics, Japan) was employed to create accurate 3D representation of both swimmers in different orientations. 3D body scanners are designed to capture the human shape when standing. After the data is collected, calculations are used to create a smooth surface representing the skin of the scanned person by utilising algorithms designed for this particular purpose. However, for the current study it was desired to scan the participants in the streamline and not in the standing position and also in two sections as the length of the swimmers in the streamline position (Table 3.1) was longer than the scan field of the Hamamatsu body line scanner (that is 2 m). As a consequence, the algorithms embedded to the scanner software could be not be used as the sections of the body scanned were not recognised by the program. For this reason the ‘scan object’ instead of the ‘scan person’ option was selected and the automatic algorithms fixing the 3D model were not employed. As a result the scanner output was neither smooth nor consecutive and additional editing was necessary.

3.5.3. 3D Scanner set up

The Hamamatsu body line scanner was positioned in a low ambient light environment in order to prevent the adverse effect of light on the scanning quality (Lemes and Uzunovic, 2009). The black swim suits were covered in talc powder in order to increase reflection of the skin surface and consequently scan the swimmers with higher accuracy. It has been reported that the reflectivity of the white colour is 80% whereas of the black colour only 8% (Boehler and Marbs, 2003). Furthermore, in order to scan the swimmers wearing their own swimming goggles (black in colour), the goggles were painted with white paint to increase the reflection of the material surface (Figure 3.10).

Figure 3.10 The swimmer's goggles were painted white and their suits were covered in talc powder when that was necessary.

Since the vertical scan field of the bodyline scanner is two meters and the height of the swimmers with their arms in streamlined position exceeded this limit (Table 3.1), the scans were performed in two stages. First the upper body got scanned with the swimmers in the 'kneeling' position (Figure 3.11a) followed by the lower body with swimmers in the 'candle' position (Figure 3.11b). The upper body scan was then aligned and merged with the lower body scan to form the final full body model (Figure 3.10c). The 'candle' position allowed also the lower part of the feet to be scanned.

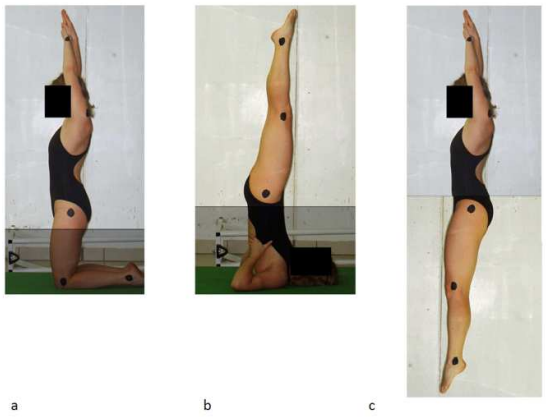

Figure 3.11 The scan of the upper part of the body (a) was merged with the scan of the lower part of the body (b) to get the full body model (c).

3.5.4. Calibrated area

The dimensions of the scanning field were equal to 2 m x 0.6 m x 1 m whereas the calibration process of the scanner was automatic without the need of any intervention of the investigator.

3.5.5. Marking

Swimmers were marked on the same six anatomical points as in the gliding data collection session. In this case the markers were used as landmarks when merging the scans of the upper with that of the lower part of the body. Since it was required for the markers to be visible on the Computer Aided Design (CAD) models exported, special markers manufactured and provided from the company that produced the scanner (Hamamatsu Photonics, Japan) were used.

3.5.6. Data collection

The 3D scanning process of both swimmers was performed with the Hamamatsu Bodyline Scanner that projects 2.048.000 points on the surface of the participants. The pitch intervals were 2.5 mm meaning that 2560 data points were projected at each of the 800 horizontal cross sections created by the scanner for the total height of 2 m (that is the length of the scanning field in the vertical direction).

When performing the scans the swimmers were instructed to breathe out as they were doing before gliding in the water. This way, there was no difference in the chest circumference length measured due to the variation of the inhaled volume of air in the lungs.

3.5.6.1. Establishing similar glide and scanned joint angles

The joint angles of the shoulders, the hips, the knees and the head during the scans were equal to the average joint angles of the same swimmers when gliding in the water. To compute the values to be prescribed when getting the scans, the joint angles of all accepted glide trials were averaged and the swimmers were required to reproduce those angles when being scanned. The accuracy of the process was ensured by the investigator with the use of a goniometer with extended sides (Figure 3.12).

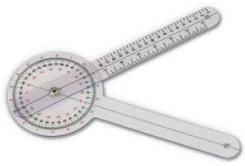

Figure 3.12 The goniometer used to calculate joint angles.

3.5.7. Data analysis

The scanned models were exported from the body line scanner in .stl (stereolithography) format and were subsequently imported to the Rhinoceros (Rhinoceros 4.0, Robert McNeel & Associates, Seattle, USA) and the Magics software (Magics, Materialise, USA) to get merged and fixed. With the use of the CAD packages the additional mesh captured by the scanner was deleted, the skin surface was smoothed and the holes were filled. Furthermore the same software was used to measure the area of each cross section of the models in the transverse plane.

3.5.7.1. Fixing the models with the use of the Magics and the Rhinoceros software

The scanned models required extensive repair to be used for accurate assessment of the swimmer's body volume as well as for CFD analysis (Figure 3.13).

The repair process involved many stages and the use of both software packages (Rhinoceros and Magics). The scanned models (of the upper and lower part of the body) were separately fixed and then merged. Initially the scanned excess mesh of both inside as well as outside the scanned model was selected and deleted with the Rhinoceros software. Areas where the captured mesh did not reflect the skin curvature were deleted also. The holes in the remaining mesh were then filled and the full segment model trimmed to include only the sections that were used for the final full body model. After that the mesh surface was smoothed and the scan of the upper and the lower part of the body merged. To achieve an accurate merge between the scans of the upper and the lower part of the body, the smoothing factors applied on the two models separately were exactly the same. Furthermore, the repair process followed was consistent across all models.

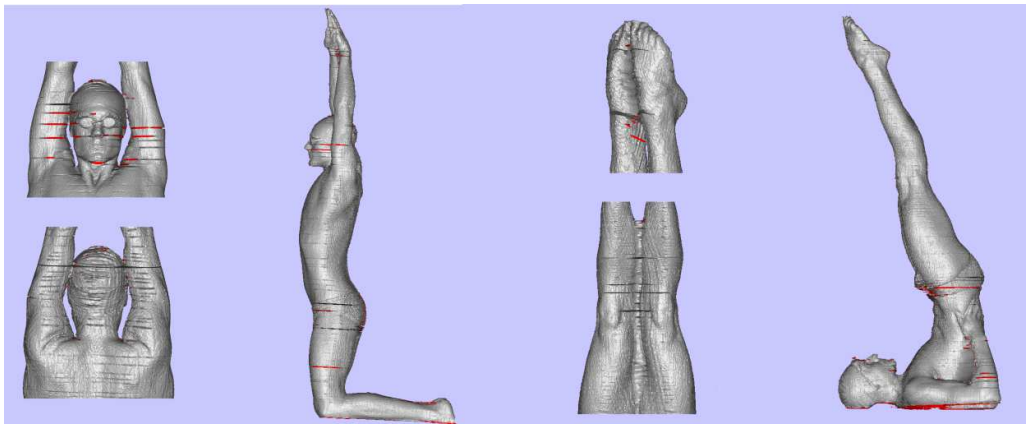

Figure 3.13 The scanned models were refined by filling the holes and smoothing the surface of the scanned mesh.

3.5.7.2. Swimmer's height in the streamlined position

Swimmer height in the streamlined position could not be measured accurately on pool-side. Even when the swimmers were asked to step on an inclined level allowing plantar flexion of the feet, the ankle joint angle was not similar to that when gliding in the water. For this reason, swimmers' geometries were scaled according to the height measured from the lateral malleolus of the fibula to the top of the fingers. Having the geometries scaled according to this length, the length from the lateral malleolus of the fibula to the end of the toes was measured from the 3D model with the Magics software (Figure 3.14).

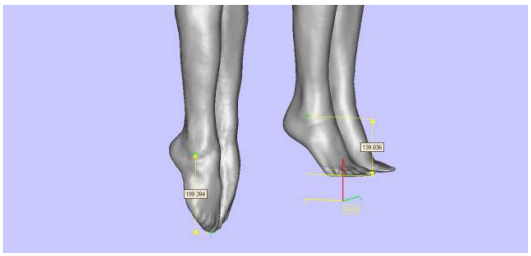

Figure 3.14 The total height in the streamline position as well as the ankle to the bottom of the toes length was measured from the 3D models.

3.5.7.3. Volume and area measurements with the use of the 3D models

Volume assessment of the entire body as well as area assessment of each cross section of the body was carried out with the use of the Magics software (Figure 3.15). However, an accurate assessment of the frontal surface area according to the angle of attack was carried out with the use of the ICEM CFD (ANSYS, Canonsburg, Pennsylvania, USA) software since the angle of attack could be prescribed with accuracy.

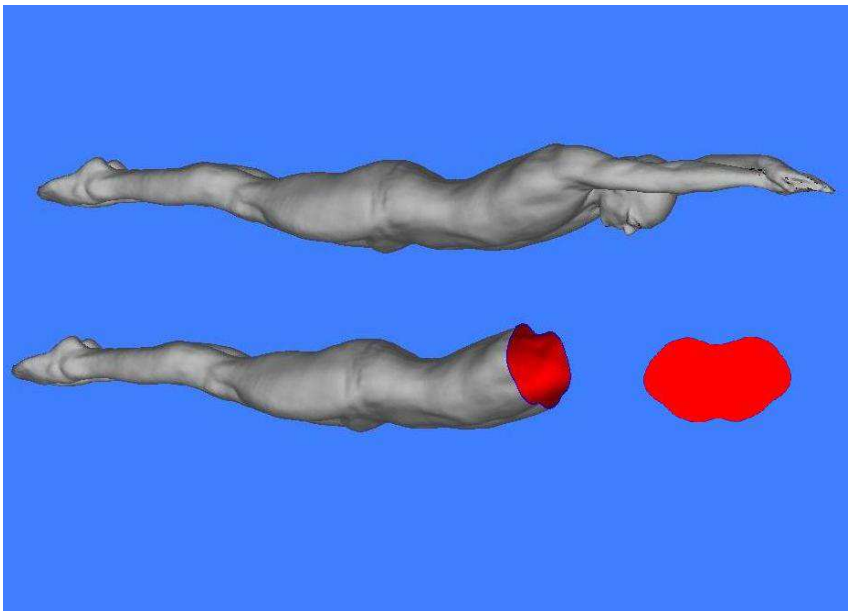

Figure 3.15 Ankle to bottom of the toes length measurement with the use of the participant's 3D models.

Chapter 4

Study 1: The effect of head position on glide performance

4.1. Introduction

The quest for higher swimming performance led to an in depth analysis of the glide phase after starts and turns. This phase is known to be a significant contributor to total swimming event time (Chow *et al.*, 1984; Vilas-Boas & Fernandes, 2003). Thayer and Hay (1984) found that the glide phase after the start for the 50 yards front crawl event is equal to 11% of the total racing time whereas the sum of all turn time for the 200 yards breaststroke event represents 39% of the total time of the event. Improved performance over the glide phase of starts and turns could improve the total event time and finishing position.

The significance of the glide phase after starts and turns has been shown also by D' Acquisto (1988) who demonstrated that the glide phase that distinguishes superior from good breaststroke swimmers.

During the glide phase the swimmer maintains the same posture and no propulsive forces are produced. The factors that determine performance in this case are the initial velocity and the hydrodynamic resistive forces acting on the swimmer's body (Lyttle, 1999, Figure 4.1). The red caption in Figure 4.1 indicates the variables of interest.

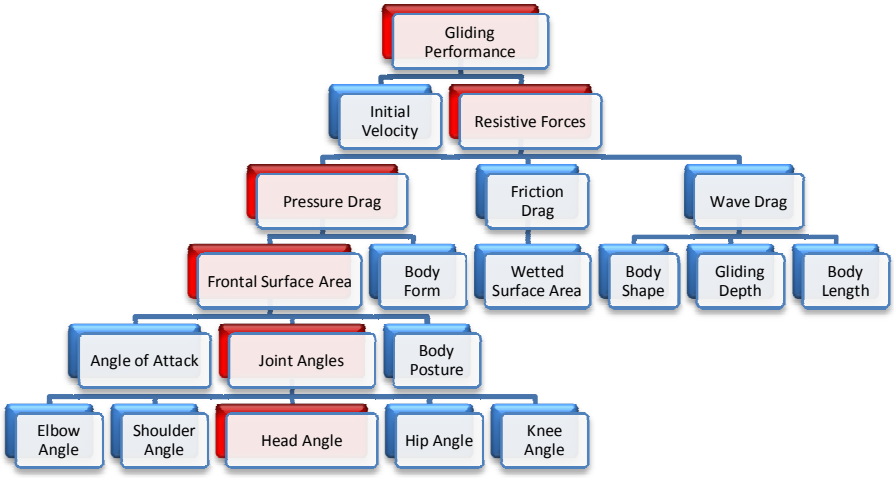

Figure 4.1.The factors affecting performance when gliding after starts and turns.

The effect of initial velocity on gliding performance is beyond the scope of this thesis and therefore the following paragraphs will focus on and detail the nature and the characteristics of the applied resistive forces.

Hydrodynamic resistance can be separated into three contributions; the pressure drag the friction drag and the wave drag (Karpovich, 1933). When the swimmer glides underwater, pressure drag has the most significant effect on the total resistive forces. The higher the gliding velocity the greater the effect of pressure drag on total resistance since pressure drag increases with the square of velocity whereas friction drag increases linearly with velocity (Vorontsov and Rumyantsev, 2000).

Rumyantsev (1982), as reported by Vorontsov and Rumyantsev (2000), found that pressure drag for an actively moving swimmer with a velocity of 2 ms^{-1} accounts for 94.9% of total drag whereas wave drag accounts 5% and friction drag only 0.05%. Despite the experimental limitations of the study and the fact that active and not passive drag was measured, the aforementioned results highlight the significant effect of pressure drag upon total resistance. Equation 4.1 describes the way total drag was calculated.

Equation 4.1

Mollendorf *et al.*, (2004) measured all contributions of drag when swimmers were towed on the surface (wearing briefs when velocity was 2.2 ms^{-1}) and found that pressure drag consists 52.1% of total drag whereas wave drag 26.5% and friction drag 21.5 respectively (D_{pr}= 44.9 N, D_w= 22.8 N and D_{fr}= 18.5 N). Even though oversimplified equations were employed for the drag contribution calculation, this study emphasised the need to decrease pressure drag in order to improve gliding performance.

The significant effect of pressure upon total drag justifies the numerous studies researchers performed over the past decades to identify the factors that could decrease this component and improve performance (Karpovich, 1933; Alley, 1952; Counsilman 1955; Schramm, 1958; Onoprienko, 1968; Clarys, 1978; Miyashita & Tsunoda, 1978; Zaidi*et al.*, 2008; Zamparo *et al.*, 2009; Vilas-Boas *et al.*, 2010).

Karpovich (1933), Onoprienko (1968) and Clarys (1978) found that the cross-sectional area has the most significant effect upon pressure drag. Later studies (Vilas-Boas *et al.*, 2010) demonstrated a significant correlation between cross-sectional area and drag.

Cappaert and Gordon (1998), Mollendorf *et al.* (2004) and Zamparo *et al.* (2009) considered also the case where the cross-sectional area does not correspond to the frontal surface area, occurring when the swimmers are not horizontally aligned. To account for the effect of the body angle, Mollendorf *et al.* (2004) and Zamparo *et al.* (2009) applied a function involving the cross-sectional area, the body surface area and the body angle to approximate the frontal surface area for different angles of attack when swimmers are gliding in the streamline posture. Nevertheless, this is not the only case that the cross-sectional area does not correspond to the frontal surface area (FSA). Likewise when the head is not positioned between the arms the FSA is increasing and consequently pressure drag increases.

The effect of the head position (head angle) on pressure drag has been investigated by Onoprienko (1968), Clarys*et al.* (1973), Miyashita and Tsunoda (1978) and Zaidi

et al. (2008). Onoprienko (1968), as reported by Vorontsov and Rumyantsev (2000), found that the tilting of the head increases the angle of attack which in turn increases total resistance by up to 40% when velocity is 1.7-2 ms^{-1}.

Similarly Miyashita and Tsunoda (1978) compared the resistive forces measured when the swimmers were towed on the surface with their head above and below the water. Higher values reported for the first condition were justified as a result of an increase in the frontal surface area.

Clarys *et al.* (1973) compared the drag forces measured when swimmers were actively swimming competition and water-polo front crawl. Results demonstrated 6 to 45% higher resistance for the water-polo front crawl swims due to lordosis in the lumbar region and an elevation of the shoulders and consequently the head.

Even though the work of Onoprienko (1968), Miyashita and Tsunoda (1978) and Clarys *et al.* (1973) has focused on the effect of the head tilt on the angle of attack, the researchers did not consider any direct effect on the frontal surface area. In addition, towing experiments conducted on the water surface did not allow an accurate comparison between the measured pressure drag values since swimmer's orientation affected also wave drag.

The methodology of Computational Fluid Dynamics has been recently employed by Zaidi *et al.* (2008) to identify the effect of head position on glide performance. The researchers used a side view picture of a female swimmer in the streamlined position (captured when lying on a chair) to create a two-dimensional geometry. The Reynolds Average Navier Stokes (RANS) equations were employed to control the turbulence fluid flow and turbulence was modelled by the standard k-ε model. Even though the effect of the head position on pressure drag was specifically assessed in this study there were limitations of the approach. These included 2D instead of 3D analysis, RANS instead of Large Eddy Simulation (LES) to model turbulence, the swimmer's geometry created according to an image captured on pool-side when the swimmer was lying on a chair instead of an image taken when the swimmer was

gliding in the water. As a result, the measured drag value was more than twice any previous reported value for swimmers experimentally or numerically tested for the same velocity.

The limitations of the methodologies described in the previous studies raise doubts about the accuracy of the computed results. Accurate assessment of the effect of the head position on gliding performance is required to define the head position with the optimum efficiency.

In light of the above considerations, the purpose of the current study was to quantify the effect of the head position on the frontal surface area and the glide performance. It is hypothesized that the high and the low head position will demonstrate the greatest frontal surface area and the lowest glide factor values amongst the conditions tested whereas the medium head position the smallest frontal surface area and the highest glide factor.

4.2. Method

For the requirements of the study a male and a female swimmer of international level whose anthropometric characteristics are presented in detail in Chapter 3 were employed. The general testing protocol is described in Chapter 3.

The study specific protocol involved additional instructions for the head angle adopted by the swimmers and the gliding depth. The participants were instructed to push off from the wall and glide in the streamlined position under three different conditions; i) with the head between the arms (medium head position) ii) with the head in cervical extension (high head position) and iii) with the head in cervical flexion(low head position) as illustrated in Figure 4.2.

Figure 4.2. Medium, high and low head position tested.

It was desirable that a number of interfering variables such as the angle of attack, the joint angles and the gliding depth would remain constant under all three conditions tested. For this reason, the participants performed a number of familiarisation glides before the beginning of the testing and feedback was provided about the corrections required. In addition to that, the glides with evident effect of the interfering variables, observed by the researcher monitoring the above and below water camera views when collecting the data, were not considered for analysis and the trials were repeated. This way, only the effect of the independent variable, i.e. the head position, was examined whereas the interfering variables that could affect the performance and influence the measured results were controlled.

Swimmers performed many glides so that there would be ten accepted trials for each condition tested. The inclusive criterion considered, after having analysed the data, was the average angle of attack variation throughout the glide (+/- 3 degrees). From the pilot study it was found that even international level swimmers could not maintain a completely streamline position for a glide interval of 1.5 s.

Considering that the flexibility of the head enabled by the atlanto-occipital joint between the first cervical bone (atlas) of the vertebra and the occipital condyle would not be the same for both participants, the swimmers were instructed to adopt the greatest possible angle for the high head position and the lowest possible angle for the low head position. For the medium head position, the swimmers were instructed to position the head between the arms so that the arms would cover the ears.

As determined by the 'GlideCoach' software protocol, the analysed gliding duration was 1.5 s. For the head angle calculation, the position coordinates of the digitised markers of the hip, shoulder and the atlanto-occipital joint were used to compute the

angle of attack of the head segment, from the shoulder to the head marker, and the upper body segment, from the hip to the shoulder marker, according to Equation 4.2. Detailed information about the exact location of the markers is presented in Chapter 3.

$$\theta_i = Arch\tan\frac{Y_{pi} - Y_{di}}{X_{pi} - X_{di}} \quad \text{(Equation 4.2)}$$

where Y_{pi} and X_{pi} are the position coordinates of the proximal joint and Y_{di} and X_{di} are the position coordinates of the distal joint of the segment at frame i. The segmental angles of attack in turn were used to compute the angle of the head segment in relation to the upper body (hip to the shoulder) segment according to equation 4.3.

$$\varphi = \vartheta_{ub} - \vartheta_h \quad \text{(Equation 4.3)}$$

where φ is the angle of the head segment, θ_{ub} is the angle of attack of the upper body segment and θ_h is the angle of attack of the head segment.

The angle of attack of the whole body in this thesis is identified as the angle between the cord linking the wrist with the ankle marker and the horizontal in the sagittal plane. The wrist and the ankle coordinates computed when the swimmers were gliding were used in Equation 4.1 for the calculation of the variable.

The head angle was computed for each frame of the glide and average values for each head position tested of each participant are reported in Table 4.1.

Table 4.1 Average head angle values for each head position adopted by the participants.

	Medium head position (degrees)	High head position (degrees)	Low head position (degrees)
Male	141.6	196.2	109.4
Female	129.3	170.5	110.3

The gliding depth for all head positions tested was 0.8 m from the water surface to avoid any adverse effect of wave drag on glide performance when gliding close to the water surface (Lyttle *et al.*, 1998).

To ensure gliding depth consistency across all trials, markers were positioned on the pool-side wall of the pool at the desired gliding depth. Glides at higher or lower depths were rejected during the data collection.

The results were comprised of displacement and frontal surface area data. The Hydro-Kinematic method (Naemi and Sanders, 2008) that enables the quantification of the glide factor from the displacement data was used to evaluate the efficiency of the performed glides.

The frontal surface area for the different head positions adopted was measured with the use of the 3D body scans of the swimmers. Average joint angles of all joints including the head were calculated from the coordinates of the tracked markers and were used to define the joint angle of the participants when getting scanned. Three full body models, one for each head condition (MH, LH, HH), were created for each participant. Figure 4.3 illustrates the 3D geometry of the male and the female swimmer in the 'medium head' position.

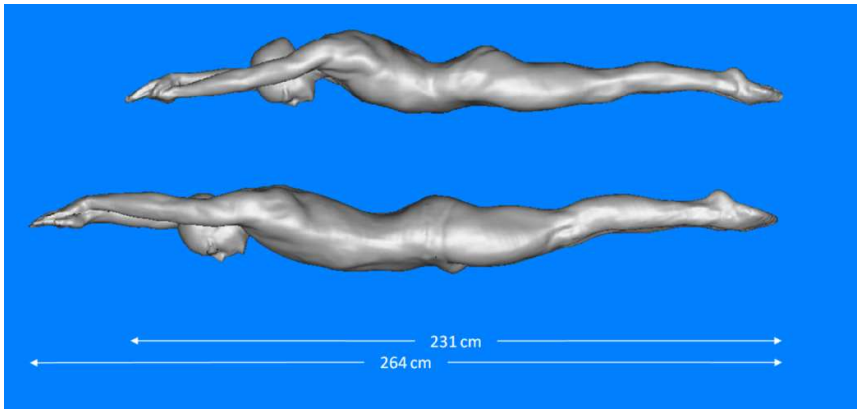

Figure 4.3 Side view of the male and the female swimmer in the 'medium head' position.

The models were imported to the ICEM software for scaling and alignment with the horizontal in space and the same software was also used to compute the frontal surface area.

Considering that a large number of familiarization glides followed by feedback was performed prior to the data collection and also that both participants participated previously in other studies that involved controlled underwater glides, it was anticipated that the order of the head positions tested would not bias the results due to any advantage of the learning effect. For this reason both swimmers performed first the glides with the medium head position followed by the high and low head position.

All procedures were in accordance to the University of Edinburgh Ethics Committee.

4.2.1. Statistical analysis

The statistical analysis was conducted using the Microsoft Office Excel (2007) and the Statistical Package for Social Sciences (SPSS, version 19). Normality of the distribution was assessed with the Shapiro-Wilk test. A dependent-samples T-Test was used to evaluate the effect of the head position on the glide factor. Pooled standard deviation was computed for each set of data according to Equation 4.4 to assist with the computation of the effect size (Cohen, 1992).

$$SD_{pooled} = \sqrt{\frac{(N_1 - 1)SD_1^2 + (N_2 - 1)SD_2^2}{N_1 + N_2 - 2}} \qquad \text{Equation 4.4}$$

N_1 and SD_1 are the number of trials and the standard deviation of the first set of data whereas N_2 and SD_2 are the number of trials and the standard deviation of the second set of data.

The effect size was computed to assess the magnitude of difference in the glide factor between the different head positions tested according to equation 4.5

$$Effect\ Size = \frac{M_1 - M_2}{SD_{pooled}}$$ Equation 4.5

M1 and M2 are the mean values of the first and second set of data.

The effect size was computed for each pair of head positions.

4.3. Results

Three different conditions were examined in the present study and the results were comprised of anthropometric and kinematic data. Figure 4.4 and 4.5 shows the medium, high and low head position adopted by the male and the female swimmer respectively. The head angle for each condition tested is presented on the left side of the figures. The data were found to be normally distributed.

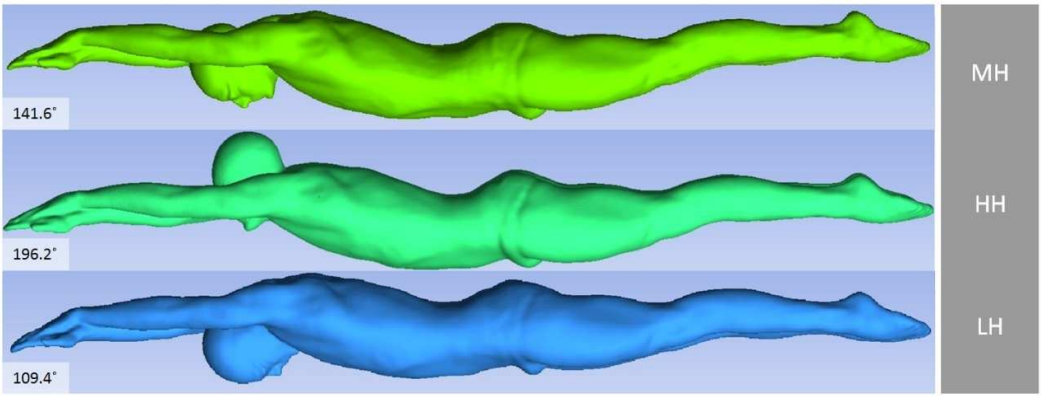

Figure 4.4 Medium, high and low head position adopted by the male swimmer.

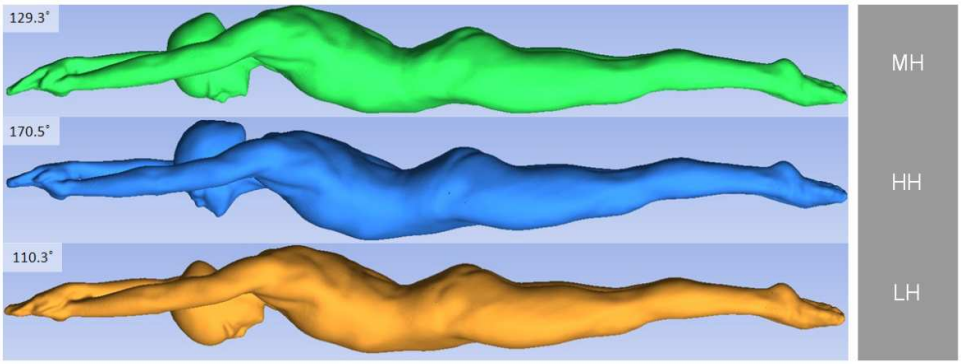

Figure 4.5 Medium, high and low head position adopted by the female swimmer.

4.3.1. Accuracy of the glide factor computation approach

As was shown in Chapter 3, the glide factor assessment accuracy increases when the displacement data of all six markers digitized are averaged for each frame of the glide interval and used for the glide factor calculation. For this reason the displacement of all markers were considered for the requirements of the current study.

4.3.2. Glide factor

Figures 4.6 and 4.7 illustrate the glide factor for each swimmer and for all three conditions tested using six markers. Table 4.2 shows the effects sizes and the significance levels obtained from the dependent-samples T-test performed for the glide factor values of both participants.

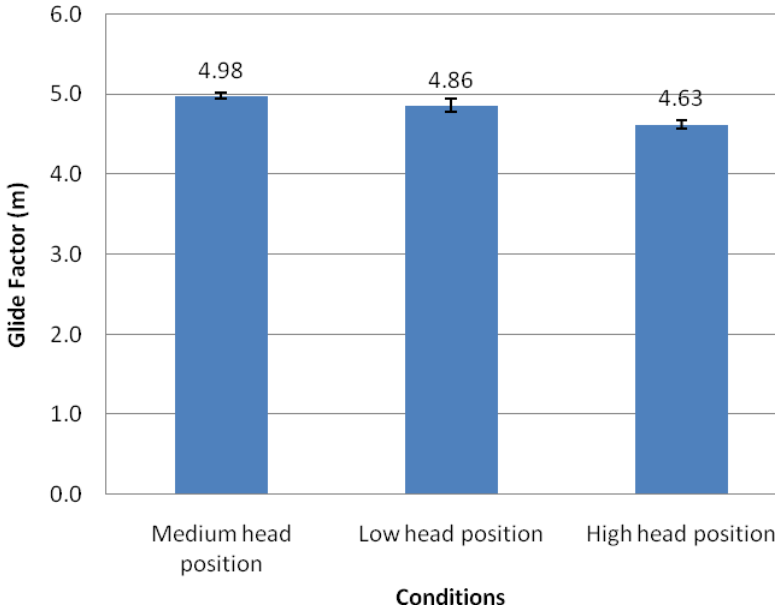

Figure 4.6. Glide factor values reported for each condition tested for the male participant. Bars represent the standard error of the mean.

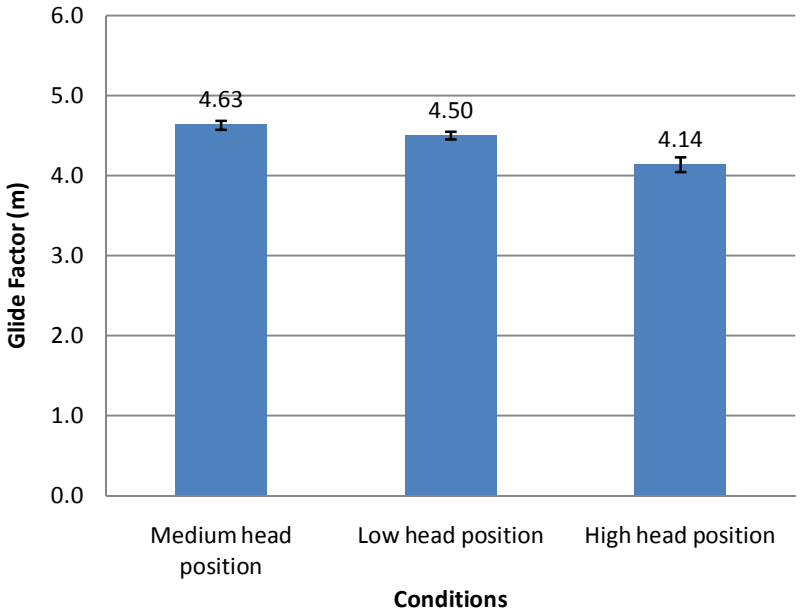

Figure 4.7. Glide factor values reported for each condition tested for the female participant. Bars represent the standard error of the mean.

Table 4.2 SD_{pooled} data, significance levels and effect sizes for each swimmer and for all head angles tested tested.

		SD_{pooled}	Significance level	Effect Size
MALE	MH / HH	0.136	.000	2.624
	HH / LH	0.277	.167	-0.645
	MH / LH	0.264	.147	0.674
FEMALE	MH / HH	0.241	.000	2.037
	HH / LH	0.229	.002	-1.587
	MH / LH	0.163	.098	0.783

4.3.3. Frontal Surface Area

Figure 4.8 shows the frontal surface area of the male and the female participant for angles of attack ranging from -3 to 3 degrees. A more detailed description of the FSA is presented in Appendix B.

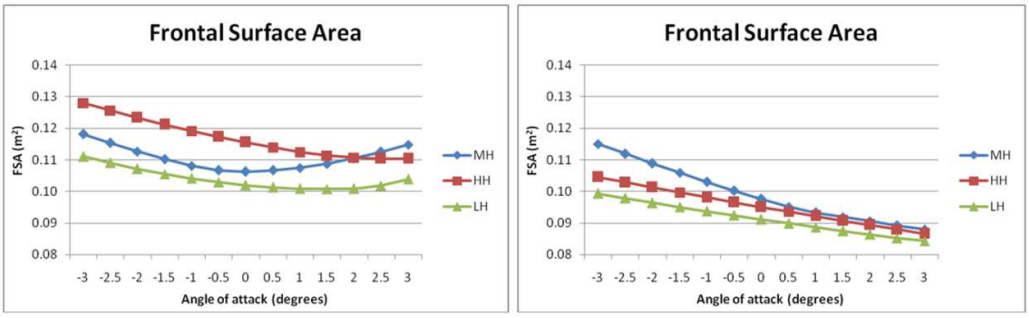

Figure 4.8. a). The frontal surface area of the male and b). the female participant for angles of attack ranging from 3 to -3 degrees.

The frontal surface area for the average angle of attack for each condition tested is presented on Figure 4.9 for the male participant and on Figure 4.10 for the female participant.

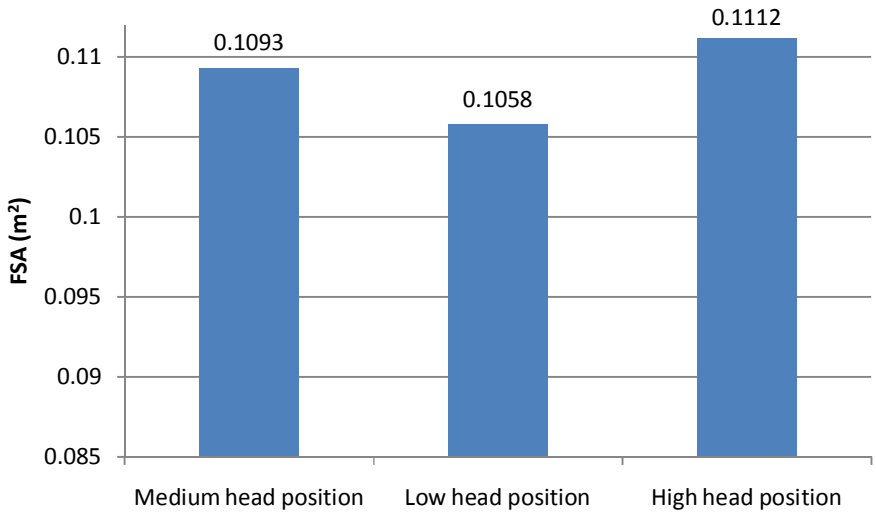

Figure 4.9. FSA values reported for each condition tested for the male participant.

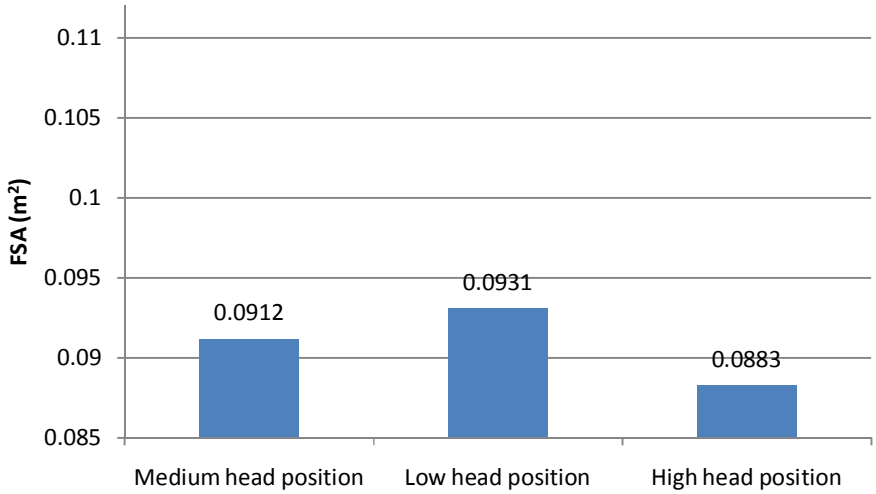

Figure 4.10. FSA values reported for each condition tested for the female participant.

4.4. Discussion

In the present study the effect of the head position on the glide performance has been assessed. What is more, the effect of head position on the frontal surface area is also reported.

The rate of deceleration when gliding was evaluated by computing the glide factor. Understanding the impact of the head position on both the glide performance and the frontal surface area provides valuable information about the optimal posture to be adopted when gliding after a dive or a turn but also is indicates whether it is the differences in the frontal surface area or the differences in the body form that actually decrease performance when the head is tilted.

As has been also indicated by the pilot study results, there were minor variations in the angle of attack as the swimmers were gliding (-1.3 ±0.86). The range of the angle of attack throughout the glide is similar to that when testing mannequins attached to steady constructions in the flume (Bixler *et al.*, 2007). Thus, the range of ±3 degrees in the angle of attack was considered unavoidable and average values were calculated and reported.

Significant difference between the medium/low and the high/low head position for both participants indicate inferior performance when raising the head towards the water surface. On the other hand, the small and not significant differences reported between the medium and low head position for both participants indicate that swimmers can choose either head position without expecting any differences in performance.

High effect size values reported between the medium and high head glide factor values (d_m=2.489 for the male participant and d_f=1.932 for the female participant) and also between the low head and high head C_G values (d_m=-1.002 for the male participant and d_f=-1.506 for the female participant) for both participants indicate differences between the sets of data. Contrarily, moderate effect size values reported between the low and high C_G values for both participants denote some similarities

between the sets of data (d_m=0.539 for the male participant and d_f=0.743 for the female participant) indicating an advantage when adopting the medium or the low head position.

According to the resutls of the current study as shown on figures 4.9 and 4.10 the increase in the FSA is not related to the gliding performance. In this case, the C_G values are induced when the head position is altered but not in relation to the FSA. The initial hypothesis that the CG and the frontal surface area are related is therefore rejected indicating that changes in the body form, as a result of the altered head position, have a stronger impact on gliding performance than the FSA itself.

Race clips of elite swimmers gliding underwater demonstrate that some of the top level athletes glide with their head between their shoulders (medium head position) such as Ian Thorpe whereas some others with their head in front of their shoulders (low head position) such as Michael Phelps(Appendix D). The results of this study demonstrating no significant difference between the two conditions indicate that swimmers can choose any of the two head positions tested according to their natural preference.

On the other hand significant differences between the high and the low/medium head position indicate that swimmers raising their head when gliding underwater should adjust their head position to further improve their gliding performance.

The complexity of the human shape in combination with the diversity of each swimmer's individual morphological characteristics renders any equation used to approximate the FSA inadequate. In this study a new approach of calculating the frontal surface area is presented. 3D body scans appear to provide precise FSA calculations. It was also attempted as part of the pilot study to record the swimmer's glide from the front view by placing a camera on the opposite wall of the pool as suggested by Cappaert and Gordon (1998). However, the swimmers were not always laterally aligned with the camera and would have to perform a significant greater number of glides in order to control this variable (a push from the wall 5 cm to the

left or to the right of the desired path would provide incorrect results). Considering the large number of glides the swimmers would have to perform to evaluate the FSA and their unavailability to attend a second data collection session, it was decided to abandon this approach.

4.5. Conclusion

The glide phase after starts and turns consist a significant part of the swim race and optimum head position should be adopted to maximize performance. Swimmers should choose either a low or medium head position to increase their gliding performance and succeed faster race times.

4.5.1. Limitations and recommendations

As the number of participants was limited it is suggested that a greater number of athletes is tested with the same methods. Additionally, to further increase the level of understanding of the forces applied when gliding underwater and also evaluate the effect of the head angle in more details it is suggested to apply the numerical technique of computational fluid dynamics where all the fluid flow and the segment parameters can be determined. This way additional interfering variables such as the angle of attack throughout the glide could be controlled. The experimental displacement and joint angle data of this study as well as the swimmer's 3D geometries comprise all the necessary data to set up the fluid flow simulations.

Chapter 5

Study 2: The effect of gliding depth on glide performance

5.1. Introduction

The gliding depth after starts and turns in competitive swimming has been associated with glide performance (Clarys, 1979). Swimmers voluntarily choose how deep they glide according to the stroke they swim, the distance of the event and their gliding posture (prone or supine). Limitations in the allowed gliding length (to 15 m) of all the official swimming events set by FINA (Federation Internationale de Natation) act as constraints in the task of optimizing performance of the glide.

According to di Prampero *et al.* (1974) performance in swimming can be improved by increasing the propulsive forces and/or minimising the resistive forces. As the swimmer is passively gliding after starts and turns, no propulsive forces are produced and performance depends on the magnitude of the applied resistive forces (Lyttle, 1999). When swimmers glide underwater in the streamlined position while maintaining the same posture, the resistive forces can be affected only by the gliding velocity and the gliding depth. The closer a swimmer glides to the water surface the greater is the wave drag contribution to total drag (equation 5.1).

$$D_{Total} = D_{Pressure} + D_{Wave} + D_{Friction} \quad \text{Equation 5.1}$$

The highlighted red cells of Figure 5.1 show how the gliding depth affects glide performance. The red caption in Figure 5.1 indicates the variables of interest.

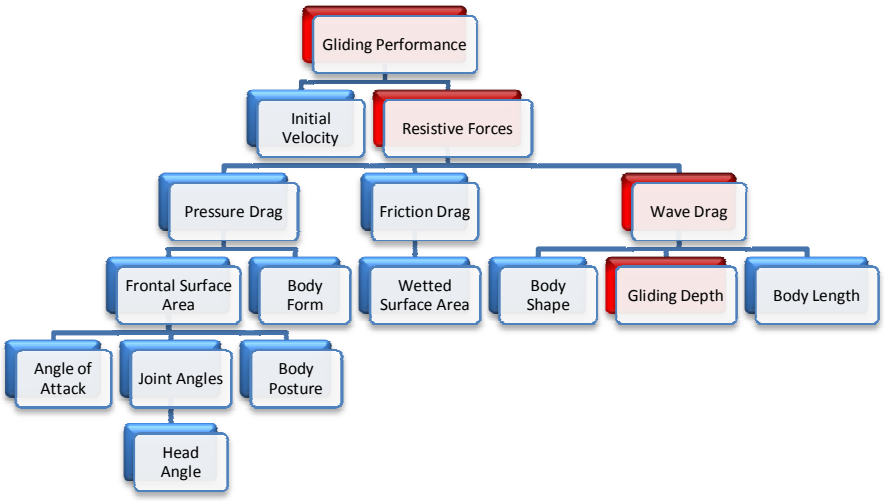

Figure 5.1. The factors affecting performance when gliding after starts and turns

Research investigating the effect of wave drag was initially undertaken for vessels. Russell (1860) as reported by Sir Henry White (1894) was the first to experimentally examine the wave making factor upon resistance and generate the wave-line theory. A few years later Michell (1898) attempted to calculate the resistance caused by the waves. Michell (1935) was the first to develop a computational method to determine the wave resistance of a vessel.

The relationship between wave drag computation and operating depth was examined half a century later when Hertel (1966) investigated the effect of surface waves, which were created by a spindle shaped object when towed at varying depths, on resistive forces. His findings suggested that wave drag becomes negligible at a depth of three times the diameter of the object. The highest drag value was reported for a towing depth of approximately 0.5 times the diameter of the object. Hertel's findings inspired other researchers to assess wave drag of species swimming close to the surface such as minks (William, 1983), muskrats (Fish, 1984), penguins (Blake and Smith, 1988), trout (Webb, Sims and Schultz, 1991), mammals (Blake, 2000), leopard frogs (Johansson and Lauder, 2004), catfish (Blake and Chan, 2007) as well

as other scientists to work on shape optimization for vessels that operate close to the water surface (Eng, 1963; Roberts and Sutton, 2006; Alvarez, Bertram and Gualdesi, 2009; Blake, 2009). The significant effect of increased wave drag and consequently resistance when swimming close to the water surface in terms of mechanical work done, has been evidently reported by Webb, Sims and Schultz (1991) who found that for trout 70% of the energy dispersion was due to the wave generation when swimming near the water surface.

The effect of wave drag has been investigated also for swimmers (Jiskoot and Clarys, 1975; Lyttle *et al.*, 1998, Maiello *et al.*, 1998; Vennell, Pease and Wilson, 2006; Machado *et al.*, 2010 and Pease and Vennell, 2011).

Jiskoot and Clarys (1975) towed forty three male physical education students at surface level and also at 60cm below the water surface at five different velocities (1.5 ms^{-1}, 1.6 ms^{-1}, 1.7 ms^{-1}, 1.8 ms^{-1}, and 1.9 ms^{-1}). The findings demonstrated higher drag values for the total immersed condition. A similar but more detailed study was conducted several years later by Lyttle *et al.* (1998). The researchers towed forty male swimmers at four different depths (0.6m, 0.4m, 0.2m and at water surface) and at six different velocities (1.6 ms^{-1}, 1.9 ms^{-1}, 2.2 ms^{-1}, 2.5 ms^{-1}, 2.8 ms^{-1} and 3.1 ms^{-1}). Their findings were contradictory to those of Jiskoot and Clarys (1975) stating that drag forces reach a maximum value when the swimmers are towed at the surface. Lyttle *et al.* (1998) in order to account also the body shape effect that could potential affect the results, considered also the surface area of the swimmers, the chest girth and the inverse ponderal index (height/weight$^{1/3}$) to represent the three components of drag namely frictional, pressure and wave drag. According to the findings both the chest girth and the ponderal index influence significantly performance. Maiello *et al.* (1998) conducted a similar study to Jiskoot and Clarys (1975) with female participants this time. The researchers towed on surface level and at 50cm below the water surface eleven female swimmers. The participants were towed at two different velocities (1.76 ms^{-1} and 1.91 ms^{-1}) and the results showed 19% lower drag values when measured below the water surface. These findings concur to those of the Lyttle *et al.* (1998) and are conflicting to those of Jiskoot and

Clarys (1975). Contradictory findings between similar studies raise some questions about the accuracy of the methodologies followed. It is apparent that Lyttle *et al.*'s (1998) experimental set up is scientifically established and the findings of the study not only confirm the theoretical computations but also correlate positively to the results scouted with the use of other methodologies (Vennell, Pease and Wilson, 2006; Pease and Vennell, 2011). However, the measurement of resistive forces when the swimmers were towed at constant speed is limiting the applicability of the findings directly by the athletes. Swimmers decelerate as they glide and it is reasonable to believe that unsteady mechanisms throughout a non steady glide might affect the impact of gliding depth on total drag.

Vennell, Pease and Wilson (2006) as well as Pease and Vennell (2011) used a flume and mannequins of only the male form for the first study and of both the male and the female form for the second study to assess the effect of gliding depth on wave drag. In their studies the mannequins were attached to a rod to minimize other equipment interference and were towed at depths from 0m to 1m at intervals of 0.1 m while velocity ranged from 0.4 ms^{-1} to 2.6 ms^{-1} at intervals of 0.2 ms^{-1}. According to the findings, drag values reached a maximum value when the mannequins were towed at the surface whereas the least drag value was reported for the glides that the depth was greater than 1.8 times the chest depth. When the drag values of the male mannequin were compared to the drag values of the female mannequin (Pease and Vennell, 2011) it was found that the contribution of wave drag to total drag was significantly higher for the female mannequin when towed at the surface. Such findings are important to understand in details the relative contribution of gliding depth and morphology upon hydrodynamic resistance particularly when the experimental set up is that much controlled and so similar to that of vessel hydrodynamics investigation (Hertel, 1966). However, it is essential that glides with unsteady velocity are also assessed.

The numerical technique of CFD has also been applied to examine the effect of gliding depth on wave drag (Machado *et al.*, 2010). The 3D model was positioned and analysed at depths of 0m, 0.1m, 0.5m and 0.9m from the water surface at

velocities of 1.5 ms^{-1}, 2.0 ms^{-1} and 2.5 ms^{-1}. Results suggest that drag decreases as the gliding depth increases. However, in this study the effect of the bottom of the pool is not considered, only the steady state condition is measured and also key methodological approaches are not mentioned.

Limitations of the aforementioned experimental studies (mannequins tested and not actual swimmers, in a flume and not in an actual swimming pool environment, when the swimmers were attached to devices and not freely gliding and finally by measuring the drag forces when the velocity was steady and not decreasing) as well as omission of key conditions of the computational methodologies followed, necessitate further experimental and computational analysis to clearly identify the relative contribution of wave drag when gliding at varying depths.

None of the previous studies has investigated the gliding depth effect on gliding performance when the velocity of the participants is decreasing. Unsteady mechanisms could potentially affect the hydrodynamics and alter the research findings.

The purpose of the current study was to evaluate the effect of gliding depth on glide performance for actual swimmers of both gender when gliding freely (and were not attached to any external device) in a swimming pool environment.

5.2. Method

A male and a female swimmer of international level whose anthropometrical characteristics are presented in details in Chapter 3 were recruited. The general methodological approach is described in detail in Chapter 3. The study specific protocol involved additional information for the gliding depth after the push from the wall. Participants (whose details are presented in Chapter 3) were instructed to push from the wall and glide in the streamlined position at four different depths; i) at 0.8 m ii) 0.6 m iii) 0.4 m and iv) 0.2 m from the water surface as illustrated in Figure 5.2.

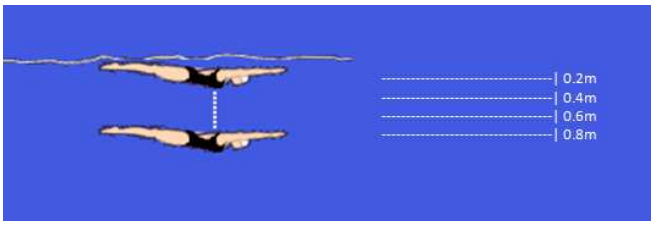

Figure 5.2. Participants performed controlled glides at a depth 0.8m, 0.6m, 0.4, and 0.2m from the water surface

Participants were asked to retain a streamlined position and also keep their head between their arms and the same joint angles for all glide depths tested. The side of the pool was marked to assist the swimmers to identifying the required gliding depth. The gliding depth, the angle of attack and the joint angles were monitored throughout the glides and the swimmers were informed after each glide whether any of the inspected variables were not adequately controlled and the trial had to be repeated. Ten successful trials were required for the analysis of the findings and participants performed so many glides so that there would be ten successful trials for each condition tested.

The video recordings were imported to the 'Glide Coach' software for digitising where MATLAB routine was used to apply the 'Hydro-Kinematic' method (Naemi and Sanders, 2008) and compute the glide factor values for each trial.

5.2.1. Statistical analysis

The Microsoft Office Excel (2007) and the Statistical Package for Social Sciences (SPSS, version 19) were employed for the data analysis.

For the gliding depth assessment, the dependent samples T-Test was used to evaluate the effect of the independent variable (the gliding depth) on the glide factor. Pooled standard deviation was computed for each set of data according to Equation 5.1 to assist with the computation of the Effect Size.

$$SD_{pooled} = \sqrt{\frac{(N_1 - 1)SD_1^2 + (N_2 - 1)SD_2^2}{N_1 + N_2 - 2}}$$ Equation 5.1

N_1 and SD_1 are the number of trials and the standard deviation of the first set of data whereas N_2 and SD_2 are the number of trials and the standard deviation of the second set of data.

Equation 5.2 was used to compute the Effect Size and assess the magnitude of difference in the Glide Factor values between the different depths tested.

$$Effect\ Size = \frac{M_1 - M_2}{SD_{pooled}}$$ Equation 5.2

M1 and M2 are the mean values of the first and second set of data.

The Effect Size was computed for each pair of gliding depths.

5.3. Results

Four different gliding depths were examined in the present study and the results comprise kinematic data and Glide Factor results. The differences between the different conditions assessed are determined by examining the C_G values for each gliding depth measured.

The C_G values reported represent the average C_G values for each condition tested. The bars represent the Standard Error of the Mean (Figure 5.3 and Figure 5.4).

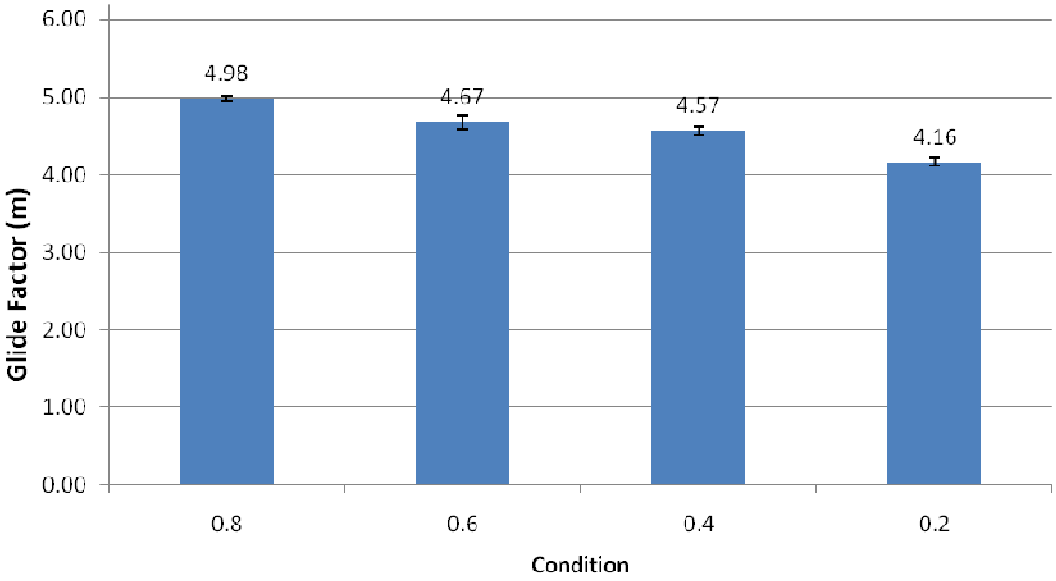

Figure 5.3. Glide Factor values reported for each depth tested for the male participant. Bars represent the Standard Error of the Mean.

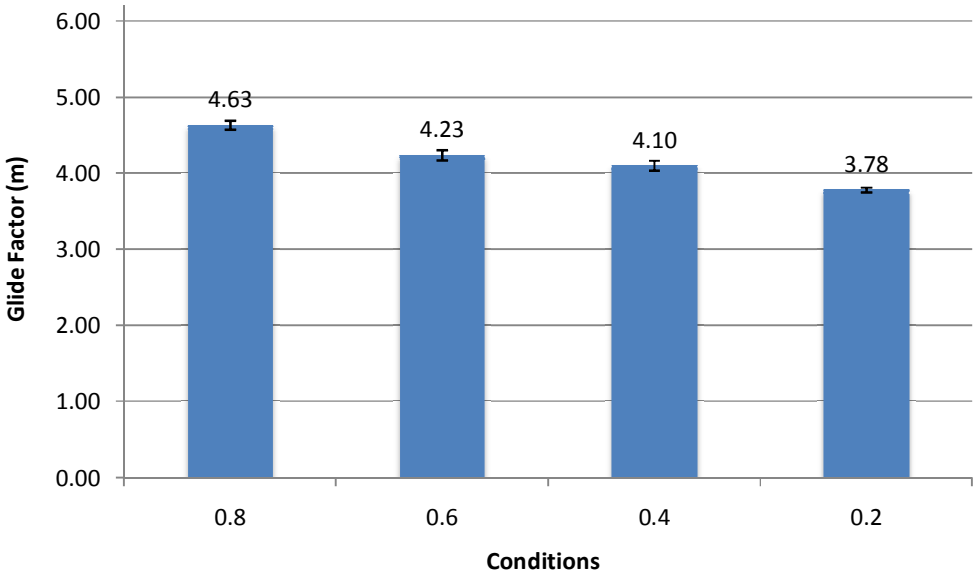

Figure 5.4. Glide Factor values reported for each depth tested for the female participant. Bars represent the Standard Error of the Mean.

Table 5.1 shows the SD_{pooled} data, the Effects Sizes and the significance levels obtained from the dependent-samples T-test comparison between the glide factor values of all the conditions tested.

Table 5.1 SD_{pooled} data, significance levels and Effect Sizes for each swimmer and for all four glide depths tested.

		SD_{pooled}	Significance level	Effect Size
MALE	0.8 m/0.6 m	0.212	.004	1.462
	0.8 m/0.4 m	0.146	.000	2.859
	0.8 m/0.2 m	0.147	.000	5.569
	0.6 m/0.4 m	0.234	.324	0.457
	0.6 m/0.2 m	0.235	.000	2.171
	0.4 m/0.2 m	0.177	.000	2.275
FEMALE	0.8 m/0.6 m	0.200	.000	1.969
	0.8 m/0.4 m	0.192	.000	2.759
	0.8 m/0.2 m	0.144	.000	5.898
	0.6 m/0.4 m	0.211	.166	0.641
	0.6 m/0.2 m	0.169	.000	2.690
	0.4 m/0.2 m	0.159	.000	2.005

The angle of attack as well as the gliding depth was monitored at all times and participants had no difficulty to control their body posture even when gliding closer to the water surface.

5.4. Discussion

The glide factor figures generally show a decreasing tendency as the participants glide closer to the surface. These findings are in agreement with previous studies assessing the effect of swimming depth on performance (Webb, Sims and Schultz, 1991) and also agree closely with findings from wave drag assessment studies for vessels (Hertel, 1966) and actual swimmers when the velocity was steady (Lyttle *et al.*, 1998, Maiello *et al.*, 1998; Vennell, Pease and Wilson, 2006; Machado *et al.*, 2010; Pease and Vennell, 2011).

The glide efficiency was assessed with the use of the glide factor. The glide factor provides an accurate indication of the efficiency of swimmers' glides while accounting differences in body sizes between individuals as well as differences in

velocities that might encounter either between trials of the same person or between trials of distinct individuals. This way a direct comparison between glides covering a range of velocities and also a range of somatotypes is possible and can provide an accurate indication of the efficiency of the glide; enabling both within and between subject comparisons.

Significant differences in C_G values for almost all conditions tested indicate that the effect of wave generation is affecting the glide efficiency of swimmers when gliding close to the surface.

As reported by Lyttle (1998), swimmers should glide at a depth of 0.4 m below the water surface for velocities ranging from 2.2 ms^{-1} to 3.1 ms^{-1}. However, deeper glides than 0.6 m were not assessed by Lyttle (1998). According to the results of the current study, the optimum glide efficiency was reported for a gliding depth equal to 0.8 m from the water surface.

A significant difference between each pair of gliding depths was reported besides the pair corresponding to 0.6 m and 0.4 m depth. Similar findings were also reported by Lyttle *et al.,* 1998 who examined the glide phase for the same depths for forty male swimmers. In their case, the participants were towed and the velocity was steady. This finding suggests that probably the same principles prevail either when the velocity is steady or decreasing. It would be interesting to examine what happens when the water flow around the swimmers is simulated and the resistive forces are computed with the use of CFD for both a steady state condition when the velocity is not changing and a transient condition when the velocity is decreasing.

An average gain of 36 cm for the male participant and 16 cm for the female participant in gliding length when choosing the optimum gliding depth in comparison to gliding close the surface (for glides of 1.5 s), highlights the significant effect of wave drag upon gliding performance. The difference in the gained advantage

between the male and the female participant is related to the different in the gliding velocity.

5.5. Conclusion

The results of this study provide information about the effect of wave drag on swimmers. With the use of the Hydro-Kinematic method the added mass was taken into account when assessing the effect of the independent variable (gliding depth). It was concluded that the glide efficiency is significantly affected by the gliding depth both for male and female swimmers while the depth at which the swimmers are affected less by drag is 0.8 m from the water surface. A non invasive approach was employed and kinematic data were used to assess the glide efficiency of decelerating glides.

5.5.1. Limitations and recommendations

In this study the glide efficiency was assessed for glides at four different depths; with 0.2 m being the closest to the water surface. As in previous towing studies (Lyttle, 1999) it was not possible to assess the effect of wave drag on glide performance for glides even closer to the surface as the duration of the glide phase analysed (1.5 s) was too long for the swimmers to maintain a steady position when parts of the body were above the water surface. It is suggested that the numerical technique of Computational Fluid Dynamics could be applied to extend the study and examine the case when the water surface is penetrated and a significant part of the body exceeds the liquid medium. Furthermore, it is hypothesised that the gliding efficiency might have been even higher if greater depths would have been also assessed. However, the maximum pool depth limitations (2m depth) prevented the assessment of greater depths due to the potential effect of the pool bottom in gliding performance.

The findings of this study will allow the swimming coaches to better design the gliding strategy of their athletes in order to further improve their performance.

Chapter 6

Study 3: The effect of full body swimsuits on glide performance

6.1. Introduction

Full body swimsuits introduced in 1998 by Adidas (Mountjoy *et al.*, 2009) and ratified in 2000 for the Sydney Olympic Games (Craik, 2011) established a new era in competitive swimming. Their launch allowed numerous world records to be broken while regular improvements in design and materials allowed a continuum in achieving faster swimming times. Research, investigating the evolution of swimmers' performance between 1990 and 2009 demonstrated a burst of more than 2% for both male and female athletes after 2000 when full body swimsuits were introduced allowing swimmers to perform beyond their previous limits (Berthelot *et al.*, 2010). Furthermore, the number of world records broken per year increased significantly after 1998 (Figure 6.1) highlighting the effect of technology and innovation on performance.

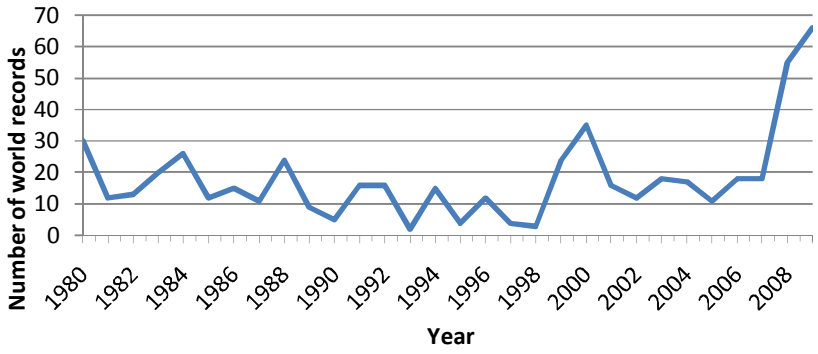

Figure 6.1The number of world records broken per year in swimming. Source: Swimming Statistics (http://www.scmsom.se/)

The second peak in the graph (in 2008) showing the number of world records broken per year (Figure 6.1) coincides with the introduction of the third generation of full body swimsuits. Polyurethane costumes made from industrial polymers were preferred by most of the top athletes participating to high level competitions. Swimmers' preference for particular brands and models such as the LZR made by Speedo at the Beijing 2008 Olympic Games and the Jaked01 made by Jaked at the Rome 2009 World Championship (Neiva *et al.*, 2011) indicate a potential advantage when compared to other competitive products of the time even though no scientific evidence was published at that time to support athletes' choices. At the Beijing 2008 Olympic Games 23 out of the 25 world records were broken by athletes wearing the Speedo LZR swimsuit and 94% of all gold medals were won by athletes wearing the same suit. Moreover, between April 2008 and November 2009, 40 out of the 41 records were broken by swimmers wearing the Speedo LZR (Mountjoy and McKeon, 2009). At the Rome 2009 World championship, 43 records were broken throughout the event when most of the swimmers chose to wear full body swimsuits (Neiva *et al.*, 2011). 47.07% of the male front crawl finalists chose to wear the Jaked01 suit at the same event (Neiva *et al.*, 2011).

But how do full body swim suits improve performance? Manufacturers claim that full body swimsuits streamline the body through a compression system that stabilizes the core and assists the swimmer to maintain a hydrodynamic posture, decrease skin friction drag with the use of low friction materials, and finally reduce muscle oscillation and skin vibration by applying a constant and firm force to the covered skin. The overall aim of all the aforementioned characteristics is performance improvement through pressure and friction drag reduction as shown in Figure 6.2. The red caption in Figure 6.2 indicates the variables if interest.

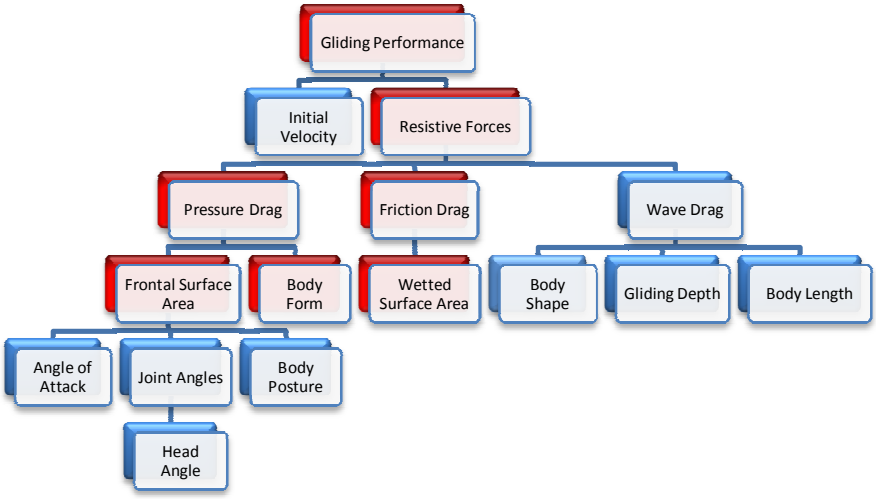

Figure 6.2 The factors affecting gliding performance.

The role of swimsuits in competitive swimming has been discussed by scientists from a philosophical point of view in an attempt to identify whether fairness is still evident and the 'spirit of sport' is implemented (Carr, 2008; Wood, 2008; Mountjoy and McKeon, 2009; James, 2010; Mayes, 2010; Craik, 2011; Partridge, 2011) but also from a performance point of view in an attempt to identify the mechanisms enhancing performance (Benjanuvatra *et al.*, 2002; Toussaint, 2002; Mollendorf *et al.*, 2004; Pendergast *et al.*, 2006; Rogowski *et al.*, 2006; Chatard and Wilson, 2008; Moria *et al.*, 2010; Moria *et al.*, 2011) and also explore the metabolic consequences when wearing the full body costumes (Rober *et al.*, 2003).

The majority of the previous performance related studies aiming to assess the benefit of wearing a full body swimsuit focused on evaluating the drag forces experienced when the athletes were towed either in a flume (Chatard and Wilson, 2008), in an annular pool (Mollendorf *et al.*, 2004; Pendergast *et al.*, 2006) or in a typical swimming pool (Benjanuvatra *et al.*, 2002). Passive and not active drag measurement techniques were chosen in an attempt to avoid including non-controlled variables in the experimental design.

Chatard and Wilson (2008) tested in the flume young, competitive and masters level swimmers when wearing normal, FB and waist to ankle suits for a period of 10 s.

The swimmers were towed on the surface after a maximal inspiration and while holding their breath; when at the same time a load cell, mounted above the water surface, was recording the passive drag values. According to the research findings, on average there was a significant reduction in passive drag equal to 6.2% ±7.9%. However, even though the effect of wearing a full body swimsuit was assessed and significant differences were found between the conditions tested, the effect of decrease in velocity when the swimmers glide after a push as well as the fact that swimmers glide underwater and not on the water surface, was not considered.

Mollendorf *et al.* (2004), besides measuring the resistive forces experienced when the swimmers were towed at the surface of an annular pool, evaluated the drag forces measured when gliding after a start or a turn with the use of the 'swim meter'. The swim meter' measures the gliding distance and the decrease in instantaneous velocity as a stainless steel wire, attached to an aluminium collar on one side and to the swim meter on the other side, is pulled out of the device (Craig and Pendergast, 1979). Even though this is the first attempt to consider that changes in velocity do affect the measured drag force when assessing the effect of wearing a full body swimsuit, experimental limitations undervalue the importance of the findings. A gliding duration of a few seconds makes it difficult for the athlete to maintain the same posture and consequently the drag force measured includes resistance induced by the body movement. Moreover, the added mass effect (mass of the water travelling along with the body) is ignored and the virtual mass is considered to be equal to the mass of the body of the swimmer. As a result the drag values measured are underestimated (Vogel, 1994). Furthermore, the velocity and the displacement data collection encompass limitations. As the wire is pulled out of the "swim meter" device, the rate of unreel that is used to compute the gliding velocity and gliding distance, is affected by the movement of the atlanto-occipital joint, the changes in the angle of attack and the contact of the wire with the body.

Pendergast *et al.* (2006) passively towed on the surface of an annular pool both male and female swimmers to assess the effect of turbulators (circular wires around the circumference of the body) on the vortex formation interruption and potentially the

reduction of the size of the wake. The turbulators were positioned at the height of the upper back, the chest and the buttocks and according to the results of the study pressure drag decreased significantly and reached the least value when all turbulators were used. However, the brand and the characteristics of the full body suit used for the requirements of the study are not specified and comparison has not been made against normal competitive suits. Moreover, the researchers did not consider that the volume of the wake is not steady when the velocity is dropping; which is the case when the athletes glide in competition after starts and turns.

Benjanuvatra *et al*. (2002) towed male and female swimmers both on the surface and under the water of a normal swimming pool with the use of a mechanical winch and according to the research findings, the swimmers experienced on average 10.2% less drag force when wearing the FB suit. However, as in previous studies (Chatard and Wilson, 2008 and Pendergast *et al.*, 2006) the velocity was kept constant throughout the whole glide. In addition, the differences reported in the net drag forces were considered to be due to the lower frictional resistance of the FB suit material and the researchers did not consider that the morphology of the body changes when wearing the FB suit and as a result pressure drag is expected to change as well.

All of the studies described demonstrate a significant advantage when wearing FB suits. Nevertheless, methodological limitations reduce the accuracy of the reported data. By towing the athletes on the water surface, the wave component of drag significantly contributes to the total measured resistance. Decomposition of total drag to the pressure, friction and wave drag contributions can then only be achieved with the use of theoretical models that introduce additional sources of error. Moreover, the waves of the water surface make it more difficult for the swimmers to maintain a streamlined posture and considering that even small alterations in the angle of attack affect the frontal surface area (FSA) (appendix B), it is reasonable to suggest that underwater analysis could increase the accuracy of the reported data. Considering also that in competition the gliding velocity is constantly reducing and that the volume of wake is constantly changing, the experimental design should include glide performance assessment under transient conditions (while the velocity is dropping).

Therefore, the purpose of the current study was to assess the effect of full body swimsuits in glide performance. It is hypothesised that the performance advantage when wearing the full body suit is directly linked to changes in swimmer's morphology. By concept, the aim of the full body suits is to reduce the friction and the pressure contribution of drag, and as such, the wave contribution in this case was eliminated by performing the glides under the water surface.

6.2. Method

A male and a female swimmer of international level, whose anthropometric characteristics are described in details in Chapter 3, volunteered to participate to the study.

The general testing protocol that involves information about the testing environment, the testing equipment and the familiarisation procedures, is described in detail in Chapter 3. For the requirements of this study, the swimmers performed 10 successful controlled glides with their normal competitive swimsuit and also 10 successful controlled glides when wearing a third generation (polyurethane) full body swimsuit. The glides were considered successful when the angle of attack and the joint angles remained constant and also no lateral deviations from the desired rectilinear gliding path were evident. In this case, the Speedo LZR and the Jacked01 costumes were employed while the body surface area covered for both types of suits was from the shoulders to the ankles (Figure 6.3b).

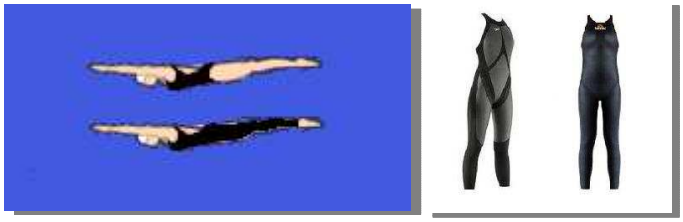

Figure 6.3 a) The normal and full body swimsuit condition tested b) The Speedo LZR and the Jacked01full body suit.

After getting marked, the swimmers submerged in the water, exhaled in order to achieve neutral buoyancy that would help them remain horizontal and performed the

glides in a rectilinear direction. To avoid any wave drag interference when collecting the data the swimmers were instructed to glide at a depth of 0.8 m from the water surface. Moreover, the trials that the athletes did not succeed in controlling their posture or the gliding depth were repeated.

The 'Glide Coach' software was employed for the data collection and also for the computation of the Glide Factor (C_G) with the use of the 'Hydro-Kinematic' method (Naemi and Sanders, 2008). Besides the C_G values, the position data of the wrist, the shoulder, the goggles, the hip, the knee and the ankle joint were extracted and the joint angles were computed. This information was used afterwards to prescribe the posture the swimmers should take when getting scanned with the use of a 3D body scanner as described in Chapter 3. The swimmers were scanned when wearing both their normal and their full body swimsuit in an attempt to measure the FSA in both cases and identify any difference in the reported values due to the use of the FB suit.

To identify whether any buoyancy benefit was evident when wearing the FB suit, the body mass was assessed in the water with both types of swimsuits after exhaling and tucking as described in the general method section of this thesis (Chapter 3).

The cross sectional area of the swimmers in the axial plane was computed for the whole body (every one centimetre) in order to assess the effect of the suit to the morphology of the body. The scanned 3D models of the male and the female swimmer are shown in Figures 6.4 and 6.5.

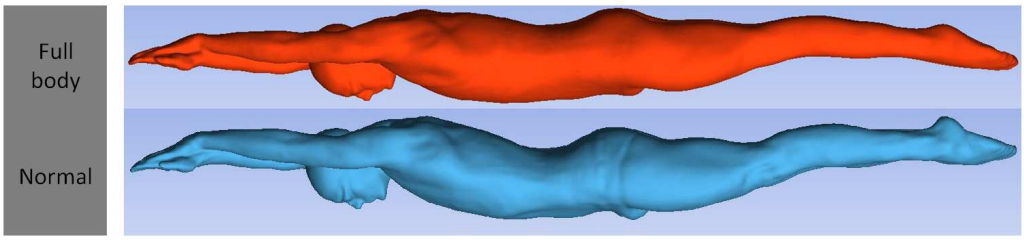

Figure 6.4 The male participant when wearing the full body and the normal swimsuit.

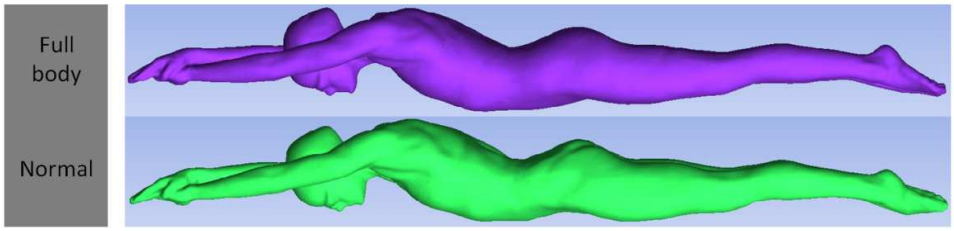

Figure 6.5 The female participant when wearing the full body and the normal swimsuit.

6.2.1. Statistical analysis

The findings of the study were analysed with the use of the Microsoft Office Excel (2007) software and the Statistical Package for Social Sciences (SPSS, version 19). Normality of the distribution was assessed with the Shapiro-Wilk test. To evaluate the effect of the FB swimsuits on gliding performance (glide factor) the dependent-Samples T-Test was employed. Pooled standard deviation was computed for each set of data according to equation 6.1 to assist with the computation of the effect size.

$$SD_{pooled} = \sqrt{\frac{(N_1 - 1)SD_1^2 + (N_2 - 1)SD_2^2}{N_1 + N_2 - 2}} \qquad \text{Equation 6.1}$$

N_1 and SD_1 are the number of trials and the standard deviation of the first set of data whereas N_2 and SD_2 are the number of trials and the standard deviation of the second set of data. The Effect Size was computed to assess the magnitude of difference in the glide factor between the different head positions tested according to equation 6.2.

$$Effect\ Size = \frac{M_1 - M_2}{SD_{pooled}} \qquad \text{Equation 6.2}$$

M1 and M2 are the mean values of the first and second set of data.

In this study the effect size was computed by subtracting the mean of the full body swimsuit C_G value from the mean of the normal swimsuit C_G value when comparing the two conditions.

6.3. Results

Two types of swimsuit were compared in this study and the performance related results comprised the glide factor values representing the glide performance of the swimmers. Furthermore, the FSA was computed for both conditions tested to identify whether the full body suit affected the streamline of the body. The cross sectional area in the axial plane was also computed for the whole body to identify any differences in the morphology of swimmers' body.

6.3.1. Glide factor

Figures 6.6 and 6.7 demonstrate the glide factor reported for the male and the female swimmer respectively. Table 6.1 presents the Effects Sizes and the significance levels obtained from the dependent-samples T-test analysis performed for the glide factor values of both participants. Table 6.1 presents the mass of both swimmers when wearing their normal and FB swimsuit.

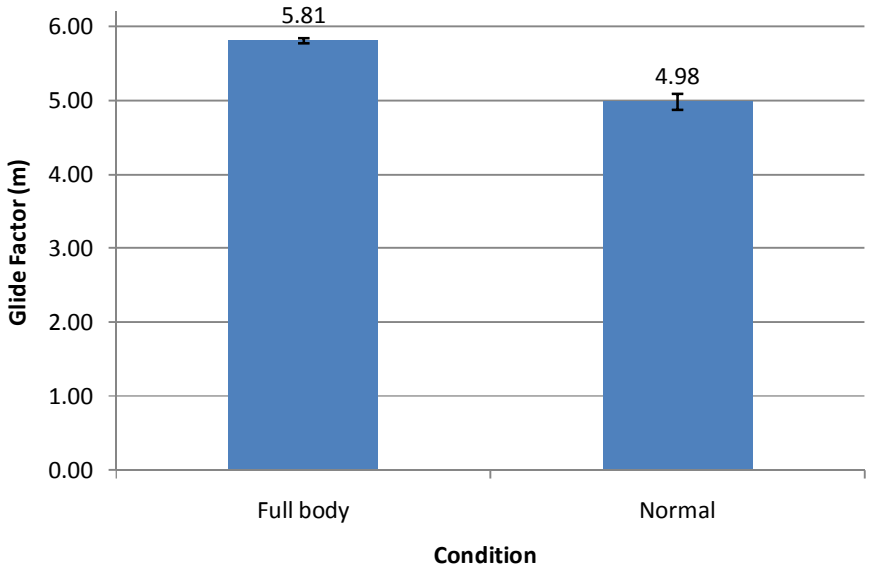

Figure 6.6 Glide Factor values reported for each condition tested for the male participant. Bars represent the Standard Error of the Mean.

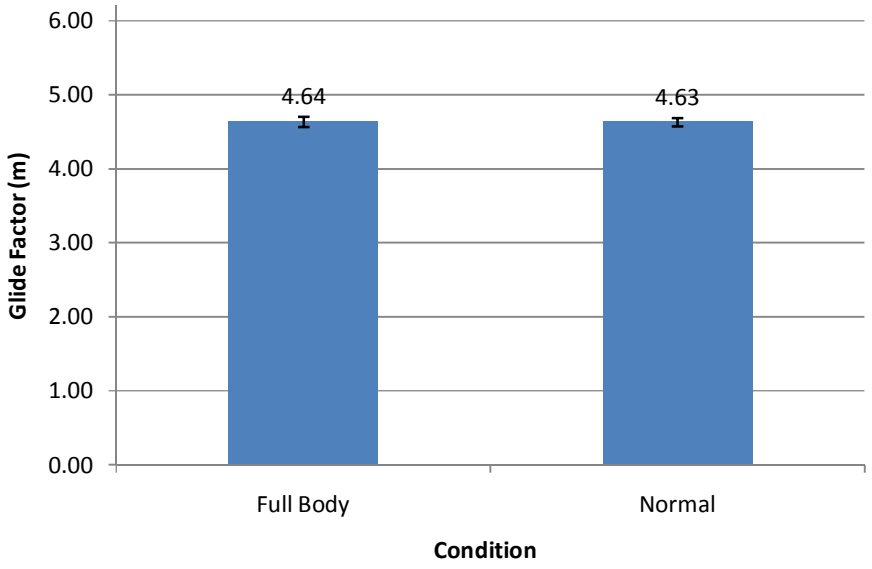

Figure 6.7 Glide Factor values reported for each condition tested for the female participant. Bars represent the Standard Error of the mean.

Table 6.1 SD_{pooled} data, significance levels and Effect Sizes for both swimmer.

		SD_{pooled}	Significance level	Effect Size
MALE	Full Body/Normal	0.249	0.000	3.317
FEMALE	Full Body/Normal	0.203	0.948	0.036

Table 6.2 Mass and standrard deviation values of both swimmers when wearing the normal competitive and the full body polyurethane swimsuit.

	Mass with the normal suit (kg)	Mass with the FB suit (kg)
MALE	3.30 (0.10)	3.27 (0.12)
FEMALE	2.87 (0.06)	2.80 (0.00)

6.3.2. Frontal Surface Area

Figure 6.8 and 6.9 show the frontal surface area for the male and the female participant when wearing the normal and the full body swimsuit.

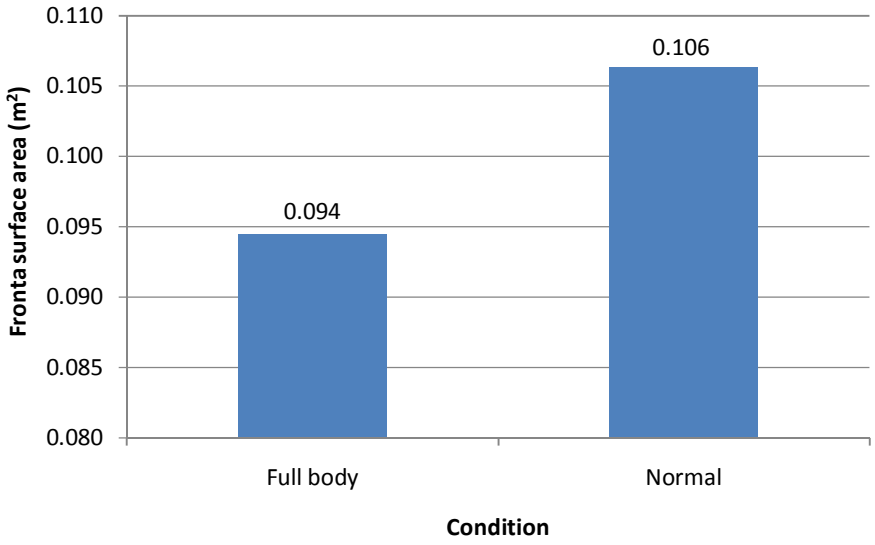

Figure 6.8 Frontal surface area values reported for each condition tested for the male participant.

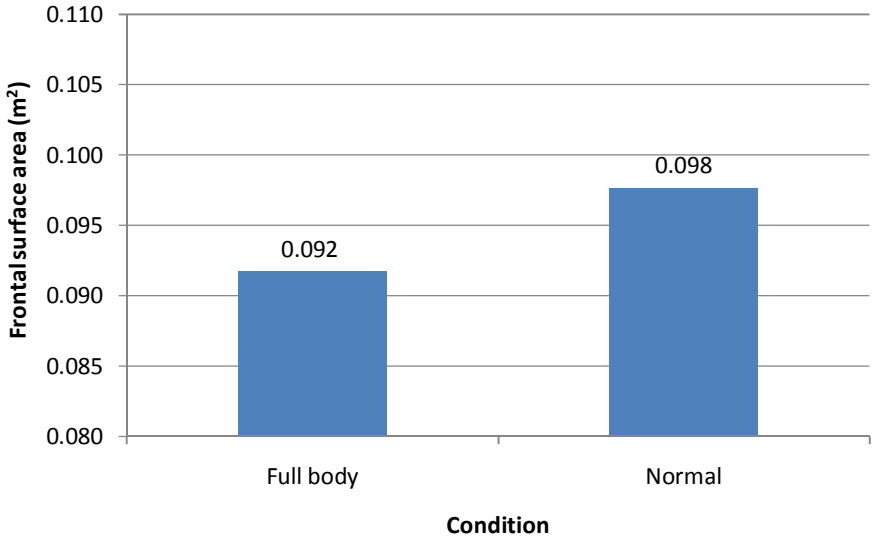

Figure 6.9 Frontal surface area values reported for each condition tested for the female participant.

6.3.3. Cross Sectional Area Measurement

Figures 6.10 and 6.11 show the cross sectional area in the axial plane for the whole body of the male and the female participant when wearing their normal and FB suit. The blue line describes the cross sectional area when wearing the FB suit whereas the red describes the cross sectional area when wearing the normal suit. The arrows indicate the sections of the body that difference in the cross sectional area is observed and is expected to affect performance.

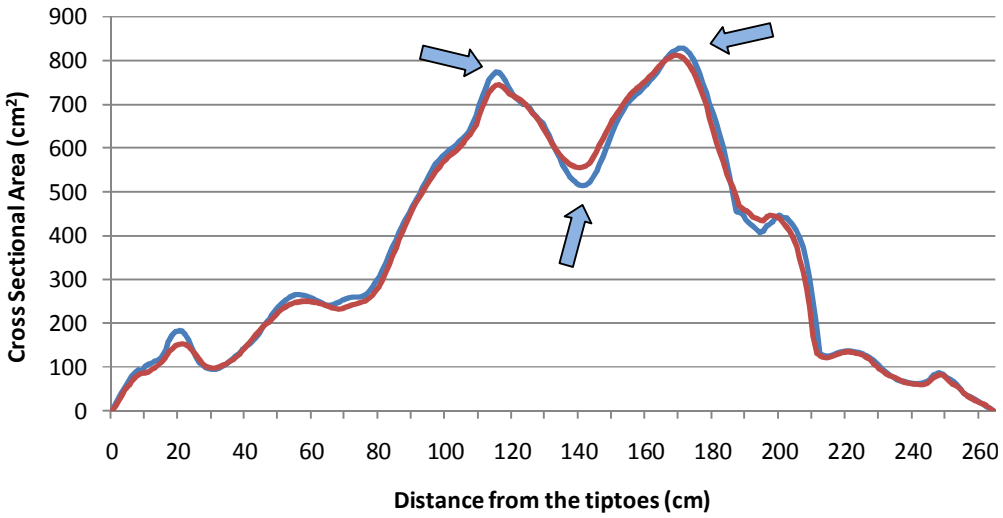

Figure 6.10 Cross sectional area values reported for each condition tested for the male participant.

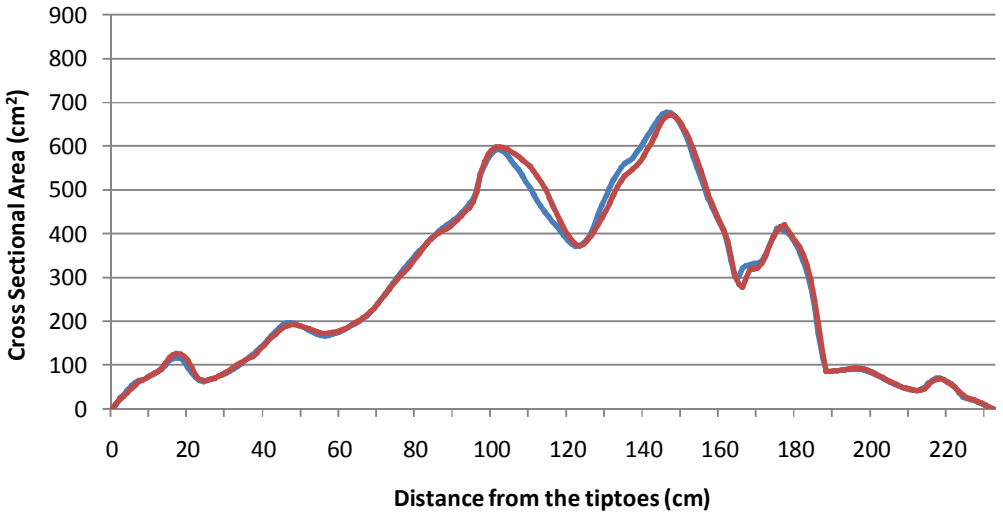

Figure 6.11 Cross sectional area values reported for each condition tested for the female participant.

6.4. Discussion

Swimming performance is determined by the magnitude of propulsive and resistive forces. In this study, the effect of the full body polyurethane swimsuits in gliding

performance has been assessed in an attempt to identify the relative advantage in competition.

According to the findings there was no significant hydrostatic mass difference between the two conditions tested for both swimmers indicating no buoyancy benefit. These findings are in accordance with previous studies (Benjanuvatra *et al.*, 2002; Chatard and Wilson, 2008) that also found no buoyancy advantage when wearing the FB suits.

Swim suit manufacturers claim that FB suits not only decreases friction drag but also change the shape of the swimmer and support them to maintain a more streamlined position. From the findings of this study it is clear that the frontal surface area of the swimmers decreased. It is also evident from the full body cross sectional measurements that the swimmer's shape became more hydrodynamic and that certain areas of the body have been compressed whereas cavities (for example at the lower back) have been covered by the suit. Figure 6.10 shows the cross sectional area measurements for the male swimmers when wearing the normal (blue line) and the full body (red line) swimsuit. The total height of the swimmer in the streamlined position was 264 cm and the cross sectional area was computed for every single cm in the axial plane (264 measurements overall).The two highest peaks in the graph correspond to the pelvis (left peak) and the thorax (right peak) whereas the trough between the two peaks corresponds to the lower back. It is clear that the suit decreased the cross sectional area for the pelvis and the thorax while increasing the cross sectional area for the lower back indicating that the surface of the swimmer's body had been flattened. However, this is not the case for the female swimmer. The FS suit did not compress the thorax and the pelvis and moreover did not increase the FSA at the level of the lower back. It is either the case that the swimmer did not select the optimum suit for her body shape or that the level of tension was not enough to change the morphological characteristics of the body. For the male swimmer the thorax cross sectional area, that corresponds also to the maximum cross sectional area of the swimmer, decreased by 1.95% whereas the pelvis cross sectional area decreased by 3.67%. The cross sectional area at the level of the lower back increased by 8.21%. For the female swimmer the thorax cross sectional area

decreased by 0.92% whereas the pelvis Cross Sectional Area increased with the FB suit by 1%. The cross sectional area at the level of the lower back increased by 0.39%.

These findings suggest that the advantage in gliding performance was a result of the morphological changes of the athletes' body. There are no similar findings in the literature comparing morphological differences when wearing FB suits. However, there have been other attempts to describe the morphology of swimmers' body such as the fineness ration (Naemi, 2007) with less success. Cross sectional measurements of 3D models have been presented only by Pease and Vennell (2011) before to describe the morphology of a male and female mannequin whose morphology was imitating that of elite level swimmers. In their case the effect of the FB suits could not have been assessed given that the mannequins were made out of solid non compressed material.

Even though full body swimsuits have been replaced by waist to knee suits for the male athletes and shoulder to knee suits for the female athletes since the beginning of 2010, understanding the hydrodynamics involved can help manufacturers to improve the design of suits that cover less parts of the body or even develop different types of suits for learners.

The same methodological approach can also be used to analyse the new waist to knee suits given that companies nowadays tend to increase the size of the suits slightly over the hips (launch of FASTSKIN3 by Speedo in November 2011) possibly in order to cover as many areas as possible.

6.5. Conclusion

The advantage in gliding performance when wearing a FB swimsuit relies on the changes in the morphological characteristics of the swimmer. This is the first time the deformation when wearing a FB suits is assessed and also the effect of the body morphology in gliding performance is examined.

The practical outcome of this study for the coaches and the swimmers is also important. Careful selection of the best suit is necessary to achieve optimal performance. Compression of the thorax and the pelvis area as well as coverage of the cavity of the lower back is essential to improve the streamline of the body.

6.5.1. Limitations and recommendations

It would be very interesting to see how the water flow is affected by the changes in morphology of the swimmers' body. CFD analysis of the scanned models could shed more light and help us compute the changes in drag in the areas of interest.

Chapter 7

Study 4: Glide performance assessment with the use of Computational Fluid Dynamics

7.1. Introduction

Performance in swimming depends on the interaction of both propulsive and resistive forces (Alexander and Goldspink, 1977 and Toussaint *et al*., 1991). In the glide phase of starts and turns, no propulsive forces are generated and performance depends exclusively on the magnitude of the resistive forces. In this phase the swimmer is passively gliding and for this reason the measured forces are also referred to as passive drag forces. For the assessment of the passive drag forces, a number of different approaches with varying degrees of error have been suggested by researchers involving either direct or indirect measurement techniques.

Direct passive drag measurement techniques have been applied since the beginning of the 20th century when Dubois-Reymond (1905) tried to measure the magnitude of passive drag with the use of a dynamometer by towing the subjects behind a rowboat. Even though no study validating the accuracy of the method has ever been published, the approach followed would not be considered reliable today since a number of interfering variables cannot be controlled. These include the velocity of the boat, the effect of sea waves, and the tension of the cord connecting the swimmer with the dynamometer. Since 1905, the testing technologies have improved and the methods have advanced. Numerous studies involving direct measurement of the resistive forces have been conducted either in a pool by towing the swimmers with the use of a pulley system and measuring the resistive force with a load cell or a dynamometer

(Amar, 1920; Karpovich, 1933; Alley, 1952; Counsilman,1955; Hairabedian, 1964; Kent and Atha, 1971; Van Manen and Rijken, 1975; Clarys *et al*., 1974; Jiskoot and Clarys, 1975; Clarys and Jiskoot, 1975; Clarys 1978a; Clarys 1978b; Clarys, 1979; Chatard *et al*., 1990; Sheehan and Laughrin, 1992; Kolmogorov and Duplisheva, 1992; Sheehan and Laughrin, 1992; Klauck, 1998; Lyttle *et al*., 1998; Lyttle *et al*., 1999; Benjanuvatra *et al*., 2001; and Mollendorf *et al*., 2004) or in a flume when the swimmer was holding a handle and drag was measured with a load cell (Miyashita and Tsunoda, 1978; Maiello *et al*., 1998; Roberts *et al*., 2003; Chatard and Wilson, 2003; and Vennell *et al*., 2006). However, even the contemporary studies involve sources of error, the swimmer is always attached to the measuring device and the gliding velocity is constant and so the swimmer is not gliding freely. Furthermore, both when towing a swimmer in a pool or in a flume, difficulties with maintaining a horizontal position are expected to increase the error involved with the measurement, particularly when different towing velocities are examined since the legs of the swimmers tend to rise when the towing velocity increases. The error associated with the force measurement device has not been assessed previously and it is expected to add to the total error. For instance hysteresis, that is the difference in the load measured when approaching a certain value with increasing and decreasing force, is expected to be evident as the force applied in the towing studies is not only increasing or only decreasing.

Indirect passive drag measurement techniques involve video based kinematic analysis (Klauck and Daniel, 1976; Oppenheim, 1997; Naemi and Sanders, 2008; and Elipot *et al*., 2009). This approach was introduced years after the towing devices were first used and coincided with the technological advances in cinematography. With the kinematic analysis the drag forces are computed when the swimmer is freely gliding without being attached to a device. This is an advantage when compared to the towing method but an equally significant source of error is involved with this approach. The mass of the water that is dragged with the swimmer called added mass, contributing to drag, cannot be calculated. The mass of the dragged water was found experimentally to be 26.8 ±2.3% of the subject's total mass (Caspersen *et al*., 2010) indicating a significant effect on drag force.

Computational fluid dynamics (CFD) is a third category of methods to assess glide performance. CFD is a numerical method used to simulate flow by solving the discretized form of the 3D governing equations of flow (namely, the continuity or conservation of mass and the Navier-Stokes (NS) equations or conservation of momentum) under geometry and flow-specific boundary conditions. The domain to be simulated is discretized into smaller 3D regions called cells (discretization/meshing) and calculations are carried out for each one of them. The accuracy of the method relies on the density of discretization (or grid/mesh density, the accuracy is better at high grid densities) employed as well as the turbulence flow model selected. The presence of eddies, that is circular flow patterns, and their unsteady nature is central to any turbulent flow and hence accurate resolution of the eddies both in space and time is essential. Eddies occur due to tiny but chaotic fluctuations in the mean flow. The main classes of turbulent models available for resolution of these eddies are: the RANS (the Reynolds Averaged Navier-Stokes) equations which use approximate closure relations for resolving the Reynolds stress term which is necessary to predict the motion of eddies, the LES (Large Eddy Simulation) approach which resolves the pure NS equations for large eddies but uses closures only for eddies smaller than the cell size and the DNS (Direct Numerical Simulation) approach where pure NS equations are solved without any approximations. In terms of the accuracy and computational cost, DNS are the most accurate but the most expensive because of the need for a very dense computational grid and RANS are the least expensive but also the least accurate because of the assumptions made for resolving the eddy motion through the Reynolds stress term. LES type simulations are placed in the middle, their accuracy is not as compromised as RANS models but not as computationally intensive as the DNS models.

The possible use of CFD for the evaluation of the passive drag forces during swimming was initially reported by Bixler (1996) using the RANS type k-ε model. Later, Bixler *et al*. (2007) compared passive drag computed experimentally in the flume with that computed by CFD analysis. The study involved an experimental part where an actual swimmer and a mannequin with similar morphology to the swimmer

posing in the streamlined position were analysed in a flume for a range of velocities and also a simulation part where the 3D model of the same shape as the swimmer and the mannequin was analysed with the use of CFD for the same range of velocities. The difference between the experimental and the computational approaches was 4% for the mannequin and 18% for the swimmer. This difference indicates that the turbulence model (*k*-ε model) selected was not accurate enough. On the contrary either the LES or the DNS approach would have increased the accuracy of the simulation and the difference between the findings would be smaller.

The water flow has been simulated also around 3D full body models of swimmers to assess the magnitude of resistive forces under different conditions (Bixler *et al.*, 2007; Marinho *et al*., 2009 and Zaidi *et al.*, 2010, Table 7.1).

Table 7.1 Previous CFD studies in swimming biomechanics involving 3D full body models (the prism cell layers are employed to increase accuracy).

Author	Segment	Analysis	Cells	Prism Cell Layers	Turbulence model
Bixler *et al.* (2007)	Full body	3D	2.6×10^6	5	RANS *k*-ε & RNG & RSM in steady state
Marinho *et al.* (2009)	Full body	3D	0.9×10^6	No	RANS *k*-ε in steady state
Zaidi *et al.* (2010)	Full body	3D	N/A	No	RANS *k*-ε and RANS *k*-ω in steady state

Overall, accuracy of the numerical technique depends on the quality of the input flow and geometry data. These include accurate representation of the 3D geometry, the choice of the turbulence flow model, the use of appropriate boundary conditions and spatial and temporal discretization schemes (Ferziger and Peric, 2002).

The representation accuracy of the 3D model imported to the simulation package for swimming analysis depends on the scanner accuracy defined by the number of points used to form the cloud representing the geometry of the athlete. Bixler *et al*. (2007)

used a laser scanner to scan the entire body of an elite male swimmer and additional higher resolution scans of the head and the hands to improve the quality of the model. The same approach was also employed in the current study. Marinho *et al*. (2009) created and analysed a human shaped computer aided design (CAD) model whereas Zaidi *et al*. (2010) and Popa *et al*. (2011) used a hand held laser scanner to scan an athlete. Besides the model used by Bixler *et al*. (2007), in all other cases the human body was misrepresented either because it was not detailed enough and the mesh was not smooth (as areas at the level thorax and the ankle joint were projected whereas others at the level of the hips and the knees were recessed) or rough assumptions about segment curvature were made when designing it (as the model comprised of flat surfaces with sharp edges at the level of the joints).

Furthermore, the accuracy of the computed results is also affected by the quality of input data in order to realistically simulate the flow. As far as swimming glide analysis is concerned, key attention should be given when setting the fluid attack velocity, which is relative to the swimmer velocity, the swimmer's orientation in relation to the water flow (angle of attack) and the joint angles. Arbitrarily chosen values not related to actual reported experimental findings lead to results with no physical meaning. In all the earlier CFD studies the velocity inlet was considered to be steady. In fact, the velocity is decreasing as the swimmer is passively gliding. Furthermore, the joint angles including the angle of the elbows, the shoulders, the hips and knees and the angle of the head, were not controlled and their effect, that has been shown to affect significantly performance, was not considered. Additionally, in all cases the angle of attack was set to zero without any justification being provided.

The performance of the different turbulence models when applied for swimming glide analysis has not been assessed thoroughly. Bixler *et al*. (2007) applied the Reynolds-averaged Navier-Stokes (RANS) equations with in the Fluent® software by first employing the standard k-ε model, then switching to the Renormalized Group (RNG) turbulence model and finally switching to the Reynolds Stress Model (RSM). The selection of turbulence models was based on previous accurate drag

measurements of a swimmer's arm (Bixler and Schloder, 1996) while the approach was initially applied to measure the drag forces of a disk similar in size to a swimmer's hand (Bixler and Riewald, 2002). Zaidi *et al*. (2010) found that the RANS equations with the standard *k*-ω model can predict the drag forces with greater accuracy than the standard *k*-ε model since the dissipation rate (ω) for modelling the near-wall region is easier to specify than the dissipation rate (ε). Non-zero and finite Reynolds stress tensors have been accounted for only by Bixler *et al*. (2007) using the RSM model by assuming approximate relations for all its nine components. However, within an in-depth study of cyclists, Defraeye *et al*. (2010), after considering various turbulence models demonstrated that the LES approach predicted the surface pressure with greater accuracy than the RANS model (7% vs 11% respectively) when compared to experimental findings since not all scales of turbulence were modelled. The only disadvantage reported for the LES model was the high computational cost, being twice the computing time of the RANS model. This is easily circumvented nowadays with ready accessibility to multi-core parallel processing. Furthermore, in flows with high Re, the small scale eddies are affected by the large scale eddies that are resolved and determined with LES (Pope, 2004). Thus, the LES model has the potential to be more accurate than the RANS model when applied to gliding swimmers.

In light of the above considerations, the purpose of the current study was to assess the transient evolution of the magnitude of resistive forces on an accurate 3D representation of a swimmer whose joint angles, the angle of attack and the gliding velocity were measured during actual glides in the pool. This information was used to define the orientation of the model in the simulation and the inlet velocity. Additionally, the glide factor determined using the Hydro-Kinematic method (experimental approach) and the glide factor determined from the resistive force output of the simulation (numerical approach) were compared. Comparisons between the LES and the *k*-ε model are also reported.

7.2. Numerical Method

The geometry of an international level swimmer was employed for the requirements of the study. The swimmer was scanned with the Hamamatsu Body Line Scanner (9036 model, Hamamatsu Photonics, Japan) and the model was treated with the Rhinoceros and the Magics software as described in detail in the method section of this thesis (Chapter 3).

Prior to the scan, the swimmer was tested in the pool according to the testing protocol described in Chapter 3 and his velocity profile, joint angles and angle of attack were measured using the GlideCoach software. The joint angles during the glides were provided as feedback to the swimmer during the scanning process. This ensured a close match between body morphology and alignment in the experimental conditions and the simulation.

7.2.1. Scaling, transformation and rotation

The model of the swimmer was imported to the ICEM CFD (12.1, Ansys Inc., Canonsburg, PA, USA), a dedicated CAD and meshing software, in a CAD (STL, stereolithography) format. ICEM CFD provides advanced measurement and spatial discretization tools to tackle complex geometries and submerged bodies. Here, the geometry was scaled to match the size and the glide orientation of the actual subject.

7.2.2. Domain

A rectangle was formed with the use of the ICEM CFD software representing the section of the swimming pool (and also the solution domain) and the swimmer was placed at the centre. The dimensions of the domain were 5.6m x 2.6m x 2.0 m (Figure 7.1b).The depth of the domain was chosen to be 2.0m that is equal to the pool depth at which the swimmer was experimentally tested, whereas the width and the length were chosen to be 2.6m and 5.6m respectively to allow enough space for the flow to develop around the swimmer (Figure 7.1b). The size of the domain was similar to that of previous CFD studies (Bixler *et al*., 2007).

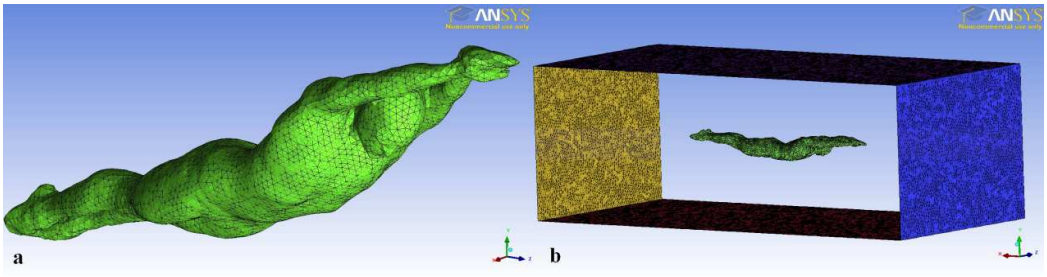

Figure 7.1. (a) The surface mesh of the swimmer consisted of 10,676 triangular surface elements. (b) The bounding box with dimensions equal to 5.6m x 2.6m x 2m.

7.2.3. Mesh generation

The pool and the swimmer were meshed with the ICEM software. The mesh type selected was tetrahedral (Tetra/Mixed) to generate the unstructured grid in the majority of the flow domain. Also, 20 layers of prismatic elements were considered around the swimmer to accurately resolve the boundary layer. Mesh independence tests employed to determine the optimum mesh size, are reported in Section 7.3.1.

7.2.4. CFD analysis

The STARCCM+ 6.04, CD Adapco Inc., Melville, NY, USA) commercial package was employed for the analysis of the 3D model.

7.2.4.1. Boundary conditions

Rather than simulating the movement of the swimmer, which is possible but beyond the scope of the current project, it is easier to simulate the flow relative to the swimmer. Experimental evidence, as shown in Chapter 4 and also in Figure 7.5, has clearly shown that a swimmer decelerates in the gliding phase over a span of 1.5 s. Therefore, at the inlet of the computational domain (Figure 7.3) a Dirichlet boundary condition of a uniform but unsteady inlet velocity as shown in Figure 7.5 was specified. A Neumann boundary condition ($\partial \underline{\mathbf{u}}/\partial \underline{\mathbf{n}} = 0$) representing fully developed flow at reference pressure was imposed for the outlet. The swimmer's surface and the bottom of the pool were modelled as smooth walls with no slip boundary conditions while the bottom wall was moving in the direction of the flow with the same velocity (Figure, 7.5).The top of the pool was modelled as a free shear

boundary (τ_{fs} = 0), indicating no tangential and normal shear stress. The swimmer performed all glides in the second lane of the swimming pool directly above the blue lane. Therefore, the distance between the swimmer's body and side of the pool was equal to 3.45m (3.75m minus half body width). This distance was considered sufficient to prevent any interaction between the swimmer and the wall and hence the sides were modelled as symmetry planes.

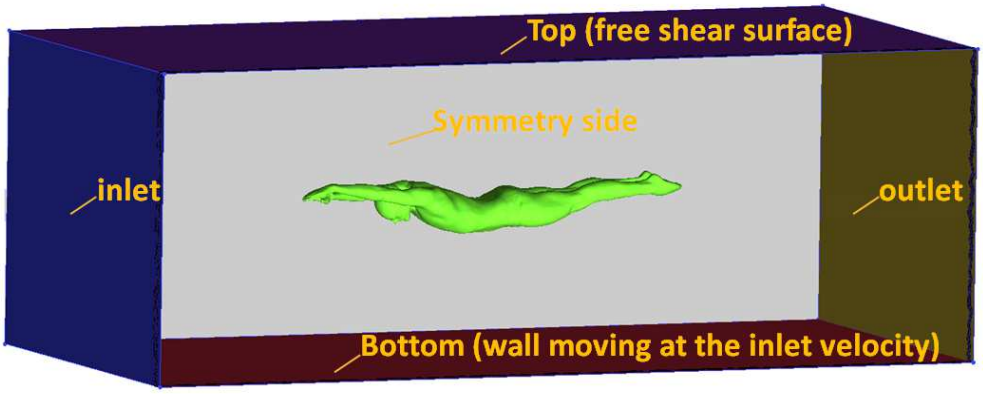

Figure 7.2.The boundaries of the computational domain.

To ensure that the initiation of the simulation would not affect the drag results of the first iterations of the analysis, 10,000 iterations with velocity equal to 2.73 ms^{-1}, being equal to the velocity of the first iteration of the analysis, preceded the transient analysis.

As far as the initial conditions of the simulation are concerned, no pressure or turbulence intensity was induced whereas the velocity was set to 2.73 ms^{-1} (equal to the velocity of the first iteration of the analysis).

The physical properties of the water were assumed to be constant and equal to the STAR CCM+ default values. The water entered the domain at a standard pressure and temperature (1 bar and 27˚C) with a free stream velocity. The magnitude of the inlet velocity was prescribed to be equal to the average gliding velocity of ten controlled glides that the participant performed in the streamlined position after a push from the wall for a total duration of 1.5 seconds (Figure 7.5). The glide velocity data were collected in the manner described in the first, second and third study of this thesis.

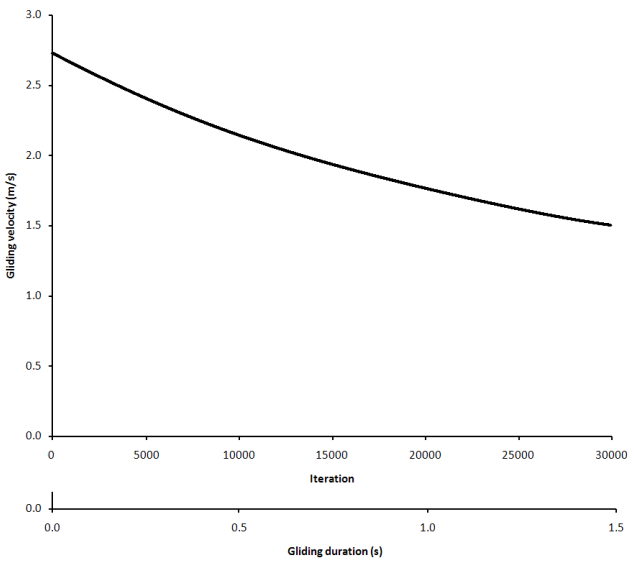

Figure 7.3 Correspondence between gliding velocity, gliding time and iteration number. This information was input to the simulation software as inlet velocity.

7.2.4.2 Flow model and simulation parameters

The LES turbulence model was employed to simulate the flow. The large scales of the motion that are solved with the LES model were filtered from the small scales of the motion that are modelled according to the filter operation of Equation 7.2. Therefore, the flow variables (U) were decomposed into the large scale ($\boldsymbol{U}$) and the subgrid scale part ($\boldsymbol{U}'$, Equation 7.1).

$$\boldsymbol{U} = \overline{\boldsymbol{U}} + \boldsymbol{U}' \qquad \text{Equation 7.1}$$

$$\overline{\boldsymbol{U}}(\mathbf{x}) = \int_A \boldsymbol{U}(\mathbf{x}'\mathrm{G}(\mathbf{x}, \mathbf{x}'; \Delta)\mathrm{d}\mathbf{x}' \qquad \text{Equation 7.2}$$

where **x** is a location in space, *A* is the domain, G is the filter function (that is either a Gausssian, cutoff or box filter that is not specified in the software used) and Δ is the filter width determining the size of the small eddies.

Equations 7.2 and 7.3 describe the form of the filtered Navier-Stokes equations used to simulate directly the large eddies.

$$\frac{\partial \overline{u'}_i}{\partial x_i} = 0$$ Equation 7.3

$$\frac{\partial \bar{u}_i}{\partial t} + \frac{\partial}{\partial x_j}\left(\bar{u}_i \bar{u}_j\right) = -\frac{1}{\rho}\frac{\partial \bar{p}}{\partial x_i} - \frac{\partial \tau_{ij}}{\partial x_j} + \nu \frac{\partial^2 \bar{u}_i}{\partial x_j x_j}$$ Equation 7.4

where ν is the kinematic viscosity and is the subgrid scale stress (defined as $\tau_{ij} = \overline{u_i u_j} - \bar{u}_i \bar{u}_j$).

As the large eddies were simulated directly (with the LES model), the small subgrid scales were analysed by modelling the subgrid scale tensor using the Boussinesq approximation (Equation 7.5) while the subgrid viscosity μ_t was modeled with the Smagorinsky subgrid scale (SSS) model (Equation 7.6). The All y^+ treatment all Treatment was selected to extend the accuracy of the near wall modelling.

$$\boldsymbol{\tau}_t = 2\mu_t \boldsymbol{S} - \frac{2}{3}(\mu_t \nabla \cdot \boldsymbol{u} + \rho\kappa)\mathbf{I}$$ Equation 7.5

where S is the strain tensor, ρ is the density, κ is the kinetic energy and **I** is the Kronecker delta.

$$\mu_t = \rho \Delta^2 S$$ Equation 7.6

where Δ is the filter width and S is the modulus of the strain rate ($S = \frac{1}{2}(\nabla u + \nabla u^T)$).

The density of the water was considered constant while the flow turbulent due to the high Reynolds number ($Re = \frac{HU_0\rho}{\mu}$ =5.28x10^6, where H is the channel width, U_0 is the maximum gliding velocity of the swimmer at t=0 in Fig 7.3, ρ is the density and μ is the viscosity) of the regime. The segregated solver was chosen and the equations were solved for every cell at the same time as the flow was incompressible and the Mach number (a dimensionless number equal to the speed of an object divided by the speed of sound) low. Given its second order accuracy, the central difference numerical scheme was employed.

As turbulence is an inherently unsteady phenomena and also to account for the time-varying inlet velocity, a transient model is used. In order to maintain computational stability and convergence (even at greater timesteps) an implicit unsteady formulation by Euler was used according to Equation 7.5 (Blazek, 2001).

$$\frac{\partial \varphi}{\partial t} = \frac{\varphi^{n+1} - \varphi^{n}}{t} = f(\varphi^{n+1}, \varphi^{n}) \qquad \text{Equation 7.5}$$

7.2.4.3. CFD reports

Drag force was computed with both the LES and the *k-ε* and plotted. Figures of the fluid domain demonstrating the velocity vector and also figures demonstrating the wall shear stress and the fluid element vorticity were exported from the simulation package and printed. Additionally, streamlines have been plotted and are also presented in section 7.3.2.

The results of the CFD model described were compared to the experimental glide factor values computed with the Hydro-Kinematic Method (HKM) when the swimmer was tested in the pool. The glide factor values for the CFD analysis were computed according to Equation 7.7 (Naemi and Sanders, 2008).

$$C_G = \frac{M}{\frac{D}{u_x^2}} \qquad \text{Equation 7.7}$$

Where C_G is the glide factor, M is the total virtual mass (kg) (equal to the mass of the swimmer plus the added mass), D is the drag force (N) and u_x is the horizontal velocity ($m \cdot s^{-1}$).

7.2.5. Statistical analysis

A One-Sample T Test analysis was performed to identify any statistically significant differences between the experimental and the numerical findings. The glide factor computed from the CFD model was used as a factor in the analysis. The analysis was performed over models using the RANS type *k-ε* turbulent model and those using the LES approach to identify any differences in the simulated results.

7.3. Simulation quality

7.3.1. Mesh independence tests

In order to determine the optimum grid mesh size, mesh independence checks were conducted by gradually refining the tetrahedral elements while maintaining the size of the prismatic elements to ensure that the computed drag value was not affected by the number of the cells. Mesh independence checks were performed with the number of total cells varying between 0.5million and 1 million (Table 7.2).

Table 7.2 Mesh independence checks were performed to define the optimum mesh size (Initial velocity, u_0=2 ms^{-1}).

	Total number of grid cells	
	0.5 million	**1 million**
Pressure (N)	52.5	56.2
Shear (N)	14.9	15
Net (N)	67.3	71.2
Computational time (s)	56802	63042

The difference between the net forces in the two cases examined for the grid independence check was found to be more than 5% (5.48%) and thus the grid with the one million cells was considered for the analysis. Accordingly, the maximum mesh size for the pool was equal to 50 mm (Figure 7.1b) whereas the maximum mesh size for the swimmer was set to be equal to 25 mm, as a larger mesh would misrepresent the surface of the swimmer because the surface would not be smooth, and edges would appear in areas with high curvature (Appendix C). The thickness of each one of the prism layers was 3 mm forming a layer of 6 cm (Figure 7.2a) in order to encompass the boundary layer (that was found to be 5.64 cm according to Equation 7.8). The calculations to compute the thickness of the boundary layer were conducted according to flat plate measurements with length equal to the swimmer's

length. Overall, 1 million cells were used to mesh the computational domain (Figure 7.2b) and the mesh file generated was then exported in a STAR CCM+ compatible format (.msh).

$$\delta = \frac{4.91L}{\sqrt{Re}} \qquad \text{Equation 7.8}$$

where δ is the boundary layer thickness, L is the swimmer's length and Re is the Reynolds number (5.28 in this case).

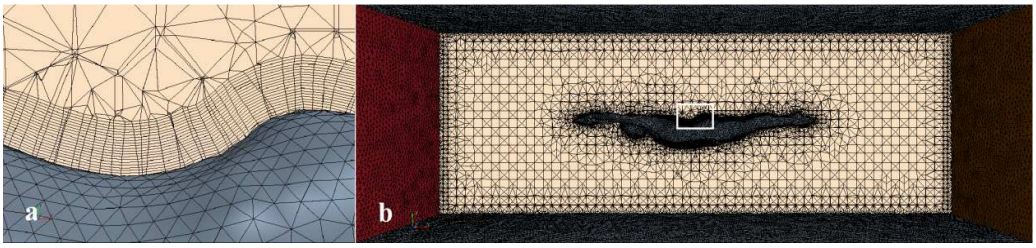

Figure 7.4 (a) 20 prism cells layers were modelled to model with higher accuracy the transition boundary layer of the swimmer. The demonstrated region is at the lower back. (b) The volume mesh generated with the use of the ICEM software.

7.3.2. Temporal independence tests

The number of time steps analysed were 3000 over the glide duration time of 1.5 s while 10 iterations were performed for each timestep. The size of each time step was selected after temporal dependence checks were performed to ensure that the measured drag was not affected by the duration of each timestep. The timestep size analysed ranged from $5x10^{-3}$ s to $5x10^{-4}$ s. This range was selected to include the timestep size that the Courant-Friedrichs-Lewy (CFL) condition was met (CFL=0). The CFL number that was computed (according to Equation 7.9) for the highest inlet velocity (that was 2.73 ms^{-1}) and the smallest cell size (that was 3 mm), was found to be one when the timestep size was equal to 1e-03 s. Therefore, the range assessed, involved timestep sizes that the CFL number was smaller (5e-04 sec) equal (1e-03 sec) and greater (5e-03 sec) than one.

$$C = \frac{u\Delta t}{\Delta x} \qquad \text{Equation 7.8}$$

where C is the CFL number.

CFL values equal to one indicate that the fluid particle displacement per timestep is equal to the mesh size whereas CFL values greater than one indicate that the displacement per timestep is greater than the mesh size. According to the literature the CFL number should be smaller or equal to one to ensure numerical stability (LeVeque, 2002). The difference in the measured drag force between the simulations conducted with timestep size equal to 1e-03 s and 5e-04 s was found to be 2.8% (or 2 N). This difference reported was considered important and all further analysis was conducted with a timestep size equal to 5e-04 s.

Table 7.3 Temporal dependence checks were performed to define the optimum timestep size (υ=2 ms^{-1}).

	Timestep size (s)		
	$5x10^{-3}$	**$1x10^{-3}$**	**$5x10^{-4}$**
Pressure (N)	53.4	55.4	56.2
Shear (N)	13.1	13.8	15
Net (N)	66.5	69.2	71.2

7.3. Results and Discussion

7.3.1. Validation

From the STAR CCM+ software 5000 values reporting the drag force applied on the swimmer model were exported and subsequently analysed with the Microsoft Excel software. The drag force values were calculated as the sum of pressure and shear force on each surface face. The time-varying inlet velocity described by Figure 7.5 was prescribed over the simulation time of 1.5 s and was interpolated every 150-250 iterations. When that was the case, fluctuations would appear in the drag force

reported for the following 5 iterations (Figure 7.6). This is expected and corresponded to the adjustment of the solution to a renewed inlet condition. For this reason the drag data were filtered with a moving average filter to eliminate these fluctuations.

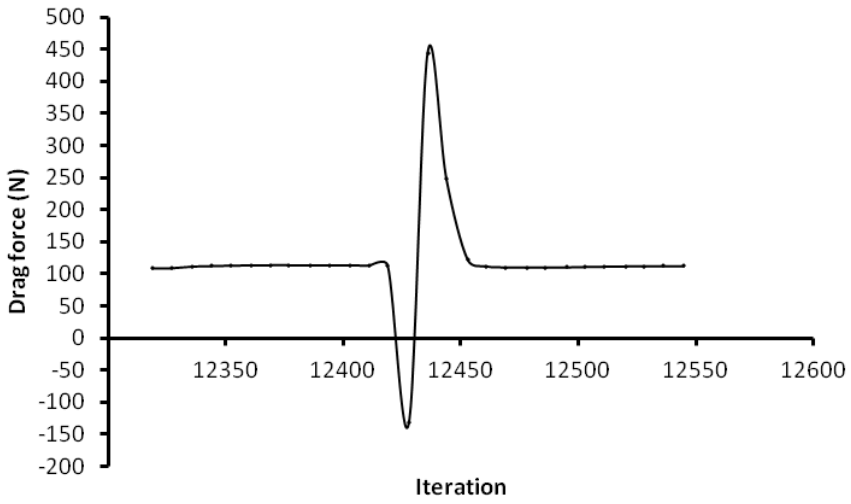

Figure 7.5 Irregularities in the drag force reported at velocity transition (the extreme values were not considered for the analysis).

The computed drag force for the whole glide (1.5 s) with the use of LES and the *k-ε* model is presented in Figures 7.7. The LES drag force reported was consistently lower than the *k-ε*. Furthermore, the *k-ε* model drag force curve was evidently smoother than the LES. This is because the RANS model decomposes the instantaneous quantities to time average and fluctuating quantities. The fluctuating quantities are modelled (with the *k-ε* model) based on a number of constants that have been empirically determined without solving the Navier Stokes equations.

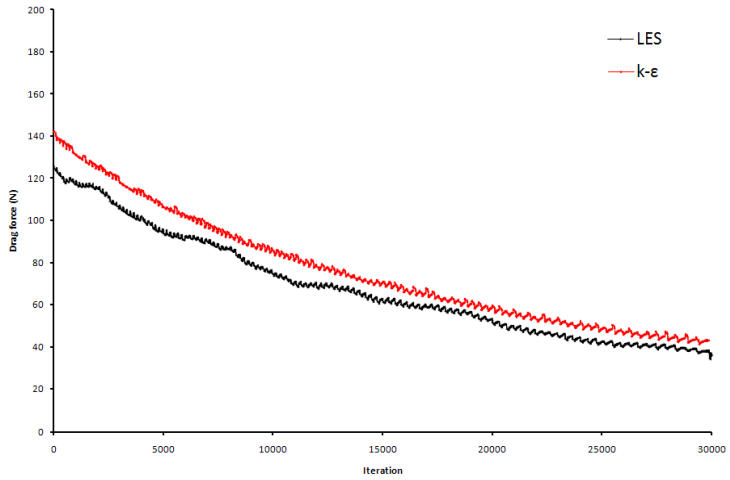

Figure 7.6 Drag force reported with the use of the LES and the *k-ε* model.

The HKM takes into account the average gliding velocity to compute the glide factor. So, the same average velocity was used to compute the glide factor from the simulation findings. The drag force when the velocity was equal to 2 ms^{-1} (that is the average velocity of the entire glide phase) was computed to be 68 N with the use of the LES model and 74 N with the use of the *k-ε* model (the standard deviation values denote the range in the computed drag force due to turbulence). The drag coefficient computed according to Equation 7.8 was found to be 0.278 and 0.303 respectively.

$$C_d = \frac{D}{\frac{1}{2}\rho\, v^2 S} \qquad \text{Equation 7.8}$$

where D is the computed drag (N), ρ is the density of the water ($kg \cdot m^{-3}$), v is the fluid velocity ($m \cdot s^{-1}$) and S is the frontal surface area (m^2).

As shown in Figure 7.6, the glide factor computed according to Equation 7.7 from the simulation findings was 5.12 when the LES model was employed and 4.70 when the *k-ε* model was employed. The glide factor computed directly from the experimental data was 4.98 (±0.11). A statistically significant difference was found between the experimental and the computational (LES) findings ($p<0.05$) and also between the experimental and the computational (*κ-ε*) findings ($p<0.001$). A factor

contributing to the difference between the simulated (both LES and κ-ε)and the experimental results could be the fact that it is difficult for the swimmer to maintain the same angle of attack when gliding in the water. The difference in the drag force reported with the two flow models, found to be *6* N for u=2 ms^{-1}, between the computational results (LES and κ-ε) demonstrate the magnitude of error that is involved when a flow model (such as the κ-ε) is employed.

Table 7.4 Glide factor values reported for the experimental and the numerical analysis.

	Experiment	**CFD (LES)**	**CFD (*k*-ε)**
Glide factor	4.98	5.12	4.70

7.3.2. Velocity, vorticity and drag fields

For the flow visualization a plane was created parallel to the flow direction (sagittal plane) at the centre of the computational domain and vector and scalar plots were applied (Figure 7.8). Areas of stagnation where velocity was significantly lower are evident between the forearms, at the front side of the cervical region and also in the lumbar region. The red circles (in Figure 7.8) indicate areas of flow recirculation. Furthermore, velocity reached extreme values in areas with a high rate of positive change of curvature such as at the occipital, the thorax, the gluteal, the crural and the calcaneal region. The direction of the flow is demonstrated in Figure 7.7 with the use of streamlines originating from a line positioned 10 cm to the front of the swimmer and perpendicular to the flow direction.

High wall shear values were evident for the sections of the body exposed to the flow such as the hands, the frontal side of the head, the subaxillary, the gluteal, the crural and the calcaneal region (Figure 7.9).

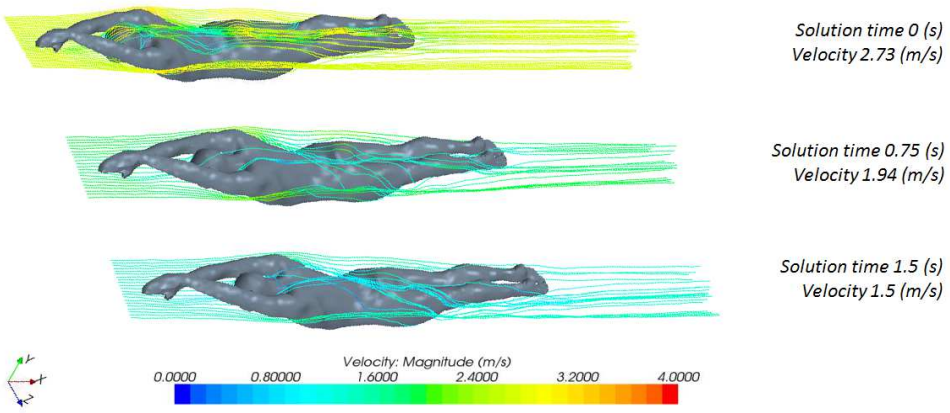

Figure 7.7 Streamlines demonstrating the flow direction and the velocity magnitude.

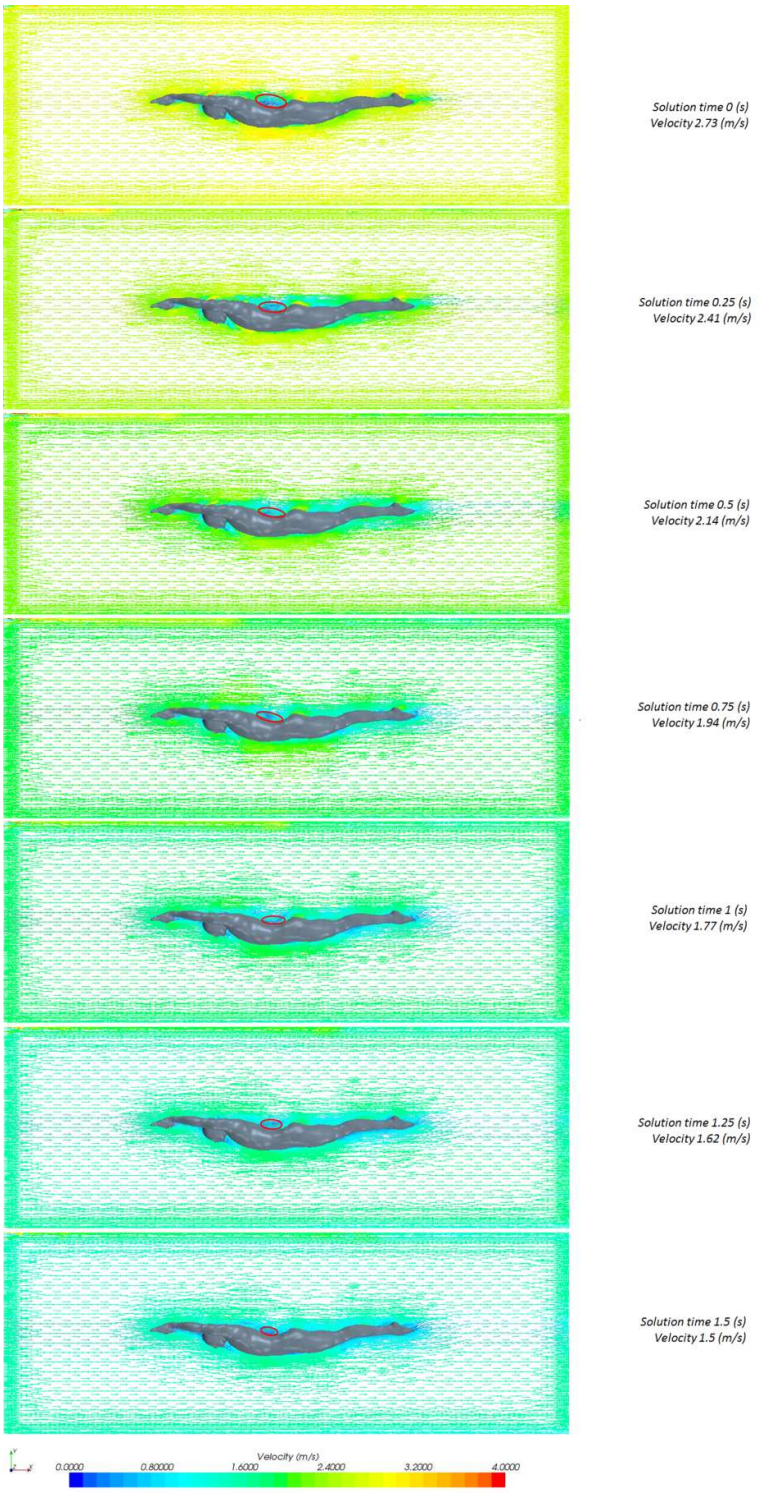

Figure 7.8 Vectors showing the velocity of the water around the swimmer's body.

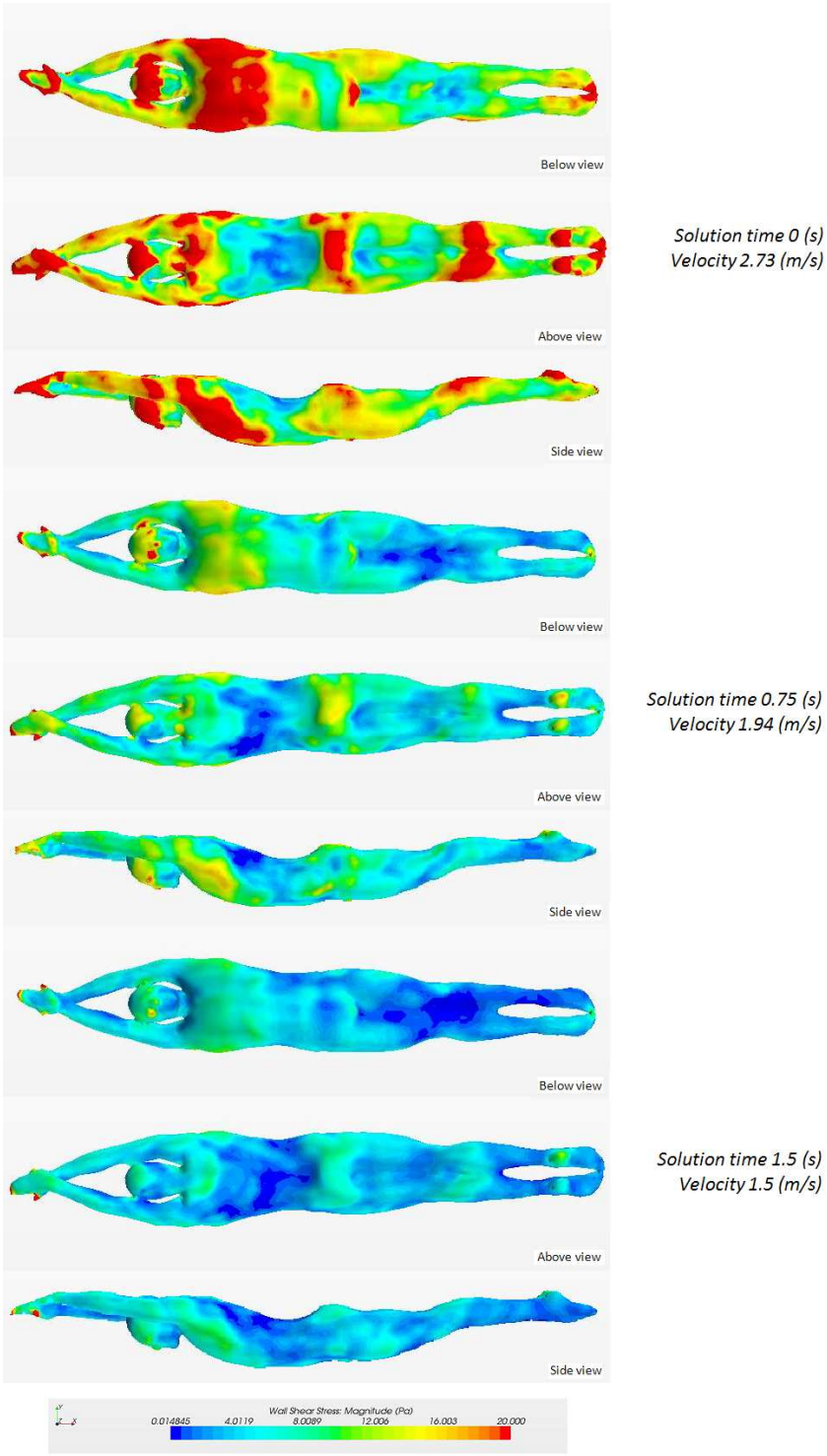

Figure 7.9 Wall shear stress magnitude scalar plots demonstrating the areas of the body with the highest wall shear.

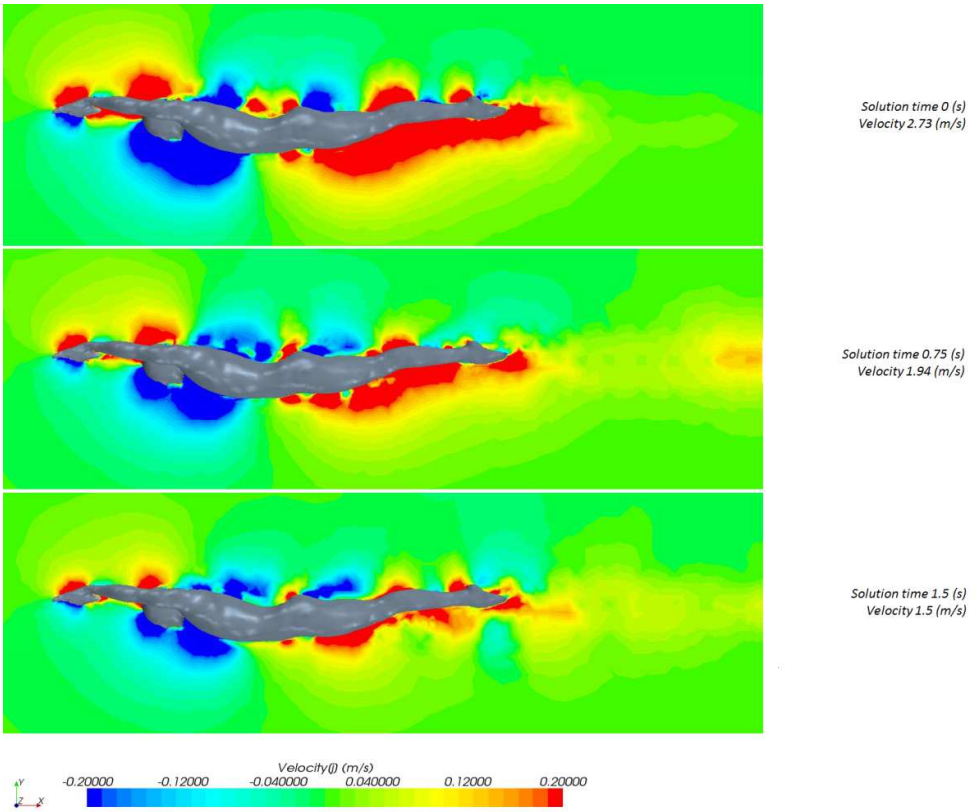

Figure 7.10 Scalar plots demonstrating the vertical component of velocity (Y axis). The positive and negative values demonstrate the direction (positive Y+ and negative Y-).

The scalar plots in Figures 7.10 and 7.11 present the vertical and the lateral component of velocity respectively. The interaction of the flow with the swimmer surface affected the direction of the flow and here the vertical and lateral component of the velocity vectors are presented.

Vortices and rotational movement of the fluid elements are positively correlated to resistance (Legendre, 2007). Figures 7.10 and 7.11 display the magnitude of the velocity components in the Y and the Z direction whereas Figures 7.11 and 7.12 display the volume of the rotating fluid elements.

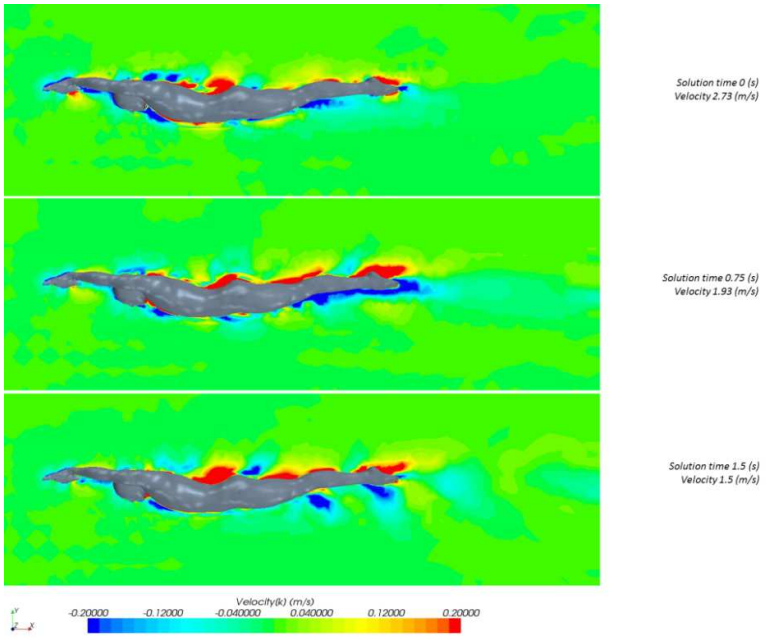

Figure 7.11 Scalar plots demonstrating the lateral direction of velocity (Z axis). The positive and negative values demonstrate the direction (positive Z+ and negative Z-).

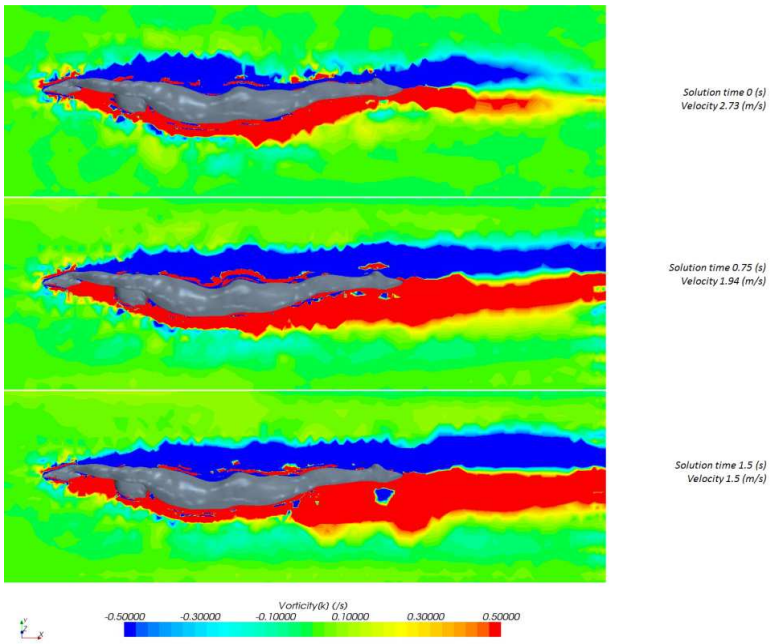

Figure 7.12 Scalar plots demonstrating the z component of vorticity. Positive values indicate regions of anticlockwise recirculation whereas negative values indicate regions of clockwise recirculation.

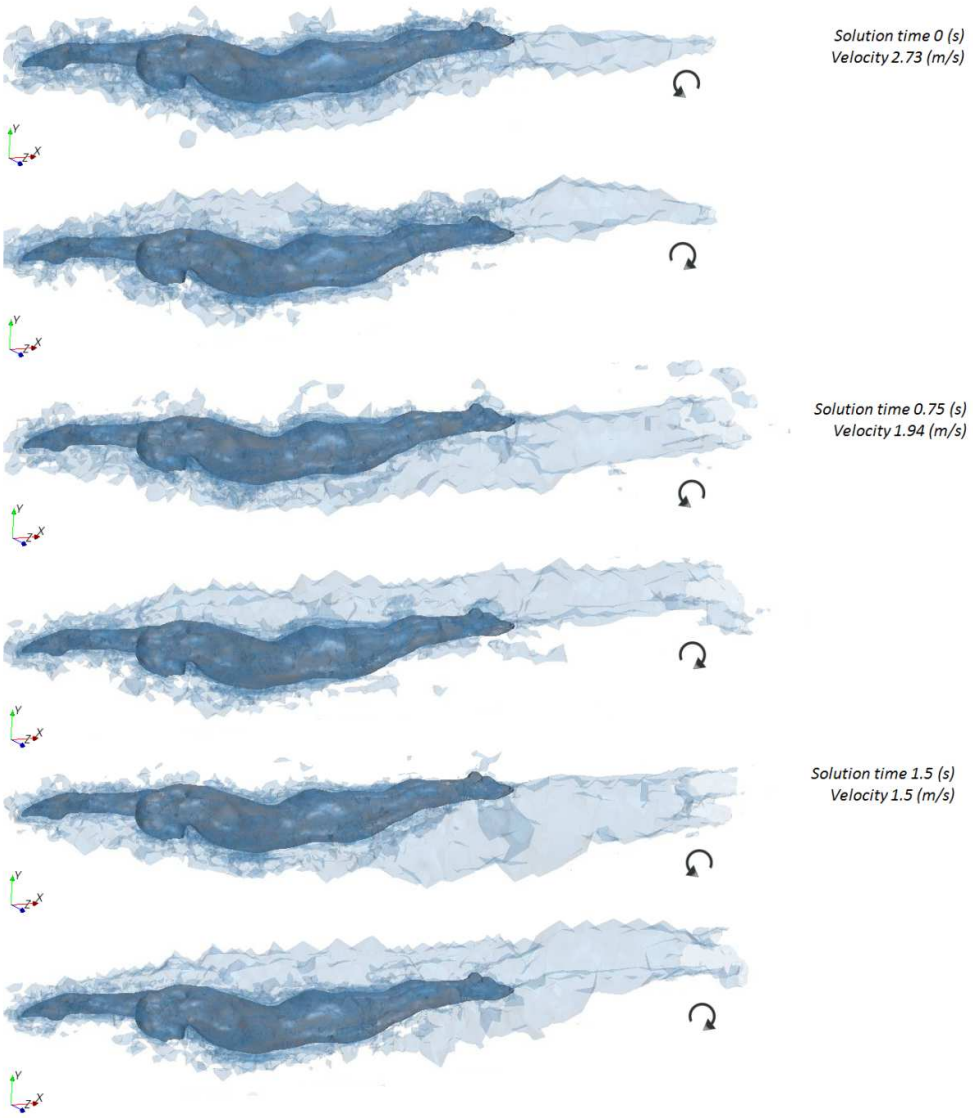

Figure 7.13 Isosurfaces of the z component of vorticity.

The vorticity Figures 7.12 and 7.13 indicate the tendency of the fluid elements to rotate around the Z axis. The rotating direction is presented separately in Figure 7.13; the top figure of each solution time, presents the volume of the elements rotating in the anticlockwise direction whereas the bottom figure presents the volume of the elements rotating in the clockwise direction. According to Figure 7.12 and 7.13 the volume of the rotating elements increased as the gliding velocity was declining.

7.3.3. Comparison with previous studies

In this study the numerical technique of computational fluid dynamics was used to assess the glide performance of an unrestricted swimmer gliding after a push from the wall. Passive drag values were computed using the LES model and the findings were validated against experimental data.

The gliding velocity input to the simulation package was based on actual data collected in the pool. The average gliding velocity of the swimmer was 2 ms^{-1}; this is also a typical average velocity of an international level male swimmer gliding for a total duration of 1.5 s. The characteristics of the actual glide of the male swimmer have been established in previous settings enabling a comparison of findings obtained by CFD and the Hydro-Kinematic Method.

The difference between the experimental and the computational results (2.73%) when the LES model was employed was significantly less than the 18% difference previously reported by Bixler *el. al.* (2007). The increase in accuracy is attributed to the transient LES turbulence model employed in this work and also due to the fact that the 3D geometry input for the CFD analysis is more accurate than the one previously used (Bixler *et al*., 2007).

In all other previous studies (Marinho *et al*., 2009; Zaidi *et al*., 2010 and Popa *et al*., 2011) the researchers employed steady models assuming isotropicity of turbulence (indicating equality of the normal stresses in all three directions), misrepresenting geometries of the human shape (critical morphological characteristics of the human body like the joints were not depicted) and did not validate their findings against experimental results.

In this study it was attempted to maximize both the computational accuracy but also to follow methodological approaches that would allow the simulation of a phenomenon as it happens in nature. For this reason, the LES model was employed despite the higher computational cost since it appears to be the most suitable approach given the characteristics of the flow and the high Re. A pure direct

numerical simulation (DNS) approach involving direct solution of the Navier-Stokes and continuity equations would have produced the most accurate result because there are no assumptions being made regarding turbulence. However, DNS would need extremely refined meshes (>5M elements) which would have been prohibitively expensive within the scope of this PhD. Moreover, kinematic data of the swimmer's actual glides were obtained. Information about his joint angles was used to set his position during scanning with a 3D laser body scanner to accurately generate the 3D geometry. The use of the Hydro-Kinematic Method of assessing the glide provided a valid criterion measure to assess the accuracy of the CFD simulation.

In absolute values the drag forces reported in this chapter (68 N) when the velocity was 2 $ms^{-1}$are comparable to those of previous studies. Bixler *et al*. (2007) reported drag values of 62.7 N for a mannequin tested in the flume when wearing swimwear for the same velocity (2 ms^{-1}). Lyttle *et al*. (2000) reported similar drag values (64.3 ±6.7 for a towing velocity of 1.9 ms^{-1}) after experimentally testing sixteen male swimmers. A direct comparison between the results of the different studies would be inaccurate since swimmers of different morphology and orientation were analysed. However, such a comparison provides a first indication about the accuracy of the measured values.

The difference between the experimental and the computational results (2.73%) can be attributed to errors in the experimental data analysis (for example errors when digitising the video files) and errors when setting up the computational analysis (the angle of attack was not constant during the glides as it was assumed when running the analysis) that cannot be evaluated. Also, approximation of the sub-grid scale eddy motion within the LED model is also a contributing factor.

7.4. Conclusion

This is the first time that a fully transient 3D CFD solution using LES turbulence for a swimmer in the same posture as when gliding in the pool, has been developed. Furthermore, this is the first attempt to analyse a full body swimming model under decelerating velocity conditions corresponding to the actual gliding velocity of the

same swimmer in an actual swimming pool. The numerical findings of the glide factor show remarkable agreement against the experimental findings.

As it has been previously suggested (Keys, 2010) and also proven for other sports (Defraeye *et al.*, 2010) the LES model appears to provide better approximations when measuring resistive forces in swimming biomechanics.

7.4.1. Limitations and recommendations

Even though it has been demonstrated with this study that the LES model performs significantly better than the RANS based k–ε model, the small scales of the motion are nonetheless modelled. A full DNS solution would be the most accurate approach to simulate the swimmer's glide as the NS equations are solved for all scales of the motion.

Chapter 8

Conclusions and Future Directions

There are two main aims of this thesis: i) to assess the effect of controllable factors that can be adjusted by the swimmers when gliding in the streamline position and ii)to assess the magnitude of resistive forces when gliding in the streamline position with the use of computational fluid dynamics.This thesis details and analyses both experimental and computational methods that were employed and discusses the results to assess the effect of the independent variables. The results were also used to validate the accuracy of the computational findings.

Previous studies assessing performance of swimmers when gliding in the streamlined position assumed that the velocity is steady during the glide phase with the only exception the inverse dynamics approach where the participants are attached to an accelerometer. In this thesis, both the experimental and the numerical methods applied to assess the gliding performance considered the rate of deceleration while the participants were not attached to any device.

In the first section of this chapter the conclusions of the studies conducted will be summarized whereas in the second section the recommendations for future studies will be presented.

8.1. Conclusions

The experimental and computational conclusions are summarized in the following subsections of the chapter.

8.1.1. Experimental Methods

In experiments, both the testing environment and the training status of the participants was controlled. The experimental data were collected in an aquatic environment where the ambient light, the temperature and the humidity was monitored and standardized. In order to prevent any confounding variables on performance, the participant's were required to avoid any stressful training and consumption of substances that could affect performance (such as alcohol and caffeine) before the testing session. The kinematic data were collected with the use of underwater cameras with about 65% lower noise than other systems reported in the literature (Machtsiras and Sanders, 2009). Finally the established Hydro-Kinematic method was employed to analyse the position data collected.

Additionally, the 3D body scanning was performed within hours from the swimming pool session to prevent any changes in the body volume characteristics of the participants. The Hamamatsu Body Line scanner was employed and a 0.6% reduction in error was reported when the measured volume of the lower limbs was compared against the water displacement method, Norton *et al.*, 2002).

By controlling the testing environment and employing low noise methods as above, it was reassured that the underwater gliding displacement data and also the swimmers' morphological representations were accurately captured. Thus, enabling a causal relationship between the head position, the gliding depth and the swimsuit worn (independent variables) and also the rate of deceleration (dependent variable) to be established.

However, the methods used were not sufficient enough to assess the magnitude of resistive forces and identify the areas of high pressure and the zones of recirculation. Investigation of other methods with such capabilities should be one of the objectives of future work (section 8.2).

8.1.1.1. Head position and glide performance

The specific purpose of the first study was to examine the relationship between the head position and performance when gliding in swimming. The results indicated that both the male and the female swimmer experienced significantly greater resistance (glide factor decreases by 7% for males and 10% for females) and thus, decelerated faster when they adopted a high head position (196.2^0, male and 170.5^0, female - angle with respect to centre of the shoulder joint and horizontal). It was also found that there was no significant difference between the medium (141.6°, male and 129.3^0, female) and low head (109.4°, male and 110.3^0, female) position for both participants indicating that swimmers can choose either position according to their natural preference. Furthermore it was found that the frontal surface variation as a result of the head position adopted was not related to the glide performance.

8.1.1.2. Gliding depth and glide performance

The specific purpose of the second study was to evaluate the effect of gliding depth on glide performance. The results demonstrated significantly higher glide factor values for the glides at a greater depth when compared to the glides closer to the water surface. The difference was found to be 16.4% for the male participant and 18.4% for the female participant when glides at 0.8 m depth and at the surface were compared.

8.1.1.3. Full body swimsuits and glide performance

The specific purpose of the third study was to assess the effect of full body swimsuits on glide performance. According to the results, even though the frontal surface area was reduced for both participants (1.95% for the male swimmers and 0.92% for the

female swimmer) when wearing the full body swim suit, the glide efficiency increased significantly only for the male swimmer (16.7%). Considering also that only the male swimmer's body morphology was altered due to the compression of the FB suit (thorax: 1.95%, pelvis 3.67% and lower back 8.21%) it was suggested that the improved gliding performance is directly linked to the local compression level of the FB suit. Additionally, the buoyancy of both swimmers was similar with either type of swimsuit when fully submerged.

8.1.2. Modeling methods

For the modelling section of the study, the 3D body scan alignment, the computational domain dimensions, the mesh generation and the fluid flow simulation model were carefully selected to maximize the accuracy of the computed results. The scan of the swimmers' upper and the lower body section was carefully merged based on landmarks placed on the athletes' body while the model was imported to the ICEMCFD software and positioned at the centre of a rectangular box representing a section of the swimming pool the swimmers were experimentally tested. The swimmer's geometry was horizontally aligned and fully submerged while the angle of attack was precisely defined based on the location of the center of the wrist and the ankle joint.

For the mesh generation, unstructured mesh with minimum mesh size of the order of 1/18.8 the boundary layer thickness was chosen. Mesh dependency tests showed that 1 million cells were necessary to achieve numerically stable results. To simulate turbulence, both the LES and the κ-εmodel were employed and according to the findings there was a better agreement to the experimental results with the LES model (difference between the experimental and LES model glide factors was around 2.8%). The gliding velocity when the participants were experimentally tested in the pool was considered and used as input into the transient inlet conditions of the simulation. After temporal dependence checks the timestep size chosen was to be equal to 5e-04 s and corresponded to half of the convective timescale.

A close match between the experimental and computational findings with the LES turbulence model was reported in this thesis primarily due to the careful completion of both sections of the study.

8.1.2.1. CFD to assess glide performance

The specific purpose of the fourth study was to assess the magnitude of resistive forces experienced when gliding in the streamlined position with the use of a numerical computational fluid dynamics method. The LES turbulence model was selected while for the first time transient analysis was conducted based on the participant's actual experimental gliding velocity. Glide factor (C_G) values were computed from the simulation findings and the results were compared to the values reported from the field analysis. Close agreement between the numerical and the experimental results (2.73%) indicated the accuracy of the numerical method.

8.1.3. General conclusions

The combination of well-established experimental methods including the 2D kinematic analysis of swimmers when gliding underwater, the Hydro-Kinematic method for glide performance assessment and3D scanning techniques allowed the assessment of association between kinematic and morphological variables. Furthermore, the data collected by the application of the aforementioned methods provided sufficient information to accurately define the initial conditions of the fluid flow simulations. This information includes the gliding velocity, the swimmer's joint angles when gliding and the swimmer's location in relation to the pool side and the bottom of the pool. Subsequently the joint angles of the scanned models were similar to the joint angles of the swimmers when gliding underwater and also the rate of deceleration used in the simulations was equal to that when the swimmers were gliding underwater. The steps followed (as described in Figure 3.1) increased the accuracy of the computed results and this process can be used as a validated methodological protocol in future studies aiming to include realistic kinematic and 3D body scan data in fluid flow simulations.

Besides the scientific implications of the studies conducted, there are also practical implications to be considered by the coaches and their athletes. These include that:

- Swimmer can adopt either a medium or low head position according to their natural preference without any significant effect on their performance.
- To minimize the resistive forces when gliding underwater, the swimmers should be gliding at 0.8 m from the water surface.
- To maximize performance when gliding underwater while wearing a full body swimsuit, swimmers should choose a costume that streamlines their body.

In addition to the research findings summarized in section 8.1.1 to 8.1.2, the data collected allowed also precise measurements of the frontal surface of the swimmers under different angles of attack and also the assessment of their body morphology.

These findings have significant implications as it has been shown that:

- Accurate assessment of the frontal surface area of swimmer when gliding underwater can be accomplished with the use of 3D body scans in the streamline position.
- Assessment of the body curvature when a swimmer is in the streamlined position can be succeeded with the use of 3D body scans and the measurement of the cross sectional area in the transverse plane across the whole body.

8.2. Recommendations for future research

8.2.1. Glide performance assessment

The use of the Hydro-Kinematic method in order to assess performance when gliding with altered head position, at different depths and with different types of swimsuit, allowed the effect of velocity decline to be considered. The same method could be

used in future studies to assess the efficiency of swimmers with varied morphological characteristics when passively gliding.

In addition to the experimental findings of the first, second and third study, CFD analysis could provide further information about the areas of high pressure and zones of recirculation when the head position is altered or a full body swimsuit is worn.

8.2.2. CFD analysis

In the fourth study it was demonstrated that the LES model performs significantly better than the RANS based k–ε model. However, future studies could employ a full DNS solution, where equations are solved for all scales of the motion, to further increase the accuracy of the findings. Additional advancement to the currently employed methods could be the use of 3D location data of each segment of the swimmer's body to better define the spatiotemporal characteristics of the simulated character.

8.2.3. Anthropometry

It was shown that precise measurements of the frontal surface area for different angles of attack can be achieved with the use of 3D body scans of swimmers in the streamlined position. Even though the application of the method requires data collection and treatment in several stages, the results could be used to assess the accuracy of indirect methods that can be applied with ease on field.

References

Alexander, R. M. & Goldspink, G. (1977). *Mechanics and Energetics of Animal Locomotion*. London: Chapman and Hall.

Alley, L. E. (1952). Analysis of water resistance and propulsion in swimming the crawl stroke. *Research Quarterly*, *23*, 257–270.

Alvarez, A., Bertram, V. & Gualdesi, L. (2009). Hull hydrodynamic optimization of autonomous underwater vehicles operating at snorkeling depth. *Ocean Engineering*, *36*(1), 105–112.

Amar, J. (1920). *The human motor*. London: G. Routledge & Sons.

Barr, I. S. (1999). Effects of Dehydration on Exercise Performance. *Canadian Journal of Applied Physiology*, *24*(2), 164–172.

Benjanuvatra, N., Blanksby, B. A. & Elliot, B. C. (2001). Morphology and hydrodynamic resistance in young swimmers. *Pediatric Exercise Science*, *13*, 246–255.

Benjanuvatra, N., Dawson, G., Blanksby, B. A. & Elliott, B. C. (2002). Comparison of buoyancy, passive and net active drag forces between Fastskin and standard swimsuits. *Journal of science and medicine in sport / Sports Medicine Australia*, *5*(2), 115–23.

Berthelot, G., Len, S., Hellard, P., Tafflet, M., El Helou, N., Escolano, S., Guillaume, M., Schaal, K., Nassif, H., Desgorces, D. & Toussaint, J. F. (2010). Technology & swimming: 3 steps beyond physiology. *Materials Today*, *13*(11), 46–51.

Bixler, B., Pease, D. & Fairhurst, F. (2007). The accuracy of computational fluid dynamics analysis of the passive drag of a male swimmer. *Sports Biomechanics*, *6*(1), 81–98.

Bixler, B. & Riewald, S. (2002). Analysis of a swimmer's hand and arm in steady flow conditions using computational fluid dynamics. *Journal of Biomechanics*, *35*(5), 713–717.

Bixler, B. & Schloder, M. (1996). Computational Fluid Dynamics: An Analytical Tool for the 21st Century Swimming Scientist. *Journal of Swimming Research*, *11*, 4–22.

Blake, R. W. (2000). Intermittent swimming in aquatic vertebrates. In P. D. Domenici & R. W. Blake (Eds.) *Biomechanics in animal behaviour* (pp. 79–102). Oxford: Bios Scientific.

Blake, R. W. (2009). Biological implications of the hydrodynamics of swimming at or near the surface and in shallow water. *Bioinspiration and Biomimetics*, *4*(1), 9.

Blake, R. W. & Chan, K. H. (2007). Swimming in the upside down catfish Synodontis nigriventris: it matters which way is up. *Journal of Experimental Biology, 210*, 2979–2789.

Blake, R. W. & Smith, M. D. (1988).On penguin porpoising. *Canadian Journal of Zoology, 66*, 2093–2094.

Blazek, J. (2001). *Computational fluid dynamics: principles and applications*. Oxford: Elsevier Science Ltd.

Bloomfield, J., Blankby, B. A., Beard, D. F., Ackland, T. R. & Elliott, B. C. (1984). Biological characteristics of young swimmers, tennis players and non-competitors. *British Journal of Sports Medicine, 18*, 97–103.

Boehler, W., Bordas Vicent, M. & Marbs, A. (2003). Investigating Laser Scanner Accuracy. *Proceedings of the XIXth CIPA Symposium.* Antalya, Turkey.

Bulgakova, N. Z. & Makarenko, L. P. (1996). Sport swimming. *Physical Culture, Education and Science*. Russian State Academy of Physical Education.

Cappaert, J. M. & Gordon, B. J. (1998). Frontal surface measurements in national calibre swimmers. *Sports Engineering*, *1*(1), 51–55.

Cappaert, J. M., Gordon, B. J. & Frisbie, K. (1997). Frontal Surface Area Measurements in National Caliber Swimmers. *Medicine and Science in Sports and Exercise*, 29(5), Supplement abstract 712.

Carr, C. L. (2008). Fairness and Performance Enhancement in Sport. *Journal of the Philosophy of Sport*, *35*, 193–207.

Caspersen, C., Berthelsen, P. A., Eik, M., Pâkozdi, C. & Kjendlie, P. L. (2010). Added mass in human swimmers: Age and gender differences. *Journal of Biomechanics*, 43(12), 2369-2373.

Chatard, J. C., Bourgoin, B. & Lacour, J. R. (1990). Passive drag is still a good evaluator of swimming aptitude. *European Journal of Applied Physiology and Occupational Physiology, 59*(6), 399–404.

Chatard, J. C. & Wilson, B. (2003). Drafting distance in swimming. *Medicine and Science in Sports and Exercise*, *7*, 1176–1181.

Chatard, J. C. & Wilson, B. (2008). Effect of fastskin suits on performance, drag, and energy cost of swimming. *Medicine and science in sports and exercise*, *40*(6), 1149–1154.

Chow, J. W., Hay, J. G., Wilson, B. D. & Imel, C. (1984). Turning technique of elite swimmers.*Journal of Sport Sciences*, *2*(3), 241–255.

Clarys, J. P. (1978). Relationship of human body form to passive and active hydrodynamic drag. In E. Asmussen & K. Jorgenson (Eds.) *Biomechanics VI-B*, 120–125. Baltimore:University Park Press.

Clarys, J. P. (1979). Human morphology and hydrodynamics. In J. Terauds & E. W. Bedingfield (Eds.) *Swimming III* (pp. 3–41). Baltimore:University Park Press.

Clarys, J. P. & Jiskoot, J. (1975). Total resistance of selected body positions in the front crawl. In L. Lewillie & J. P. Clarys (Eds.) *Swimming II* (pp. 110–117). Baltimore:University Park Press.

Clarys, J. P., Jiskoot, J., Rijken, H. & Brouwer, P. J. (1974). Total resistance in water and its relation to body form. In R. C. Nelson & C. A. Morehouse (Eds.) *Biomechanics IV* (pp. 187–196). Baltimore:University Park Press.

Cook, T. S., Couch, G., T., C., William, W. K. & Boonn, W. (2012). Using the Microsoft Kinect for Patient Size Estimation and Radiation Dose Normalization: Proof of Concept and Initial Validation. *Society for Imaging Informatics in Medicine*. Orlando.

Counsilman, J. E. (1955). Forces in swimming two types of crawl stroke. *Research Quarterly*, *26*, 127–139.

Craig, A. B. & Pendergast, D. R. (1979). Relationships of stroke rate, distance per stroke, and velocity in competitive swimming. *Medicine and Science in Sports*, *11*(3), 278–283.

Craik, J. (2011). Introduction: Re-fashioning the Swimming Body. *Journal of Current Cultural Research*, *3*, 71–82.

Cureton, T. K. (1975). Factors governing success in competitive swimming: a brief review of related studies. In L. Lewillie & J. P. Clarys (Eds.) *Swimming II* (pp. 9–41). Baltimore: University Park Press.

Dabnichki, P. & Avital, E. (2006). Influence of the position of crew members on aerodynamics performance of two-man bobsleigh. *Journal of Biomechanics*, 39, 2733- 2742.

Dal Mutto, C., Zanuttigh, P. & Cortelazzo, G. M. (2012). Microsoft Kinect Range Camera. In: *Time-of-Flight Cameras and Microsoft Kinect™* (pp. 33–47). Boston, MA: Springer US.

Deffeyes, J. & Sanders, R. H. (2005). Elliptical Zone Body Segment Modeling Software: Digitizing, Modeling and Body Segment Parameter Calculation. In Wang, Q. (Eds.) *Proceedings of the XXIII International Symposium on Biomechanics in Sports* (pp. 749–752). Beijing, China.

Defraeye, T., Blocken, B., Koninckx, E., Hespel, P. & Carmeliet, J. (2010a). Computational fluid dynamics analysis of cyclist aerodynamics: Performance of different turbulence-modelling and boundary-layer modelling approaches. *Journal of Biomechanics*, *43*(12), 2281–2287.

Defraeye, T., Blocken, B., Koninckx, E., Hespel, P. & Carmeliet, J. (2010b). Aerodynamic study of different cyclist positions: CFD analysis and full-scale wind-tunnel tests. *Journal of biomechanics*, *43*(7), 1262–1268.

D'Acquisto, L. J., Costill, D. L., Gehtsen, G. M. & Wong-Tai, Y. Lee, G. (1988). Breaststroke economy skill and performance: study of breaststroke mechanics using a computer based "velocity video." *Journal of Swimming Research*, *4*, 9–14.

di Prampero, P. E., Pendergast, D. R., Wilson, D. R. & Rennie, D. W. (1974). Energetics of swimming in man. *Journal of Applied Physiology*, *37*(1), 1–5.

Eik, M., Berthelsen, P.A. Caspersen, C., Pakozdi, C. & Kjendlie, P. L. (2008). Validity of a velocity decay method for estimating passive drag in swimmers. In J., Cabri, F., Alves, D., Araujo, L., Berreiros, J., Diniz & A. Veloso (Eds.) *Proceedings of the 13th Annual Congress of the ECSS.* Estoril, Portugal.

Elipot, M., Hellard, P., Taïar, R., Boissière, E., Rey, J. L., Lecat, S. & Houel, N. (2009). Analysis of swimmers' velocity during the underwater gliding motion following grab start.*Journal of Biomechanics*, *42*(9), 1367–70.

Eng, K. & Hu, P. N. (1963). *Wave resistance reduction of near surface bodies*. Hoboken, NJ: Stevens Institute of Technology, Davidson Lab.

Fish, F. E. (1984). Mechanics, power output and efficiency of the swimming muskrat (Ondatra zibethicus). *Journal of Experimental Biology*, *110*, 183–201.

Fish, F. E. (1993). Power output and propulsive efficiency of swimming bottlenose dolphins (Tursiops truncatus). *Journal of Experimental Biology*, *185*, 179-193.

Fish, F. & Lauder, G. V. (2006). Passive and active flow control by swimming fishes and mammals. *Annual Review of Fluid Mechanics*, *38*, 193–224.

Gardano, P. & Dabnichki, P. (2006). On hydrodynamics of drag and lift of the human arm. *Journal of biomechanics*, *39*(15), 2767–2773.

Graham, T. E. (2001). Caffeine and exercise: Metabolism, Endurance and Performance. *Sports Medicine (Auckland, N.Z.)*, *31*(11), 785–807.

Gunther, P., Nathan, D. & Francois, F. (2012). Patterns of correlation between vehicle occupant seat pressure and anthropometry. *WORK*, 2226–2231.

Hairabedian, A. (1964). *Kinetic Resistance Factors Related to Body Position in Swimming*. Stanford University.

Hay, J. G. (1986). Swimming biomechanics: a brief review. *Swimming Technique*, *23*(3), 15–21.

Hertel, H. (1966). *Structure, Form, Movement*. New York: Reinhold.

Hollander, A. P., de Groot, G., van Ingen Schenau, G. J., Toussaint, H. M., de Best, H., Peeters, W., Meulemans, A. & Schreus, A. W. (1986). Measurement of active drag forces during swimming. *Journal of Sports Sciences*, *4*, 21–30.

Holmer, I. (1974). Physiology of swimming man. *Acta Physiologica Scandinavica*, *407*, 1–55.

Huijing, P. A., Toussaint, H. M., Mackay, R., Vervoorn, K., Clarys, J. P., de Groot, G. & Hollander, A. P. (1988). Active drag related to body dimensions. *Swimming Science V*. (pp. 31–37). Human Kinetics Publishers Inc.

Hwang, S. J. (2001). *Three dimensional body scanning systems with potential for use in the apparel industry*. North Carolina State University.

James, D. (2010). The ethics of using engineering to enhance athletic performance. *Procedia Engineering*, *2*(2), 3405–3410.

Jiskoot, J. & Clarys, J. P. (1975). Body resistance on and under the water surface. In J. P. Clarys & L. Lewillie (Eds.) *Swimming II* (pp. 105–109). Baltimore: University Park Press.

Johansson, L. C. & Lauder, G. V. (2004). Hydrodynamics of surface swimming in leopard frogs (Rana pipiens). *Journal of Experimental Biology*, *207*, 3945–3958.

Jones, P. R. M., West, G. M., Harris, D. H. & Read, J. B. (1989). The Loughborough anthropometric shadow scanner (LASS). *Endeavour*, *13*(4), 162–168.

Karpovich, P. V. (1933). Water resistance in swimming. *Research Quarterly*, (4), 21–28.

Kent, M. R. & Atha, J. (1971).Selected critical transient body positions in breast stroke and their influence upon water resistance. In L. Lewillie & J. P. Clarys (Eds.) *Proceedings of the First International Symposium on Biomechanics in Swimming* (pp. 119-125).Brussels: Universite libre de Bruxelles.

Keys, M. (2010). *Establishing Computational Fluid Dynamics models for swimming technique assessment. Stroke*. The University of Western Australia.

Kirchhoff, R. H. (1998). Inviscid incompressible flow – potential flow. In: Johnson, R. W. (Eds.) *The handbook of fluid dynamics*. Boca Raton, USA: CRC press.

Kjendlie, P. L., Alves, F. B., Berthelsen, P. A., Caspersen, C., Eik, M., Marinho, D. A., Pâkozdi, C., Rouboa, A. I., Silva, A. J. & Vilas-Boas, J. P. (2009). Added Mass Of Human Swimmers: A Comparison Of Computational And Experimental Results. *Medicine & Science in Sports & Exercise, 41* (Supplement 1), 386–387.

Klauck, J. (1998). Man's water resistance in accelerated motion: An experimental evaluation of the added mass concept. In K. Keskinen, P. V. Komi, & P. Pitkanen (Eds.)*Proceedings of the VIII International Symposium on Biomechanics and Medicine in Swimming* (pp. 83–88). Saarijavi, University of Jyvaskyla.

Klauck, J. & Daniel, K. (1976). Determination of man's drag coefficients and effective propelling forces in swimming by means of chronocyclography. In P. V. Komi (Ed.), *Biomechanics VB* (pp. 250–257). Baltimore: University Park Press.

Kolmogorov, S. V. & Duplishcheva, O. A. (1992). Active drag, useful mechanical power output and hydrodynamic force coefficient in different swimming strokes at maximal velocity. *Journal of Biomechanics, 25*(3), 311–318.

Kolmogorov, S. V. Rumyantseva, O. A., Gordon, B. J., & Cappaert, J. M. (1997). Hydrodynamic characteristics of competitive swimmers of different genders and performance levels. *Journal of applied biomechanics, 13*, 88–97.

Kwon, Y. H. (1999). Object plane deformation due to refraction in two- dimensional underwater motion analysis. *Journal of Applied Biomechanics, 15*, 396–403.

Kwon, Y. H. & Casebolt, J. B. (2006). Effects of light refraction on the accuracy of camera calibration and reconstruction in underwater motion analysis. *Sports Biomechanics, 5*, 95–120.

Lecrivain, G., Slaouti, A., Payton, C. & Kennedy, I. (2008). Using reverse engineering and computational fluid dynamics to investigate a lower arm amputee swimmer's performance. *Journal of Biomechanics, 41,* 2855–2859.

Lemes, S. & Zaimović-Uzunović, N. (2009). Study Of Ambient Light Influence On Laser 3D Scanning. *7th International Conference on Industrial Tools and Material Processing Technologies ICIT & MPT* (pp. 327–330). Ljubljana, Slovenia.

Lyttle, A. D. (1999). *Hydrodynamics of the human body during the freestyle tumble turn*. The University of Western Australia.

Lyttle, A. D., Benjanuvatra, N., Blanksby, B. A. & Elliott, B. C. (2000). Morphology and hydrodynamic resistance in young swimmers.In Hong, Y., Johns, D. P. & Sanders, R. (Eds.) *Proceedings of the XVIII International Symposium on Biomechanics in Sports.* Hong Kong, China.

Lyttle, A. D., Blanksby, B. A., Elliott, B. C. & Lloyd, D. G. (1998). The role of drag in the streamlined glide. *Journal of Swimming Research, 13*, 15–22.

Machtsiras, G. & Sanders, R. H. (2009). Accuracy of a Portable (PTZ Digital) Camera System Designed for Aquatic Three-Dimensional Analysis. In Harrison, A. J., Anderson, R. & Kenny, I. (Eds.) *International Symposium on Biomechanics in Sports* (pp. 451). Limerick, Ireland.

Machtsiras, G. & Sanders, R. H. (2012). A Comparison of elliptical zone and 3D scanning calculating methods of estimating swimmer's body segment volumes. In R., Meeusen, J., Duchateau, B., Roelands, M., Klass, B., De Geus, S., Baudry & E. Tsolakidis (Eds.) *Proceedings of the 13th Annual Congress of the ECSS* (pp. 462). Bruges, Belgium.

Maiello, D., Sabatini, A., Demarie, S., Sardella, F. & Dal, M. A. (1998). Passive drag on and under the water surface. *Journal of Sports Sciences, 16*(5), 420–421.

Marinho, D. A., Reis, V. M., Alves, F. B., Vilas-Boas, J. P., Machado, L., Silva, A. J. & Rouboa, A. I. (2009). Hydrodynamic drag during gliding in swimming.*Journal of Applied Biomechanics, 25*(3), 253–257.

Marinho, D. A., Reis, V. M., Vilas-Boas, J. P., Alves, F. B., Machado, L., Rouboa, A. I. & Silva, A. J. (2010). Design of a three-dimensional hand/forearm model to apply computational fluid dynamics. *Brazilian Archives of Biology and Technology, 53,* 436–442.

Mayes, R. (2010). The Modern Olympics & Post-Modern Athletics: A Clash in Values. *The Journal of Philosophy, Science & Law, 10*, 1–17.

Minetti, A. E., Machtsiras, G. & Masters, J. C. (2009).The optimum finger spacing in human swimming. *Journal of Biomechanics, 42*(13), 2188–2190.

Mittal, R., Dong, H., Bozkurttas, M., Najjar, F. M., Vargas, A. & von Loebbecke, A. (2008). A Versatile Sharp Interface Immersed Boundary Method for Incompressible Flows With Complex Boundaries. *Journal of computational physics*, *227*(10), 4825–4852.

Miyashita, M. & Tsunoda, R. (1978). Water resistance in relation to body size. In B. Eriksson & B. Furberg (Eds.) *Swimming Medicine IV* (pp. 395–401). Baltimore: University Park Press.

Molland, A. F. (2008). *The maritime engineering reference book. A guide to ship design, construction and operation*. Burlington: Elsevier Ltd.

Mollendorf, J. C., Termin, A. C., Oppenheim, E. & Pendergast, D. R. (2004). Effect of Swim Suit Design on Passive Drag. *Medicine & Science in Sports & Exercise*, *36*(6), 1029–1035.

Moretti, G. & Abbett, M. (1966). A time-dependent computational method for blunt body flows. *AIAA Journal*, *4*(2), 36–41.

Moria, H., Chowdhury, H., Alam, F. & Subic, A. (2011). An evaluation of swimsuit performance. *Procedia Engineering*, *13*, 382–388.

Moria, H., Chowdhury, H., Alam, F., Subic, A., Smits, A. J., Jassim, R. & Bajaba, N. S. (2010). Contribution of swimsuits to swimmer's performance. *Procedia Engineering*, *2*, 2505–2510.

Mountjoy, M., Gordon, I., McKeown, J. & Constantini, N. (2009b). Technology in sport: Medical and Ethical Repercussions. *Clinical Journal of Sport Medicine*, *19*(6), 443–4.

Naemi, R. (2006). *A "Hydro-kinematic" Method for Quantifying Glide Efficiency of Swimmers. The University of Edinburgh.*

Naemi, R. & Sanders, R. H. (2008). A "Hydrokinematic" Method of Measuring the Glide Efficiency of a Human Swimmer. *Journal of Biomechanical Engineering*, *130*(6), 061016.

Neiva, H. P., Vilas-Boas, J. P., Barbosa, T. M., Silva, A. J. & Marinho, D. A. (2011). 13th FINA world championships: analysis of swimsuits used by elite male swimmers. *Journal of Human Sport and Exercise*, *6*(1), 87–93.

Newman, J. N. (1977). *Marine hydrodynamics*. Cambridge, Mass. MIT Press.

Nickoloff, E. L. & Alderson, P. O. (2001). Radiation exposures to patients from CT: reality, public perception and policy. *American Journal of Roentgenology*, 285–287.

Nomura, T., Goya, T., Matsui, A. & Takagi, H. (1994). Determination of active drag during swimming. In M. Miyashita, Y. Mutoh, & A. B. Richardson (Eds.) *Medicine and Science in Aquatic Sports* (pp. 131–136). Basel, Switzerland.

Norton, J., Donaldson, N. & Dekker, L. (2002). 3D whole body scanning to determine mass properties of legs. *Journal of biomechanics*, *35*(1), 81–6.

Oeffner, J. & Lauder, G. V. (2012). The hydrodynamic function of shark skin and two biomimetic applications. *The Journal of experimental biology*, *215*(5), 785–795.

Onoprienko, B. I. (1968). Relationship of hydrodynamic drag and swimmer's body position. *Theory and Practice of Physical Culture*, *9*, 12–15.

Oppenheim, E. (1997). *Model Parameter and Drag Coefficient Estimation from Swimmer Velocity Measurements*. University of Buffalo.

Orszag, S. & Patterson, G. S. (1972). Numerical simulation of turbulence, Statistical Models and Turbulence. *Lecture Notes in Physics* (Vol. 12, pp. 127–147). New York: Springer.

O'Brien, C. P. & Lyons, F. (2000).Alcohol and the athlete. *Sports medicine (Auckland, N.Z.)*, *29*(5), 295–300.

Partridge, B. (2011). Fairness and Performance-Enhancing Swimsuits at the 2009 Swimming World Championship: The "Asterisk" Championship. *Journal of Sport, Ethics and Philosophy*, *5*(1), 63.

Pease, D. (2009). *Wave drag and its implications for performance*. University of Otago.

Pease, D. & Vennell, R. (2011). Comparison of wave drag for both the male and female form. *Portugese Journal of Sport Sciences*, 11, 355–358.

Pendergast, D., Mollendorf, J. C., Zamparo, P., Termin, A. C., Bushnell, D. & Paschke, D. (2005). The influence of drag on human locomotion in water. *Undersea & hyperbaric medicine: journal of the Undersea and Hyperbaric Medical Society, Inc*, *32*(1), 45–57.

Pendergast, D. R., Mollendorf, J. C., Cuviello, R. & Termin, a. C. (2006). Application of theoretical principles to swimsuit drag reduction. *Sports Engineering*, *9*(2), 65–76.

Popa, C. V., Zaïdi, H., Arfaoui, A., Polidori, G., Taïar, R. & Fohanno, S. (2011). Analysis of wall shear stress around a competitive swimmer using 3D Navier-Stokes equations in CFD. *Acta of bioengineering and biomechanics*, *13*(1), 3–11.

Pope, S. B. (2004). Ten questions concerning the large-eddy simulation of turbulent flows. *New Journal of Physics*, *6*, 1–24.

Psycharakis, S. (2006). *A three-dimensional analysis of intra-cycle kinematics during 200m freestyle swimming*. *The University of Edinburgh*.

Rennie, D. W., Pendergast, D. R. & Di Prampero, P. E. (1975). Energetics of swimming man. In J. P. Clarys & L. Lewillie (Eds.) *Swimming II* (pp. 97–104). Baltimore: University Park Press.

Riewald, S. & Bixler, B. (2001). CFD Analysis of a swimmer's arm and hand, acceleration and deceleration. In Blackwell, J. R. & Sanders, R. (Eds.) *Proceedings of the XIX International Symposium on Biomechanics in Sports*. San Francisco, USA.

Roberts, B. S., Kamel, K. S., Hedrick, C. E., McLean, S. P.& Sharp, R. L. (2003). Effect of a FastSkin suit on submaximal freestyle swimming. *Medicine and science in sports and exercise*, *35*(3), 519–24.

Roberts, G. N. & Sutton, R. (2006). *Advances in unmanned marine vehicles*. Hertfordshire: IEE Press.

Rogowski, I., Monteil, K., Legreneur, P. & Lanteri, P. (2006). Influence of swimsuit design and fabric surface properties on the butterfly kinematics. *Journal of applied biomechanics*, *22*(1), 61–6.

Robinette, K. M., Daanen, H. & Paquet, E. (1999). The CAESAR project: a 3-D surface anthropometry survey. In: *Proceedings of Second International Conference on 3-D Digital Imaging and Modeling* (pp.380-386). Ottawa, Canada.

Rouboa, A. I., Silva, A. J., Leal, L., Rocha, J. & Alves, F. B. (2006). The effect of swimmer's hand/forearm acceleration on propulsive forces generation using computational fluid dynamics. *Journal of biomechanics*, *39*(7), 1239–48.

Royal Institution of Naval Architects (1860). *Transactions of the Royal Institution of Naval Architects*. London.

Rumyantsev, V. A. (1982). Biomechanics of sport swimming. *Central State in Institute for Physical Culture*. Moscow.

Rushall, B. S., Holt, L. E. & Sprigings, E. J. (1994). A re-evaluation of forces in swimming. *Journal of Swimming Research*, *10*, 6–30.

Ryder, J. R. & Ball, S. D. (2012). Three-Dimensional body scanning as a novel technique for body composition assessment: A preliminary investigation. *Journal of Exercise Physiology*, *15*(1), 1–14.

Schleihauf, R., Gray, L. & DeRose, J. (1983). Three-dimensional analysis of hand propulsion in the sprint front crawl stroke. In A. P. Hollander, P. A. Huijing, & G. de Groot (Eds.) *Biomechanics and Medicine in Swimming* (pp. 173–183). Human Kinetics.

Schlichting, H. & Gersten, K. (2000). Boundary-Layer Theory (8th ed). London: Springer.

Sharp, R. L., & Costill, D. (1989). Influence of body hair removal on physiological responses during breaststroke swimming. *Medicine & Science in Sports & Exercise*, *21*(5), 576–580.

Sharp, R. L., Hackney, A. C., Cain, S. M. & Ness, R. J. (1988).Effect of shaving body hair on the physiological cost of freestyle swimming. *Journal of Swimming Research*, *4*, 9–13.

Sheehan, D. P. & Laughrin, D. M. (1992). Device for qualitative measurements of hydrodynamic drag on swimmers. *Journal of Swimming Research*, *8*, 30–34.

Shuter, B. & ASlani, A. (2000). Body surface area: Du Bois and Dubois revisited. *European Journal of Applied Physiology*, *82*, 250–254.

Taïar, R., Bertucci, W., Letellier, T. & Benkemis, I. (2005). Experimental assessment of the drag coefficient during butterfly swimming in hydraulic flume. *Acta of Bioengineering and Biomechanics*, *7*(2).

Taïar, R. & Lodini, A. (2005). Estimation of swimmers anthropometric parameters and surface areas in real swimming conditions. *Acta of Bioengineering and Biomechanics*, *7*(1), 85-95.

Takagi, H., Shimizu, Y. & Kodan, N. (1999).A hydrodynamic study of active drag in swimming. *JSME International Journal (Series B)*, *42*(2), 171–177.

Takagi, H., Shimizu, Y., Kurashima, A. & Sanders, R. H. (2001).Effect of Thumb Abduction and Adduction on Hydrodynamic Characteristics of a Model of the Human Hand. In Blackwell, J. R. & Sanders, R. (Eds.) *International Symposium on Biomechanics in Sports* (pp. 122–126). San Francisco, USA.

Toussaint, H. M. (2002). The Fast-Skin body suit: hip, hype, but does it reduce drag during front crawl swimming? In Giannikelis K. (Eds.) *XXV International Symposium on Biomechanics in Sport* (pp. 15-24). Cacares, Spain.

Toussaint, H. M., De Looze, M., van Rossem, B., Leijdekkers, M., & Dignum, H. (1990). The effects of growth on drag in young swimmers. *International Journal of Sports Biomechanics*, *6*, 18–28.

Toussaint, H. M., Janssen, T. & Kluft, M. (1991). Effect of propelling surface size on the mechanics and energetics of front crawl swimming. *Journal of Biomechanics*, *24*, 205–211.

Toussaint, H. M., Van Stralen, M. & Stevens, E. (2002). Wave Drag in Front Crawl Swimming. In Giannikelis K. (Eds.) *XXV International Symposium on Biomechanics in Sports* (pp. 1–4). Cacares, Spain.

Ungerechts, B. E. & Niklas, A. (1994). Factors of Active Drag Estimated by Flume Swimming. In M. Miyashita, Y. Mutoh, & A. B. Richardson (Eds.) *Medicine and Science in Aquatic Sports* (pp. 137–142).

Van Manen, J. D. & Rijken, H. (1975). Dynamic measurement techniques on swimming bodies at the Netherlands ship model basin. In L. & J. P. & J. P. Clarys (Eds.) *Swimming II* (pp. 70–79). Baltimore: University Park Press.

Vennell, R., Pease, D. & Wilson, B. (2006). Wave drag on human swimmers. *Journal of biomechanics*, *39*(4), 664–671.

Vilas-Boas, J. P. Alves, F. B., & Marques, A. (2006). Biomechanics and Medicine in Swimming *Biomechanics and Medicine in Swimming* (Vol. 6, p. 148). Porto.

Vilas-Boas, J. P., Costa, L., Fernandes, R., Ribeiro, J., Figueiredo, P., Marinho, D. A., Silva, A. J., Rouboa, A. & Machado, L. (2010). Determination of the drag coefficient during the first and second gliding positions of the breaststroke underwater stroke. *Journal of applied biomechanics*, *26*(3), 324–31.

Vilas-Boas, J. P. & Fernandes, R. (2003). Swimming starts and turns: determinant factors of swimming performance. In M. Sidney & P. Pelayo (Eds.) *Actes des 3emes Journees Specialisees deNatation* (pp. 84–95). Paris: Publibook.

Vogel, S. (1994). *Life in Moving Fluids; The physical biology of flow (2nd ed)*. Princeton: Princeton University Press.

von Loebbecke, A., Mittal, R., Fish, F. & Russell, M. (2009b). Propulsive efficiency of the underwater dolphin kick in humans. *Journal of Biomechanical Engineering*, *131*(5), 054504.

von Loebbecke, A., Mittal, R., Mark, R. & Hahn, J. (2009). A computational method for analysis of underwater dolphin kick hydrodynamics in human swimming. *Journal of Sports Biomechanics*, *8*(1), 60–77.

Vorontsov, A. R. & Rumyantsev, V. A. (2000). Propulsive Forces in Swimming. In V. M. Zatsiorsky (Ed.), *Biomechanics in Sports: Performance Enhancement and Injury Prevention* (p. 667).

Wang, J., Gallagher, D., Thornton, J. C., Yu, W., Horlick, M. & Pi-Sunyer, F. X. (2006). Validation of a 3-dimensional photonic scanner for the measurement of

body volumes, dimensions, and percentage body fat. *American Journal of Clinical Nutrition*, *83*(4), 809.

Webb, P. W. (1975). Hydrodynamics and energetics of fish propulsion. *Bulletin of Fisheries Research Board of Canada*, *190*, 1–60.

Webb, P. W., Sims, D. & Schultz, W. W. (1991). The effects of air–water surface on the fast-start performance of rainbow trout (Oncorhynchus mykiss). *Journal of Experimental Biology*, *155*, 219–226.

White, W. H. (1894). *A manual of naval architecture for the use of officers of the Royal Navy, officers of the Mercantile Marine, yachtsmen, shipowners, and shipbuilders* (p. 768). London: Murray, J.

Wibowo, A., Sakamoto, D., Mitani, J. & Igarashi, T. (2012). DressUp: a 3D interface for clothing design with a physical mannequin. In S. N. Spencer (Ed.), *Proceedings of the Sixth International Conference on Tangible, Embedded and Embodied Interaction* (pp. 99–102). New York: ACM.

Williams, T. M. (1983). Locomotion in the North American mink, a semi-aquatic mammal: I. Swimming energetics and body drag. *Journal of Experimental Biology*, *103*, 155–168.

Williams, T. M. (1999). The evolution of cost efficient swimming in marine mammals: limits to energetic optimization. *Philosophical Transactions of the Royal Society B: Biological Sciences*, *354*(1380), 193–201.

Williams, T. M. & Kooyman, G. L. (1985).Swimming performance and hydrodynamic characteristics of harbour seals. *Physiological Zoology*, *58*, 576-589.

Wilson, B. D. & Thorp, R. (2003). Active drag in swimming. In J. C. Chatard & J. M. Puget (Eds.) *Proceedings of the IX World Symposium of Biomechanics and Medicine in Swimming* (pp. 21–26). St Etienne, France.

Wood, J. (2008). Record breaking or rule breaking? *Materials Today*, *11*(6), 1.

Yeon, S. L., Jong, K. S., Shin, V. I., Kim, G. H. & Jeon, M. (2008). Anatomical evaluation of CT-MRI combined femoral model. *Biomedical Engineering*, *7*(6), 1–12.

Zaïdi, H., Fohanno, S., Taïar, R. & Polidori, G. (2010). Turbulence model choice for the calculation of drag forces when using the CFD method. *Journal of biomechanics*, *43*(3), 405–11.

Zaïdi, H., Taïar, R., Fohanno, S. & Polidori, G. (2008). Analysis of the effect of swimmer's head position on swimming performance using computational fluid dynamics. *Journal of Biomechanics*, *41*(6), 1350–1358.

Zamparo, P., Gatta, G., Pendergast, D. & Capelli, C. (2009). Active and passive drag: the role of trunk incline. *European journal of applied physiology*, *106*(2), 195–205.

Zamparo, P., Pendergast, D. R., Mollendorf, J., Termin, A. & Minetti, A. E. (2005). An energy balance of front crawl. *European Journal of Applied Physiology*, *94*, 134–144.

Appendix A

Appendix A comprises the information sheets provided to the participants prior to the data collection sessions.

Informed Consent Form

Participant's Name: _____ **Sex:** Male / Female

Date of Birth:_____

Investigator: Georgios Machtsiras
(g.machtsiras@sms.ed.ac.uk)

Supervisor: Prof. Ross Sanders
(r.sanders@ed.ac.uk)

Ethics Committee Approval Number:

Project Title:

'The effect of head position on resistive forces when gliding in swimming'

Participant Statement

1. I fully understand what is involved in taking part in this study.	YES / NO
2. Any questions I have about the study, or my participation in it, have been answered to my satisfaction.	YES / NO
3. I understand that I do not have to take part and that I may decide to withdraw from the study at any point without prejudice.	YES / NO
4. My concerns regarding the study have been answered and such further concerns as I have during the time of the study will be responded to.	YES / NO
5. I consent to participate on this research study.	YES / NO
6. I grant my permission for the video recordings to be shown to others for educational purposes, for example on the World Wide Web.	YES / NO

Signature of the Participant _____ Date _____

Signature of the Investigator _____ Date _____

Participant Information Sheet

Dear Swimmer,

Aim of the study
The aim of this study is twofold. First to identify the relative effect of key factors in gliding performance and second to determine the accuracy of Computational Fluid Dynamics (CFD) in analyzing swimming hydrodynamics. For this reason a three dimensional model of your body will be created, analyzed and findings will compared to real data collected when gliding in the water.

What is expected from you
Your participation involves two separate sessions.
Session 1. The first session will take place at St Leonard's swimming pool, Edinburgh.
Pre-test. You will be marked with black marker on 6+7=13 anatomical points. Height, weight in water and weight out of the water will be assessed and two sets of two pictures will be taken (front view and side view) when standing in the anatomical position.
Test. After that, you will do a warm-up of 200 m and a set of familiarization glides until you feel confident you can glide on a horizontal streamlined position. The data collection comprises three sections. For the first section of the study, you will perform 10 glide with high head position, 10 with medium and 10 with low head position. Trials that you did not manage to control your body posture (body alignment, head position, joint angles and gliding depth) will be repeated. For the second section, you will perform 10 glides at 0.6 m depth (from the water surface), 10 at 0.4 m depth and 10 at 0.2 m depth. The third and last section involves 10 glides when wearing a full body swimsuit. The gliding depth for all sections will be 0.8 m from the water surface. During the glides the relative position of all marked anatomical points will be computed to estimate your glide efficiency.
Feedback will be provided throughout the session.
Approximate duration: 6 hours with breaks between.

Session 2. The second session will take place at the Department of Health Science at Robert Gordon University, Aberdeen.
Pre-test. You will be marked on the same 13 anatomical points with the first session with stickers visible on the Computer Aided Design (CAD) model.
Test. After adopting a streamlined position on land identical to the gliding one, you will be scanned in two stages; first your upper body (Figure 1) followed by your lower body (Figure 2). In total eight scans will be performed with altered joint angles. These scans will be used as an input to a software package that will simulate the water flow around your body and estimate drag forces.
For the scans you will be required to wear your swimming suit (full body swimming suits for two of the scans) and a white swimming cap (this is provided).
Approximate duration: less than two hours.

Benefit from your participation
A copy of your recorded glides as well as a short report on your gliding performance will be provided to you and your coach after the completion of the study.

Notes
Your participation is completely voluntarily and you can withdraw from the study at any time.
All recorded files and information data will be treated as case sensitive. The video files and the 3D models will be securely stored and all information, which could identify the participants, will be coded.

Investigator: Georgios Machtsiras
E-mail: g.machtsiras@sms.ed.ac.uk
Tel. 0131 651 6408

Supervisor: Prof. Ross Sanders
E-mail:r.sanders@ed.ac.uk
Tel. 0131 651 6580

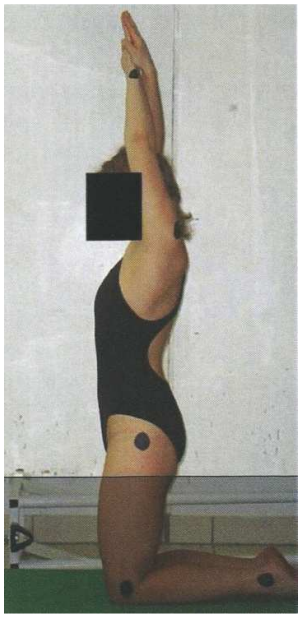

Figure 1

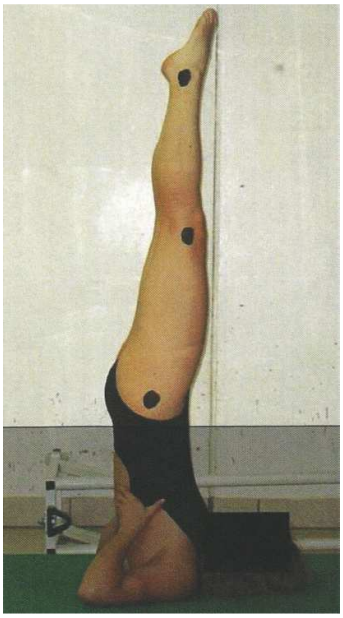

Figure 2

Pre Activity Questionnaire

Participant's Name: _____ **Sex:** Male / Female

Date of Birth:_____

Investigator: Georgios Machtsiras
(g.machtsiras@sms.ed.ac.uk)

Supervisor: Prof. Ross Sanders
(r.sanders@ed.ac.uk)

For you own safety complete the following questions

Do you have a heart condition?	YES / NO
Have you ever experienced chest pains when exercising?	YES / NO
Do you feel dizzy; lose balance or ever lost consciousness?	YES / NO
Do you suffer from any joint problem?	YES / NO
Is there any other reason why you should not undergo physical activity?	YES / NO

I_____ hereby declare that all sections have been completed according to the best of my knowledge. Date _____

Signature of the Investigator _____ Date _____

Appendix B

Differences in the angle of attack when a swimmer is gliding underwater are expected to affect the frontal surface area. However, this increment is not linear and is associated to the individual morphological characteristics of the athlete and the adopted joint angles. In Appendix B the frontal surface area is presented of both swimmers for angles of attack ranging from -3 to 3 degrees.

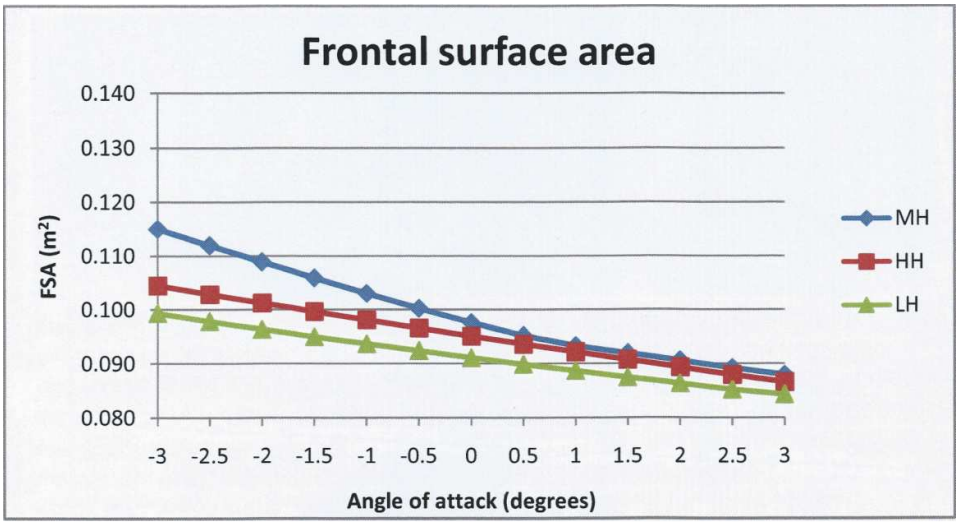

Figure AP.1 The frontal surface area profile for the female swimmer for angles of attack ranging from -3 to 3 degrees.

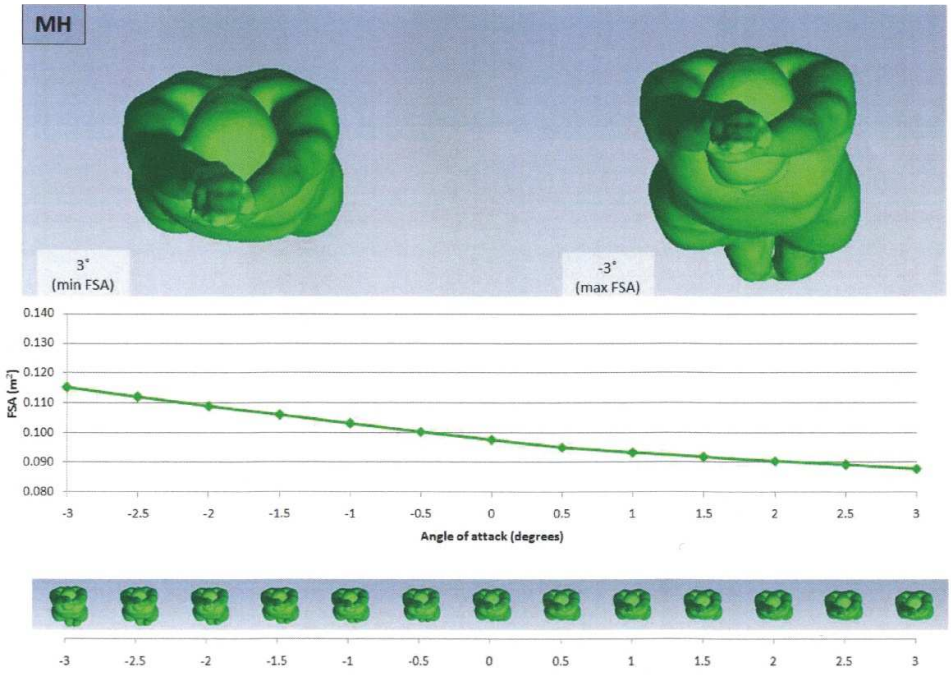

Figure AP.2 The frontal surface of the female swimmer in the medium head position.

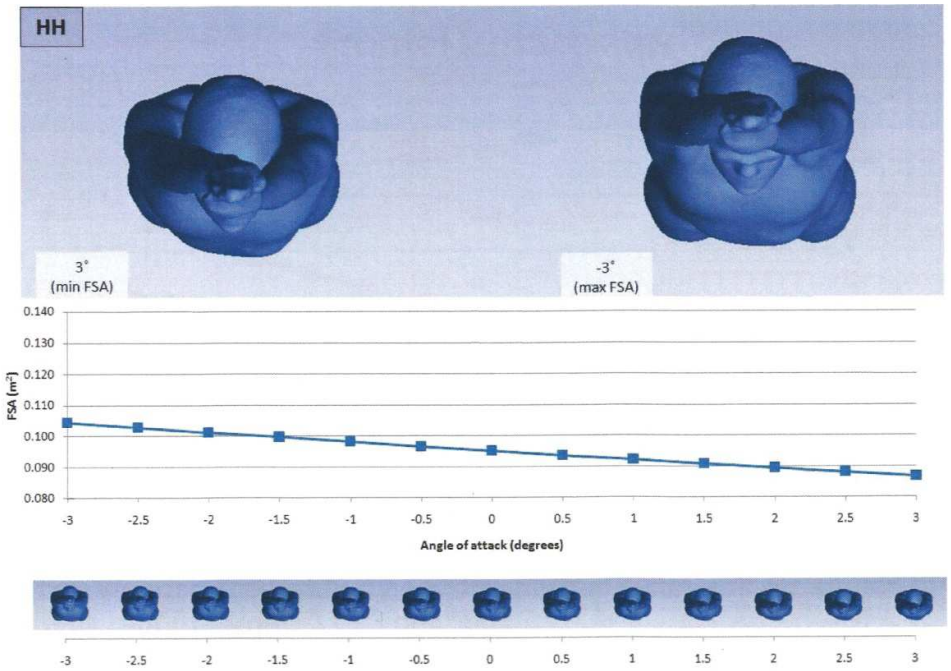

Figure AP.3 The frontal surface area of the female swimmer in the high head position.

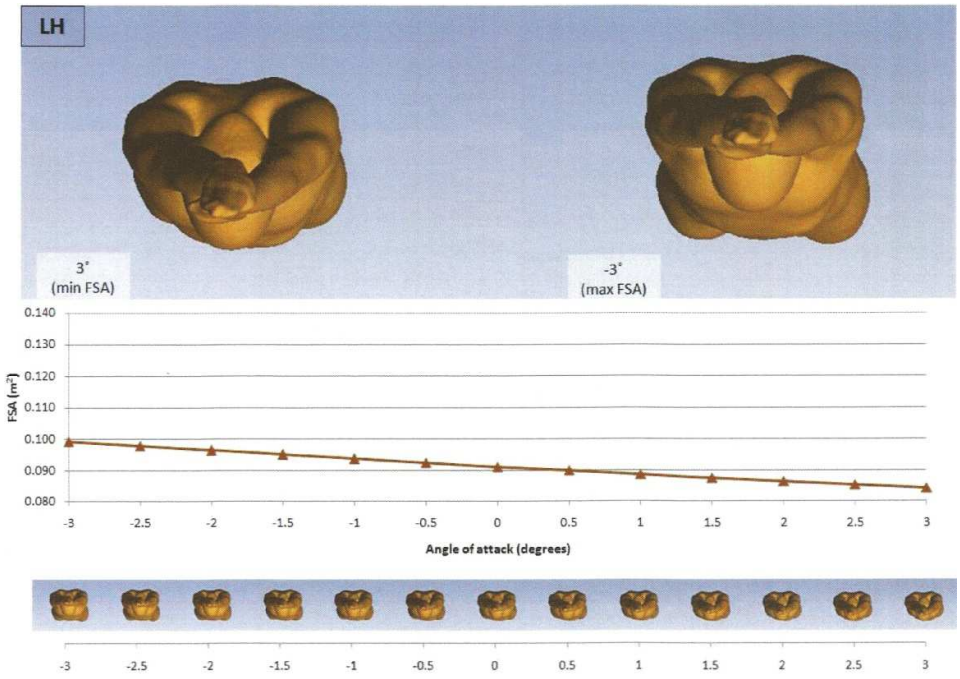

Figure AP.4 The frontal surface of the female swimmer in the low head position.

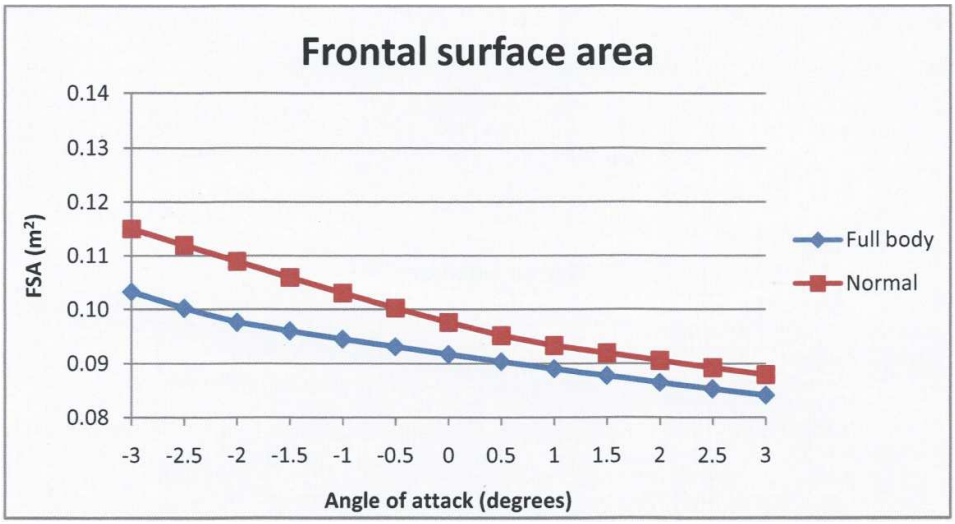

Figure AP.5 The frontal surface area profile for the female swimmer when wearing the full body and the normal swimsuit for angles of attack ranging from -3 to 3 degrees.

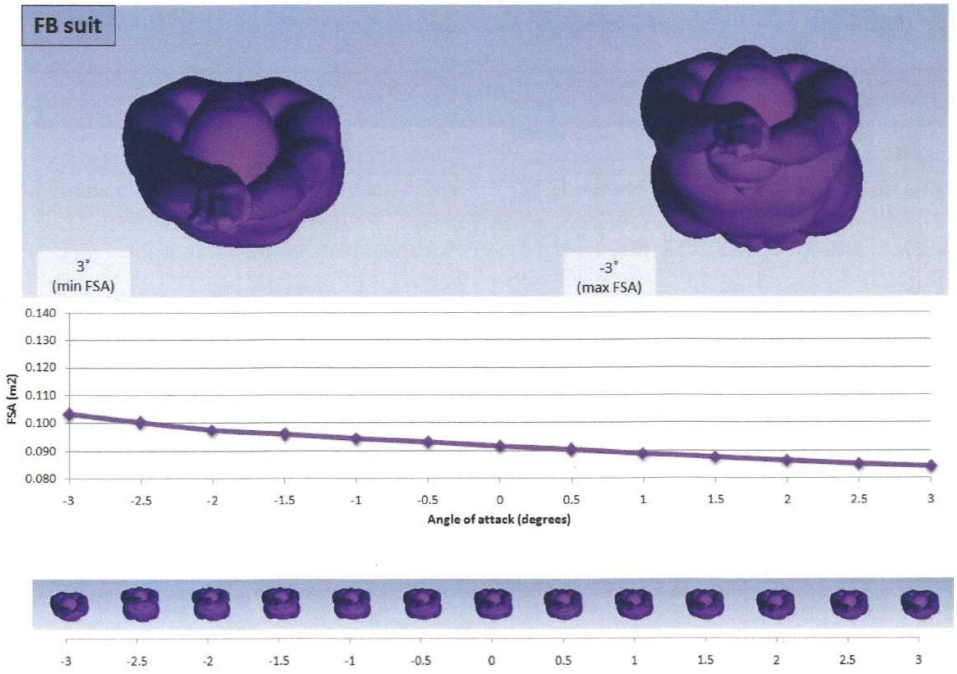

Figure AP.6 The frontal surface of the female swimmer when wearing the full body swimsuit.

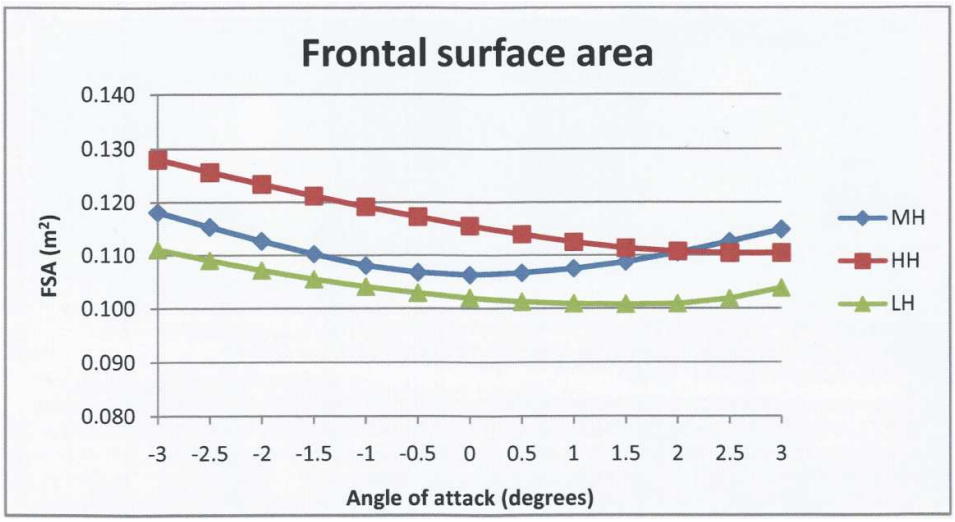

Figure AP.7 The frontal surface area profile for the male swimmer for angles of attack ranging from -3 to 3 degrees.

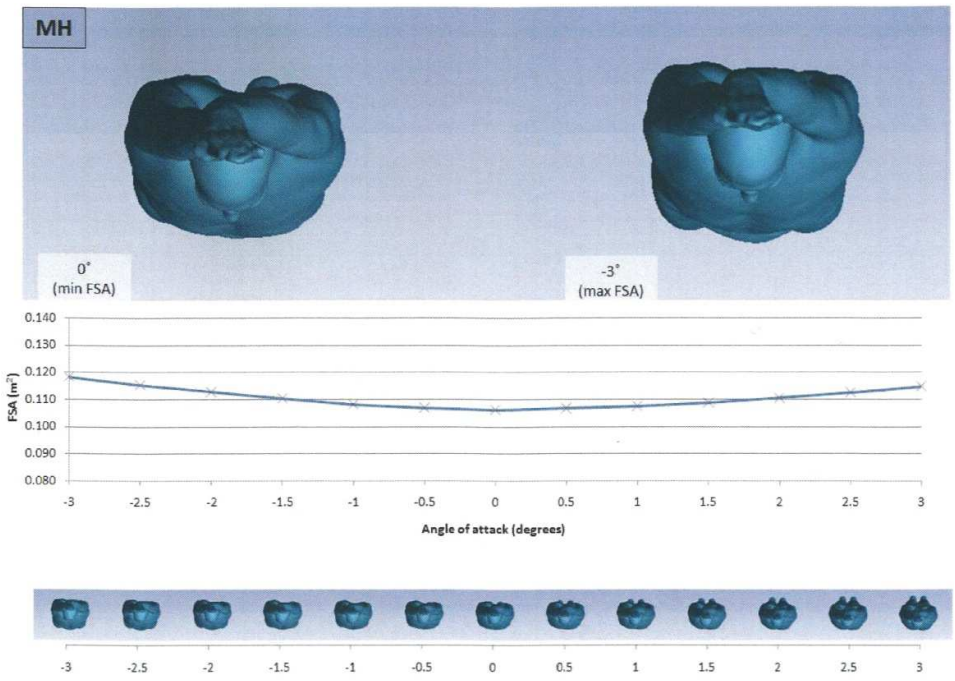

Figure AP.8 The frontal surface of the male swimmer in the medium head position.

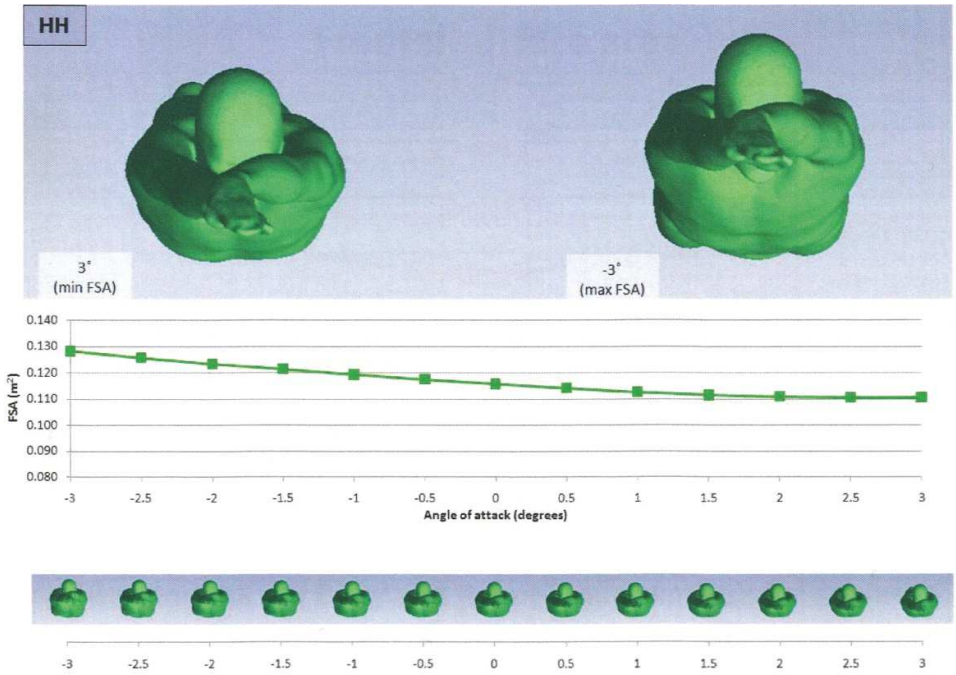

Figure AP.9 The frontal surface area of the male swimmer in the high head position.

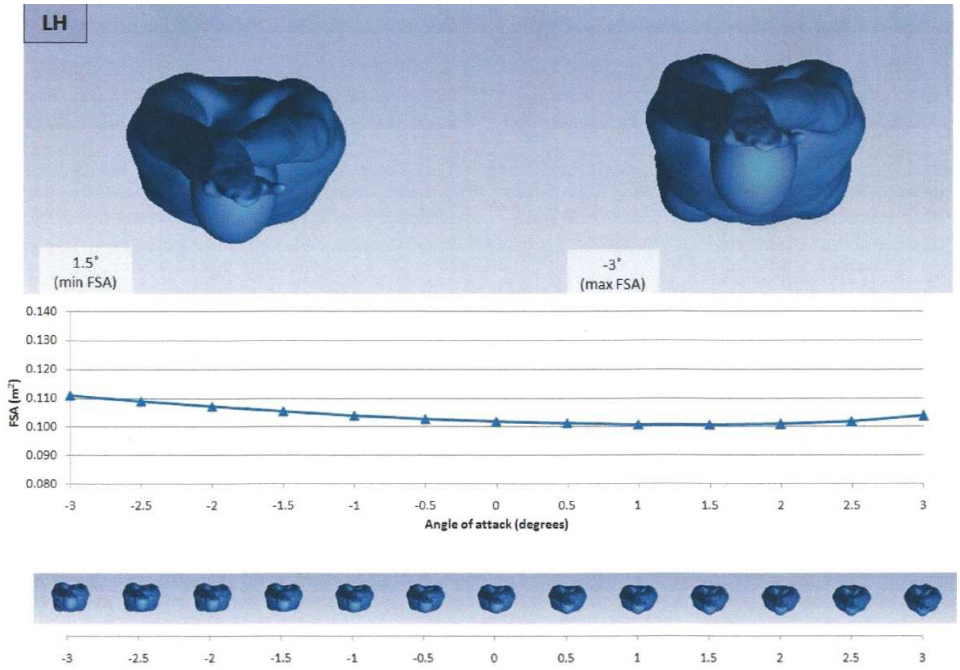

Figure AP.10 The frontal surface of the male swimmer in the low head position.

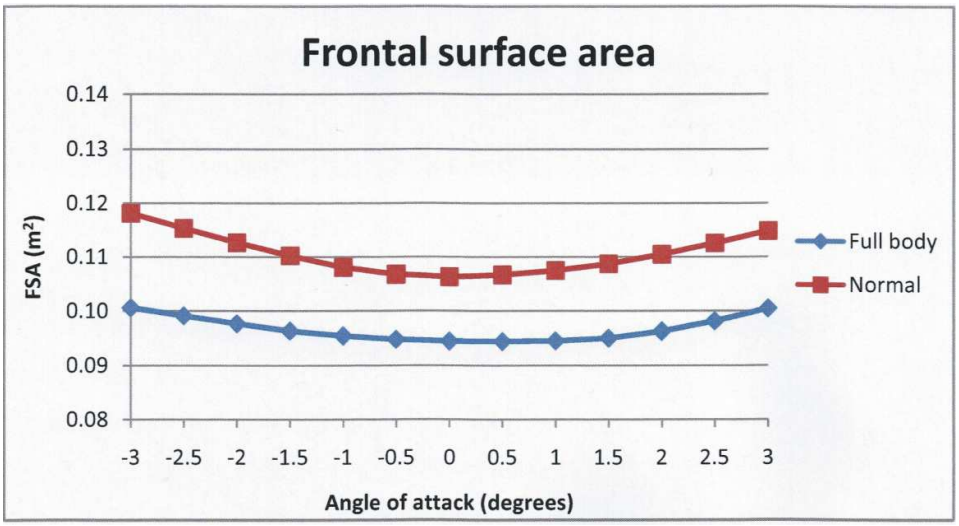

Figure AP.11 The frontal surface area profile for the male swimmer when wearing the full body and the normal swimsuit for angles of attack ranging from -3 to 3 degrees.

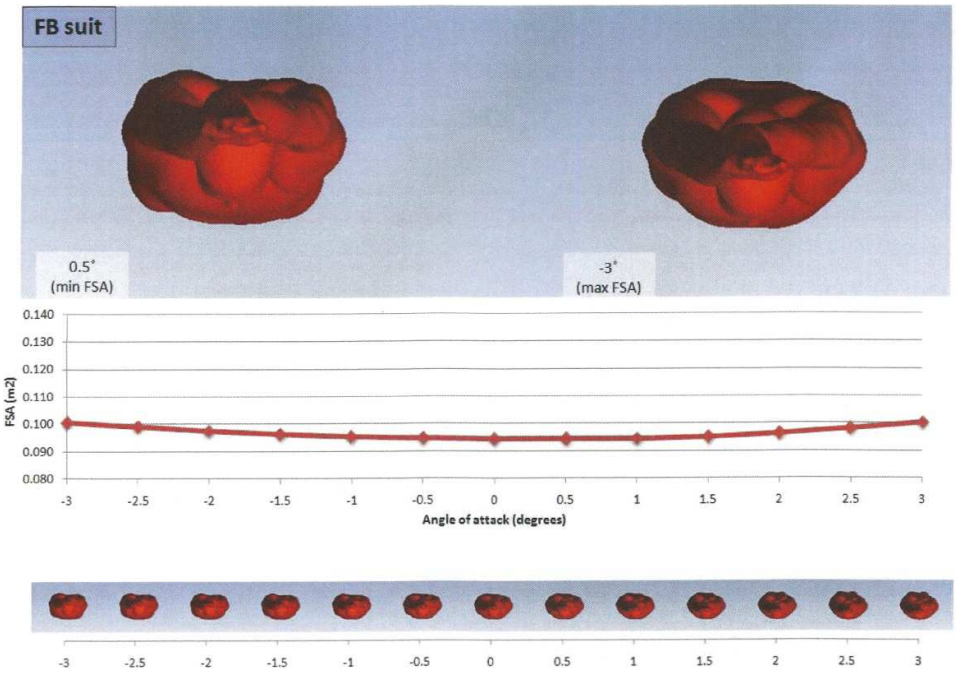

Figure AP.12 The frontal surface of the male swimmer when wearing the full body swimsuit.

Appendix C

A swimmer's scanned 3D model is consisted of a cloud of points whose number can be altered according to the requirements of the study to be conducted. Subsequently, any alteration is directly affecting the accuracy of the body shape representation.

The density of the cloud of points in this study is defined as the maximum distance between two adjoining points and consequently the longer the distance the lower the quality of the representation. Figures AP.13 to AP.18 demonstrate this difference for the model of the male swimmer when gliding in the medium head position.

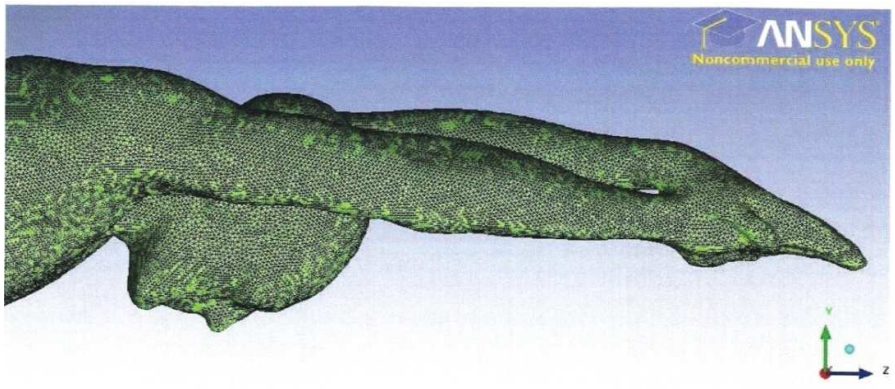

Figure AP.13 Maximum mesh size 5 mm.

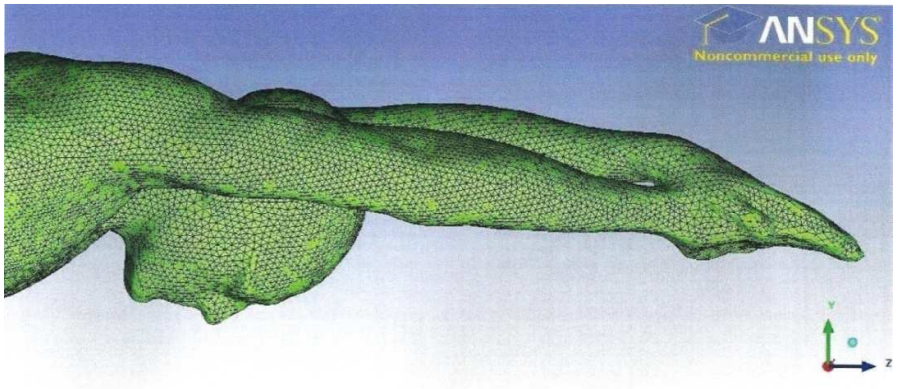

Figure AP.14 Maximum mesh size 8 mm.

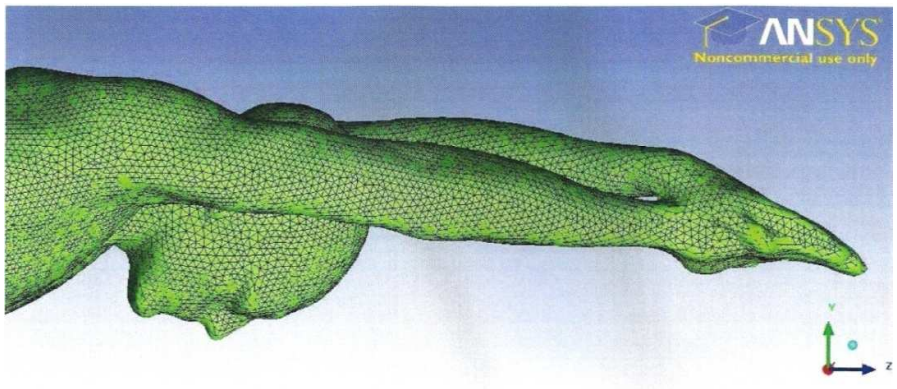

Figure AP. 15 Maximum mesh size 9 mm.

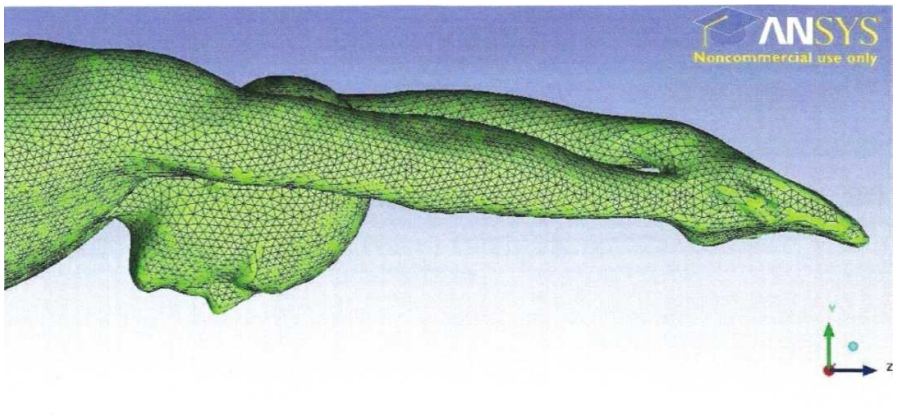

Figure AP. 16 Maximum mesh size 10 mm.

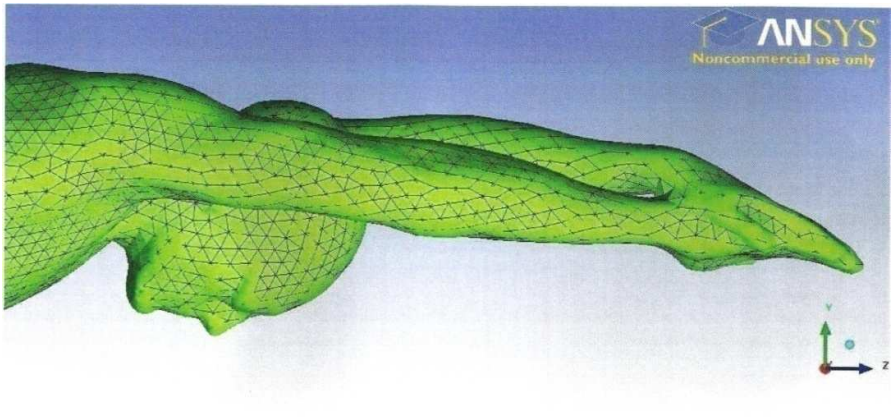

Figure AP. 17 Maximum mesh size 20 mm.

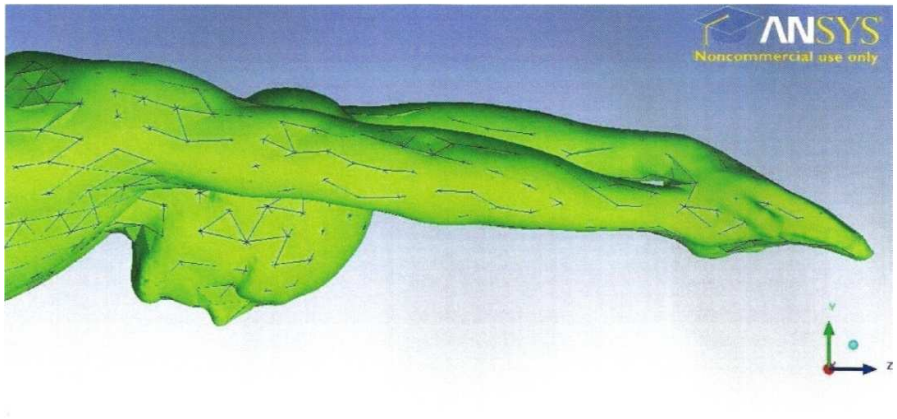

Figure AP. 18 Maximum mesh size 40 mm.

Appendix D

Appendix D shows the low and medium head position adopted by two of the most successful swimmer's.

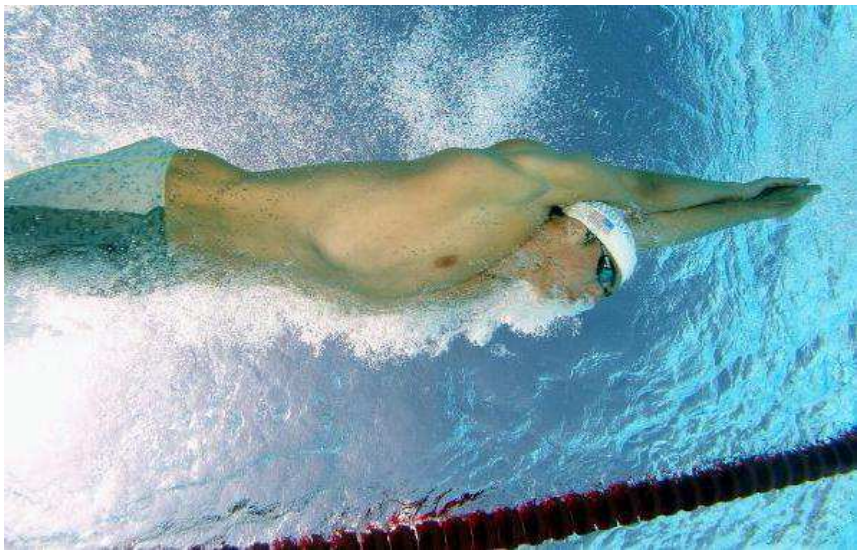

Figure AP. 19 Michael Phelps gliding underwater with a low head position.

Figure AP. 20 Ian Thorpe gliding underwater with a medium head position.

Sections of the second chapter have been published in:

Sanders, R.H., Psycharakis, S.G., Naemi, R., McCabe, C. & Machtsiras, G. (2008). *Swimming*. In: Hong Y. & Bartlett R. (Eds.) Routledge Handbook of Biomechanics and Human Movement Science. Oxford: Taylor & Francis Publisher. pp: 323-339.